Simulation of viscous instabilities in miscible and immiscible displacement

by Eli Gilje

Master thesis
Petroleum technology – reservoir chemistry

Department of Chemistry
University of Bergen
June 2008

Preface

The work presented in this thesis has been carried out at the Centre for Integrated Petroleum Research, CIPR, at the University of Bergen.

Advisors on this thesis are professors Arne Skauge and Harald Høiland at the University of Bergen. I would like to express my gratitude towards Arne for helping me throughout the work, and to Harald for being my contact to the Institute of Chemistry at UIB. I am very thankful to Terje Finnekås for being an exceptional student advisor. I am also grateful to all my colleagues at CIPR for their support and encouragement, especially Alif Be for valuable help towards the end.

At the beginning of this thesis, I spent one week at the University of Texas at Austin. During this week I was trained in the UTCHEM simulator by Mojdeh Delshad. As Mojdeh has continued to be a support throughout the work, I am very grateful to her as well.

I would like to thank my friends and family, in particular my father Eimund Gilje, StatoilHydro, for valuable help and advice during this work.

Finally I would like to thank my dear Håvard for all his support.

Eli Gilje (Bergen, 9 June, 2008)

Abstract

This study includes modeling of viscous instabilities at both miscible and immiscible displacement. Oil recovery of heavy oil leads to unstable displacement for adverse mobility ratio for both miscible and immiscible displacement.

Simulation studies of viscous fingering in miscible and immiscible displacements were performed in order to history match 2D slab laboratory experiments performed at CIPR, Centre for Integrated Petroleum Research. History matching of a polymer flood experiment is also included in this thesis. All simulations were performed using UTCHEM, a chemical flooding simulator developed at the University of Texas at Austin.

In the laboratory experiment, viscous fingering was observed for the miscible displacement at unfavorable mobility ratio. For the miscible displacement at favorable mobility ratio, an indifferent displacement process (more piston-like displacement) was observed. For the immiscible displacements, both at unfavorable mobility ratio, viscous fingering was only observed in the case with zero initial water saturation. The presence of capillary pressure, however, smeared out the front of the fingers, turning the displacement process indifferent over time.

At unfavorable mobility ratio, a water flood experiment was followed by a polymer flood. During the polymer flood an oil bank was accumulated, and considerable additional oil was produced.

To history match the miscible displacement an approach was tried by using variation in local grid block permeability. This approach with large variation in permeability field, miscible displacement showed overall good agreement with the experimental results. The miscible displacement at favorable mobility ratio, when simulated in UTCHEM, showed an indifferent type displacement process. The simulation model of the miscible displacement at unfavorable mobility ratio, showed the formation of viscous fingering very similar to that obtained in the laboratory experiment. The applied method of permeability distribution seems to match both displacements at favorable and unfavorable mobility ratio.

The simulated model for immiscible displacement at S_{wi}=0, did not generate viscous fingers. The establishment of water films is most likely a fast kinetic reaction that is not included in the simulator and is therefore not observed in UTCHEM. The UTCHEM simulator did, however, provide similar results for

the immiscible displacement at S_{wi}=0.12. The applied capillary pressure in the immiscible displacements causes smearing of the front, which results in an indifferent type displacement.

The simulation model of the polymer flood following a water flood showed the accumulation of an oil bank very similar to observed experimental results. In order to match the oil bank formation and oil recovery by polymer flooding, the residual oil saturation in the simulation model had to be reduced from the residual oil saturation by water flooding ($S_{or,w}$=0.47), to a lower residual oil saturation after polymer flooding ($S_{or,p}$=0.31). The approach of only changing endpoint saturations and including the physical chemistry properties of the polymers, was able to give a good history match of the experiment.

Table of contents

1 Introduction

Water injection is the principal form of secondary oil recovery, and is widely practiced in the North Sea. Reasons for this is that supply of water is often plentiful, and therefore inexpensive, and that it is usually more stable frontal displacement than other forms of secondary recovery. The purpose for injecting water is both in upholding reservoir pressure, and in displacing the oil towards the production wells as illustrated by Fig 1.1. Water injection, as a method for secondary recovery, has been applied in the oil industry for many years [1].

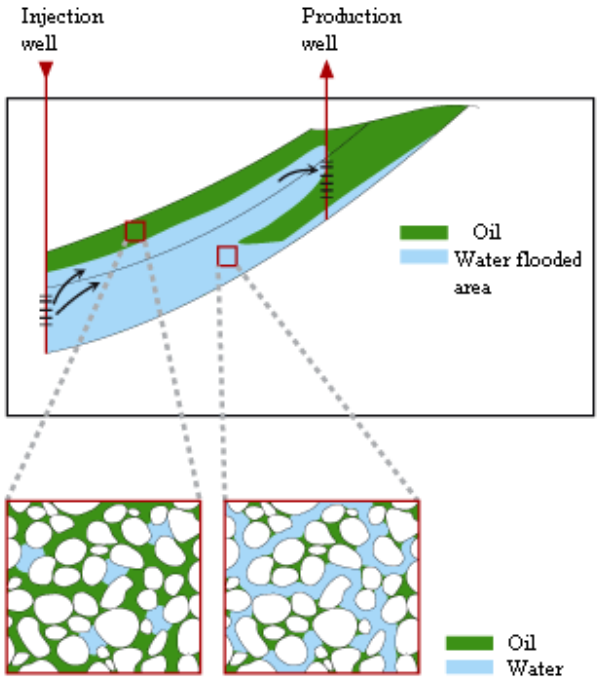

Figure 1.1: Schematic illustration of water injection in an oil reservoir. Cross sections show the distribution of oil and water before and after the water has displaced the oil [72].

The stability of a water flood depends on the mobility ratio between oil and water, heterogeneity of the porous medium, segregation of the fluids in the reservoir, and dissipation of fluid fronts caused by capillary pressure. Instabilities may occur in both miscible and immiscible processes, and originate on the interface between oil and water. These frontal instabilities are often characterized by a number of penetrating fingers of displacing fluid.

The mobility ratio is defined as the mobility of the displacing fluid over that of the displaced fluid [2] and is given by Eq. 1.1,

$$M = \frac{k_{rw} / \mu_w}{k_{ro} / \mu_o} \tag{1.1}$$

The mobility ratio dictates the efficiency of the water-oil displacement on a microscopic scale. In a one-dimensional water flooding experiment of a homogeneous core plug, a less than unity mobility ratio (M<1), gives a completely stable displacement. If M<1, the injected water can not travel faster than the oil, and it is therefore displaced in a piston-like manner which is the most favorable form of displacement as shown in Fig. 1.2,

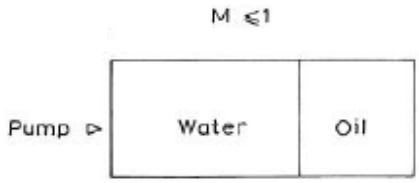

Figure 1.2: Waterdrive experiment at favorable mobility ratio, in a one-dimensional homogeneous core plug [1].

Most NCS fields have low oil viscosity, typically less than one centipoise (mPa*s). Using typical endpoint parameters for North Sea fields for viscosities and endpoint relative permeabilities gives a mobility ratio as shown in Eq. 1.2,

$$M^0 = \frac{k_{rw}^0 / \mu_w}{k_{ro}^0 / \mu_o} = \frac{0.3 / 0.4 mPa \cdot s}{1 / 0.8 mPa \cdot s} = 0.6 \tag{1.2}$$

which is well below unity. Because of the low oil viscosity, most North Sea fields have quite favorable mobility ratios and are therefore suitable for water flooding.

Many of the oil field around the world contains high viscous oil, which gives a mobility ratio greater than unity (M>1). Such mobility ratios are unfavorable and may cause the occurrence of frontal instabilities [3]. If M>1, the injected water may channel through the oil in an unstable manner, see Fig. 1.3. This viscous fingering leads to premature breakthrough of water and a poor volumetric sweep.

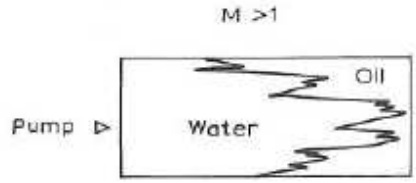

Figure 1.3: Waterdrive experiment at unfavorable mobility ratio, in a one-dimensional homogeneous core plug [1].

In cases where the mobility ratio is unfavorable and the reservoir heterogeneity is significant, polymers may be added to the injected water in order to increase its viscosity and thus improve the volumetric sweep of the reservoir. The effect of mobility control on the performance of water floods was first presented by Muskat. The fact that a small amount of polymer added to water reduces its mobility significantly was established in 1964 [4,5]. Fig. 1.4 illustrates a polymer flooding sequence.

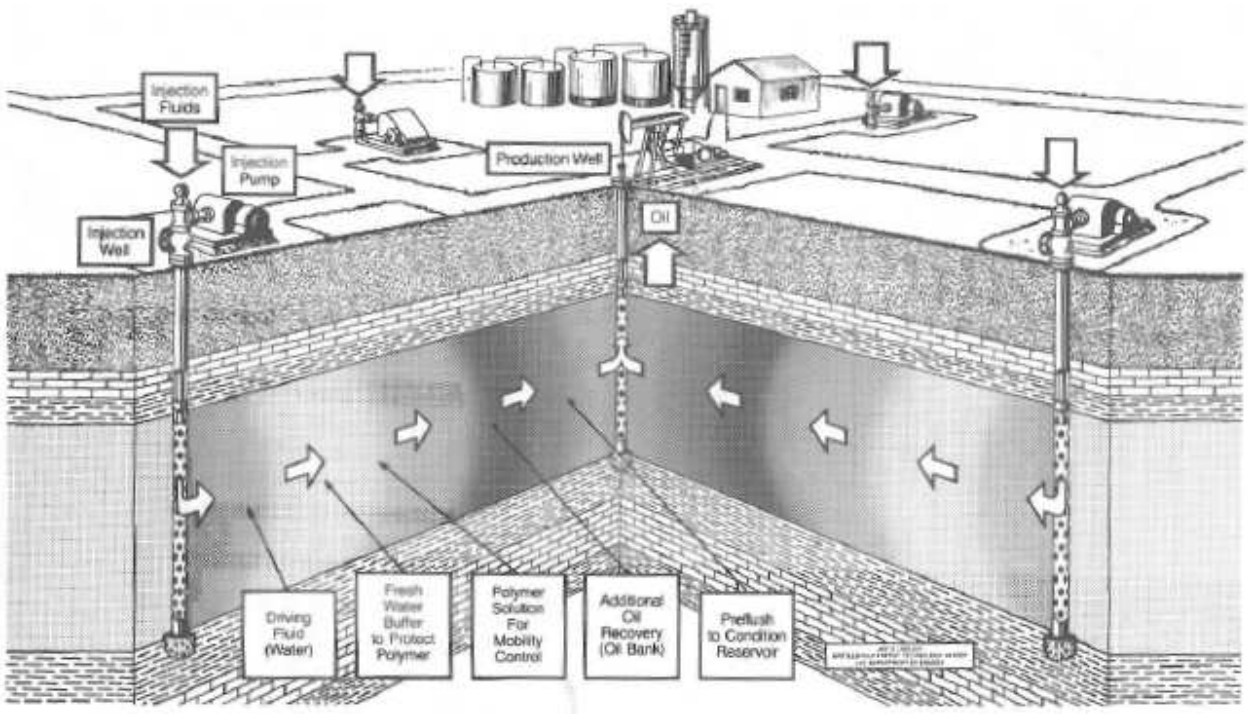

Figure 1.4: Schematic illustration of a polymer flooding sequence, using a single 5-spot pattern [71].

In principle, an increase in water viscosity should give lower residual oil saturation due to an increase in the capillary number. This increase is, however, normally too small to significantly effect the residual oil saturation. Thus the residual oil saturation will be much the same for the polymer flood as it is for a water flood. The main effect of a polymer flood will be to accelerate reserves and improve volumetric sweep efficiency.

The mobility ratio for NCS fields are quite favorable, but they are very heterogeneous. The effect of a polymer injection is rather small for a heterogeneous reservoir if the mobility ratio is favorable. NCS fields are therefore not the best candidates for polymer flooding. Other fields around the world, containing more viscous oil, make for better candidates.

An experimental study of increased oil recovery in adverse mobility reservoirs has been carried out at the Centre for Integrated Petroleum Research, CIPR, at the University of Bergen. This study includes the use of a 2D-scanner to identify flow regimes in miscible oil-oil displacements with unfavorable mobility ratio, and in immiscible water-oil displacements with capillary pressure. In this thesis the chemical flooding simulator, UTCHEM, has been used in order to history match the experimental displacements. The experimental study included an investigation of oil recovery when modifying the mobility ratio between oil and water by introducing polymers to the system. The UTCHEM simulator was also utilized to history match the experimental polymer flood [6].

2 Theory

The displacement of one fluid in a porous medium by another fluid depends both on heterogeneities and the interaction of several forces. The acting forces include viscous forces driven by adverse viscosity ratios, gravity forces driven by fluid density gradients, capillary forces due to interfacial tension between immiscible fluids, and dispersive forces caused by concentration gradients between miscible forces. The effect of one or several of these forces might cause an unstable displacement process. Viscous forces can cause viscous fingers to develop along the displacement front. If the displacement rates a low, the gravity forces may cause segregation of the fluids leading to gravity over- or under-ride of one fluid with respect to the other fluid. Dispersive and capillary forces have a tendency to smear out and dampen viscous fingers in miscible and immiscible displacements, respectively. The main focus of this thesis will be on fingering caused by viscous forces.

2.1 Viscous fingering

Viscous instabilities are associated with displacement processes where the displaced fluid has a higher viscosity than the displacing fluid. The less viscous displacing fluid generally flows more easily than the more viscous displaced fluid, causing the occurrence of perturbations which finger through the system. Several parameters affect the initiation of viscous fingers, for instance the balance between capillary and gravitational forces and the heterogeneity of the rock. Once occurred, the viscous fingering increases with the viscosity ratio, between the displaced and displacing fluids. Viscous fingering can have dramatic effect on the sweep efficiency of a displacement process. Unstable displacement processes due to viscous fingering are often associated with early breakthrough of the displacing fluid. Fig. 2.1 illustrates viscous fingering in a quarter of a 5-spot model.

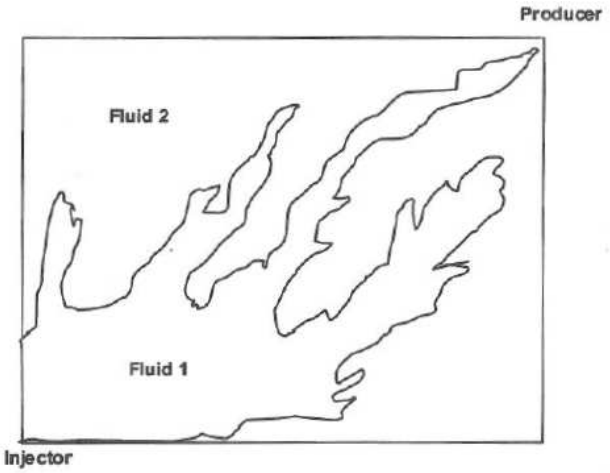

Figure 2.1: Viscous fingering in a quarter of a 5-spot model with a mobility ratio of 17 [70].

The following example [7] illustrates why an unfavorable mobility ratio may result in displacement front instabilities. Fig. 2.2 [7] illustrates the linear displacement of oil by a solvent in a porous medium. The porous medium is initially fully saturated by oil. In such a case the mobility ratio is merely the viscosity ratio between the oil and the solvent. Longitudinal dispersion is assumed negligible in this example. If heterogeneities are absent the displacement front should remain a plane surface during the displacement. However, if the stable front were to encounter a small region of higher permeability, the part of the front entering this region would momentarily travel faster than the rest of the front.

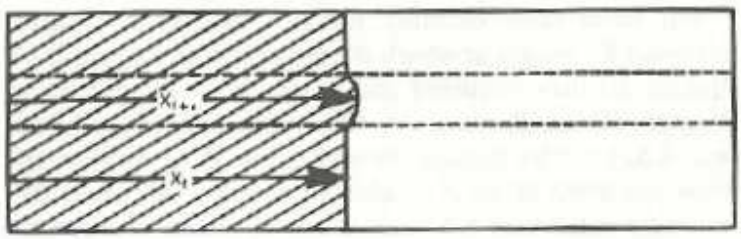

Figure 2.2: A simplified model of frontal instability [7].

As illustrated in Fig. 2.2, this would cause the faster moving part of the front to protrude a distance ε from the otherwise stable interface. Thus $x_f + \varepsilon$ is the distance from the inflow end to the front in the high permeable region, where x_f is the distance to the undisturbed front. Using Darcy's equation, the velocity of the undisturbed front can be expressed by Eq. 2.1,

$$\frac{dx_f}{dt} = \frac{k\Delta p}{\phi\mu_s\left[ML + (1-M)x_f\right]} \tag{2.1}$$

where μ_s is the viscosity of the solvent. The velocity of the front in the high permeable region may be expressed by Eq. 2.2,

$$\frac{d(x_f + \varepsilon)}{dt} = \frac{k\Delta p}{\phi\mu_s\left[ML + (1-M)(x_f + \varepsilon)\right]} \tag{2.2}$$

From Eq. 2.1 and Eq. 2.2 and provided that $\varepsilon << x_f$, Eq.2.3 follows,

$$\frac{d\varepsilon}{dt} = \frac{-k\Delta p(1-M)\varepsilon}{\phi\mu_s[ML+(1-M)x_f]^2} \tag{2.3}$$

Integrating Eq. 2.3 gives $\varepsilon = e^{Ct}$, where C is given by Eq. 2.4,

$$C = \frac{-k\Delta p(1-M)}{\phi\mu_s[ML+(1-M)x_f]^2} \tag{2.4}$$

Immediately after the formation of the perturbation, ε will initially increase exponentially with time as long as M > 1. If M < 1, ε will decrease exponentially with time. Thus this example illustrates how viscous forces may cause frontal instabilities arising from permeability heterogeneities. The example is extremely simplified, and had dispersive or capillary forces been present the growth of the frontal instability might been opposed.

The viscous instability phenomena consist of both the initiation of fingers and finger growth. Small scale permeability heterogeneities are often the cause for finger initiation [8]. A criteria for conditions where perturbations might occur, is a mobility ratio greater than one. As this seems valid for miscible processes, such factors as capillary pressure might complicate the situation for immiscible processes.

2.1.1 Finger initiation

Initiation of viscous fingers is generally attributed to the presence of permeability heterogeneities. In porous media, finger initiation is easily visualized as pore structure is microscopically random, even in packs of glass-beads that appear macroscopically homogeneous [9]. Such microscopic variations are sufficient to initiate viscous fingers. Under certain appropriate displacement conditions, viscous fingering are even observed in laboratory Hele-Shaw models [9]. Hele-Shaw models are constructed of two parallel plates with a liquid filled gap between them. Microscopic variations at the plate surfaces and gap width sufficiently initiate viscous fingering.

Several mathematical investigations of finger initiation by the frontal perturbation method has been performed [10,11,12,13,14]. The frontal perturbation method assumes a spectrum of wavelengths of the perturbations at the front. For instance that a Fourier series may be used to describe the variations of the

frontal positions about an average smooth line. For any given set of conditions, all perturbations below a critical wavelength are eliminated due to dispersion. Perturbations above the critical wavelength continue to grow at an unfavorable mobility ratio.

For the case of an initially sharp solvent/oil interface the following expression for the critical wavelength in a miscible displacement, Eq. 2.5, was proposed by Gardner and Ypma [14],

$$\lambda_c = 2^{5/2} \cdot \pi \cdot \frac{\mu_o + \mu_s}{\mu_o - \mu_s} \cdot \frac{K_t}{v} \tag{2.5}$$

Where λ_c is the finger width in cm, μ_s and μ_o are the respective solvent and oil viscosities. K_t is the transverse dispersion coefficient in cm^2/s, and v is the average interstitial velocity in cm/s.

From numerous experiments [15,16,17,18,19,20,21,22] it has been concluded that dispersion is not sufficient to damp out all flow perturbation in systems of reservoir dimensions. This is also true about most of the systems of laboratory dimensions.

In an experimental study of viscous instabilities in both linear and radial models performed by Perkins et al. [22], observations show that a small region at the inlet of their models were devoid of fingers. It was proposed that even though viscous fingers are initiated by permeability variations at the inlet, the growth rate in length of the finger exceed the initial growth rate of the longitudinal mixed zone before propagation of the fingers. A fairly simplified expression for the growth rate in finger length were developed by Perkins et al. [22]. These authors also proposed an approximate calculation of the linear and radial distances of where fingering first would be observed. Different expressions of growth rate for finger length have been proposed by other authors [23,24]. However, any expression for growth rate of finger length used with the finger initiation calculations proposed by Perkins et al., show that the initial region that is devoid of fingers is negligible on reservoir scale and on most laboratory scales [22].

2.1.2 Finger growth

Once perturbations occur above the critical wavelength, they begin to grow in length. New fingers may initiate from the ends of already growing fingers. This result in a finger pattern looking somewhat like that in Fig. 2.3 a).

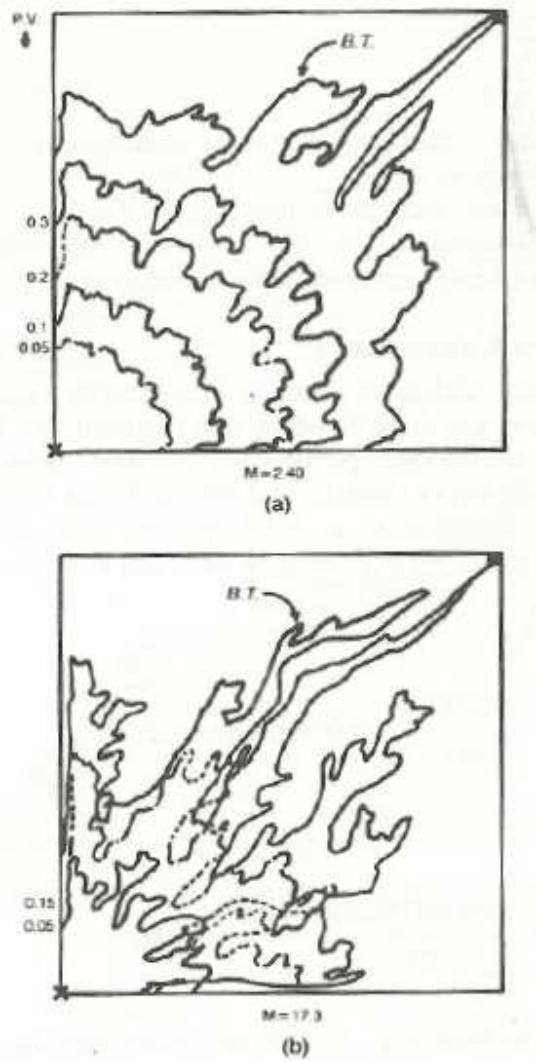

Figure 2.3: Displacement fronts for different mobility ratios, (a) 2.4 and (b) 17.3, and at different injected PV until breakthrough. The figure shows a quarter of a five-spot model [16].

An increase in mobility ratio results in an increase in viscous instability which consequently increases the growth rate of the viscous fingers [9].

The growth of the finger occurs both in length and in average width. In length, the finger growth is approximately linear with time. For dispersive type growth, however, the displacement front mixing zone grows with the square root of time. Finger growth in width is a combination of spreading by transverse

dispersion, by merging and coalescence of smaller fingers into larger fingers [22]. This merging of smaller fingers can be observed in Fig. 2.3 b). As a result, oil may be trapped between two merging fingers. During the merging the oil is mixed into the larger finger that forms [22]. During the mixing of oil and solvent, the effective viscosity ratio is reduced. This process results in fewer and fewer fingers growing larger during the displacement.

Longitudinal dispersion have been found to be relatively unimportant in the growth of finger length [15,17,25]. Transverse dispersion, however, if at high rates, may erase fingers completely or reduce them to one or two larger fingers creating a more stable displacement [15,21,26]. Importance of transverse dispersion in a miscible displacement may be characterized by the dimensionless transverse dispersion group, K_tL/vW^2 [9]. Here L is total displacement length, and the reservoir width over which the fingers occur are represented by W. Transverse dispersion has an increasing effect on the displacement as the value of the transverse dispersion group increases.

Several mathematical treatments have been developed of miscible displacement with viscous fingering [10,22,27,28,29]. By use of a finite-difference technique, Peaceman and Rachford [28] solved the diffusion-convection and continuity equations numerically in 1962. The authors used the mathematical model to calculate the behavior of two-dimensional laboratory experiments. Unfavorable mobility ratios were used. Finger growth in the mathematical model was initiated by small random permeability variations. The finger development calculated by the mathematical model were less complex than that observed in laboratory experiments. However, the calculated propagation rate of the fingers were in good agreement with experimental observations. A near linear relationship was found between the length of the finger region and PV injected. At the time when this method was presented, number of grids and computing time made it unpractical for reservoir problems.

Several mathematical studies have shown a linear relationship between length of fingered region and injected PV, as long as the transverse dispersion is not extensive [15,22,23,24]. This have been observed for both linear and diverging radial systems. The relationship for finger growth, however, varies between the theories.

A mathematical treatment of viscous fingering analogous to the Buckley-Leverett [30] method for calculating immiscible displacement, was developed by Koval [24]. The method proposed by Koval, gave good predictions of the results of experimental laboratory miscible displacements under conditions where

the growth of viscous fingers were not appreciably affected by transverse dispersion. Predictions by Koval method were in good agreement with experimental data presented by Blackwell et al. [15], Brigham et al. [31], and Handy [32]. It was reported by Claridge [33] that the method worked well for radial data, and good agreement was found by Kyle and Perrine [20] between Koval method and experiments. Not all available data, however, were adequately predicted by Kovals method [22].

2.1.3 Literature overview

The literature available on viscous fingering can be divided into three areas, experimental, analytical and numerical. The literature concerning experimental work involves laboratory core floods at adverse mobility ratios [14]. The analytical work concerns the mathematical description of the inception and modeling of viscous fingering [14,34,35]. Different methods used for scaling fingers to reservoir conditions [24,36] is also part of this area. The last area, concerning numerical work, concerns the use of different simulation techniques in predicting and simulating the physical behavior of the viscous fingers [28,37,38,39,40,41,42].

Replicas of real well patterns, such as five spots, have been used in experimental studies of both viscous fingering and sweep efficiency. An overview of these studies are provided by Stalkup [9]. Some researchers have used X-ray in the observation of finger evolution in slabs of quarried rock [43,44,45,46]. Others have used backlighting in the visual spectrum in observing the displacement of fluids in this layers of packed fine sand or glass beads [11,15,16,18,21,22,25,26,47,48,49,50,51]. The use of computer image processing in studying viscous fingering in corefloods were proposed by Peters et al. in 1987 [52]. The objective of their study was to extract quantitative information from the digital images of viscous fingering in order to get better insight into unstable displacements.

Numerous of the experimental results showing viscous fingering have been obtained by studying two-dimensional fluid displacement between two parallel plates [53,54]. This type of apparatus is named after its inventor and is called a Hele-Shaw cell [55]. The first application of the Hele-Shaw cell in viscous fingering problems were made by Saffman and Taylor [56]. As both the velocity of a fluid in a porous medium and the velocity of a fluid in a Hele-Shaw cell obey Darcy's law, Saffman and Taylor suggested that the behavior of a Hele-Shaw cell could represent flow in a porous medium. Hele-Shaw cells are very suitable in observational studies of flow in porous media due to direct optical access [57]. Since the late 1950s the Hele-Shaw cell have been widely used in studies of viscous fingering.

Pioneers in the study of viscous fingering [11,56] focused on the basic issues of understanding the conditions for onset of fingering. Chuoke et al. [11] proposed that instabilities with wavelengths greater than a critical value propagates at displacement velocities greater than a critical velocity. If the wavelengths are less than the critical wavelength, the growth of viscous fingers are inhibited by surface tension. Capillary number, or a modified version of capillary number, have also been used in describing viscous fingers in linear Hele-Shaw cells [56,58].

Some concerns on the use of Hele-Shaw cells in studies of viscous fingering have been expressed. Due to the heterogeneity of the wettability of the glass surfaces in Hele-Shaw cells, Perkins and Johnston [49] switched to packs of glass beads. Claridge [59] proposed that Hele-Shaw cells are more suitable in miscible displacements than in immiscible displacements. This is due to the absence of capillary dispersive forces in the cell during immiscible displacements. Dispersion in miscible flow, however, can be related to the gap between the glass plates [17].

A substantial amount of theoretical literature have been presented on viscous fingering. However, there is no widely accepted model of the phenomena. Four theoretical areas have been emphasized in recent work. A random walk model of finger growth have been proposed, where viscous fingering is related to diffusion limited aggregation. Another area concern stability analysis of fingering, often in Hele-Shaw cells. Description of displacements at unstable mobility ratios using fractals have also been presented. The last area concern the possibility that viscous fingering may be a chaotic phenomenon in the sense that flow behavior is very sensitive to initial conditions.

Theories based on diffusion limited aggregation and random walk models commonly lacks generality in the solutions. In those approaches one simulation is only the answer for one set of parameters. This is true also for probabilistic models like Monte Carlo simulations [60,61].

Studies on stability analysis have dealt with both immiscible and miscible isothermal displacement processes. The study of immiscible displacements were pioneered by the work of Chuoke et al [11], and followed by Rachford, Hargoort, and Peters and Flock [50,62,63]. These authors all represented the smearing effect due to the capillary transition zone in porous media, by a surface tension term. Several studies [10,14,23,64,65] concerning the instability of miscible processes are based on the same primary assumption when analyzing the perturbed functions. The primary assumption is that the unperturbed solvent profile is at a quasi-steady state. Lee et al. [66] presented a linear perturbation analysis of instability

in miscible displacement processes without the assumption of a quasi-static solvent profile. The hydrodynamic dispersion expressions were considered dependent on velocity. Solutions of the analytical perturbation equations gave the necessary and sufficient conditions for instability in miscible displacements.

Later interest in the Saffman-Taylor problem has led to the recognition that viscous fingering under certain circumstances can be described by fractals [67]. Mandelbrot [68] first introduced the concept of fractals, fractal dimension, in the description of complex geographical curves. The description of fingering patterns by a fractal relationship between the maximum finger length and area swept, was first proposed by van Damme et al in 1986 [67]. Several experiments performed on radial Hele-Shaw cells or radial porous discs using near miscible fluids gave a fractal dimension in the order of 1.6 to 1.7 [47,67,73]. These fractal measurements were all performed on systems of diverging radial flow. Gharbi et al.[74] used imaging techniques to visualize the behavior of several displacement processes. These behaviors were then characterized by fractal models in order to accurately predict their performance.

Chaotic concepts were applied to the description of fingering by Christie and Bond [38]. The proposed idea was to impose a boundary condition with a random distribution about a user specified average value. Using nonlinear miscible displacement models they were able to generate finger patterns numerically. Fanchi et al. [61] used a nonlinear dynamical stability analysis to study the viscous fingering problem. They found that the growth of perturbations from equilibrium is a mechanism for generating local instabilities.

In the numerical work on matching experimental laboratory data, several different techniques have been used including finite-difference simulations [24,28,38,41,42], a method of weighted residuals [39], and random walk models [40]. Most of these techniques were reasonable successful in matching experimental data, which indicates that the numerical simulators are able to mimic the physical phenomena of viscous fingering under some conditions.

While analysis of linear stability provide useful information concerning the early stages of finger growth, it tells little of the subsequent growth of viscous fingers. Thus, investigators of viscous fingering phenomena have relied on numerical solutions of the convection dispersion equation. In the use of finite-difference calculations some form of initial perturbation in permeability or composition proved necessary for generating viscous instabilities [28,38,41,75]. Christie and Bond [38] performed calculations that when compared to the experimental results of Blacwell et al. [15] showed reasonable agreement.

King and Scher [76], DeGregoria [77], and King and Scher [78] used a probabilistic interpretation of the flow equations producing fingering behavior qualitatively similar to observed experiments. The quantitatively agreement with experimental observations, however, is quite poor. Solutions are strongly dependent on the size of the mesh used in the calculations.

Several authors [39,79] have used spectral methods to investigate the growth of fingers. Spectral methods provide very useful information concerning the fluid mechanics of fingers, and have high accuracy. Tan and Homsy [79] have reported calculations showing that after initiation, fingers spread at the tip. This makes the finger tip unstable, causing it to split again. These authors, however, did not compare their calculations to experimental data.

Araktingi and Orr [80] used a particle-tracking computational technique to investigate finger initiation and growth in a heterogeneous porous media. This model used a finite-difference solution of the material balance equation in determining the local fluid velocity field when the distribution of permeability is given. Finger evolution is calculated by following the motion of tracer particles in the velocity field. Dispersion effects are included by random perturbations of particle positions in both transverse and longitudinal directions. Simulation results obtained with the particle-tracking model are in good agreement with experimental data of unstable displacements.

2.1.4 Miscible displacement

Miscible displacements are, in theory, a rather efficient process of enhanced oil recovery. However, due to hydrodynamic instabilities, viscous fingering occur at the displacement front [81]. Such problems reduce the efficiency of miscible displacements.

In miscible displacements there are no active capillary forces. Dispersion, however, play the same role as interfacial tension does in immiscible flows as will be discussed in section 2.1.2. As the effect of interfacial tension is given by the capillary number, the effect of dispersion is given by the Peclet number. The Peclet number is the ratio of viscous to dispersive forces, and was presented by Christiansen and Fanchi [82].

Dispersion in a miscible displacement reduces the instabilities by dampening the growth of viscous fingers. If the dispersive forces were given enough time to act, all miscible processes would in principle be stable. During a miscible flow both spreading splitting of fingers, as will be described in section 2.1.2, occur

during the process. Shielding of fingers, however do not occur at the same rate as observed in immiscible flow [8].

Early literature provide several stability analysis on miscible displacements [10,14,23,29,35,65,66,83]. All studies involve the following steps in analyzing the displacement stability. The first step is to specify an unperturbed mathematical model. Secondly, perturbations are introduced into dependent variables of the model. The resulting equations are then subtracted from the unperturbed mathematical model. This results in the deriving of hydrodynamic equations for the perturbations. These equations may be solved either analytical or numerical, and from these solutions stability conclusions are draw. The displacement is judged to be stable if the perturbations diminish with time, and unstable if the perturbations grow with time.

The perturbation equations are of nonlinear nature, which causes problems. It is therefore customary to linearize them, resulting in a linear stability theory. This linear theory can be used to determine the conditions for onset of instabilities, but not the long term behavior of the unstable displacement.

In 1984, Peters et al. [34] presented a dimensionless stability number for miscible displacements. The critical value for predicting the onset of instabilities is $4\pi^2$. If the stability number exceeds this value, the miscible displacement will be unstable. The dimensionless stability number is presented in Eq. 2.6,

$$\frac{-k\left(\frac{u}{k}\frac{d\mu}{dc}-\frac{d\rho}{dc}g\right)L_x^2L_y^2}{\phi\delta\bar{\mu}D_T\left(L_x^2+L_y^2\right)} \tag{2.6}$$

In unstable miscible displacements the viscous fingering are mildly sensititive to displacement rate, due to the effect of increased dispersion with increasing rate [34].

During an unstable miscible displacement there are three active displacement mechanisms [84]. At first the unstable miscible displacement gradually gives a complete sweep of the area initially contacted by the viscous fingers, the first mechanism. After breakthrough the fingers continue to grow, invading and sweeping areas originally passed by, the second mechanism. At last the transition zones grow laterally due to dispersion, causing a spread across the full width of the model, the third mechanism. Given enough time these three displacement mechanisms will combine to give a 100% displacement efficiency.

2.1.5 Immiscible displacement

During immiscible displacements interfacial tension, and thus capillary pressure, have an effect on the displacement efficiency. Due to capillary trapping, some residual saturation will always be present after an immiscible displacement. Viscous instabilities as a result of an unfavorable mobility ratio, contributes to this residual saturation. The effect of the interfacial tension may be quantified by the capillary number, presented by Eq. 2.7, which is the ratio between viscous and capillary forces.

$$N_c = \frac{\mu u}{\sigma} \tag{2.7}$$

For unstable immiscible flow the interfacial tension may have both a dampening and promoting effect on viscous fingers. The interfacial tension generally works to suppress an increase in surface area, but in the case of an already developed finger, interfacial tension will prevent the development of small perturbations on the finger surface. This results in all the fluid flowing into the already developed finger, promoting it's growth.

As the capillary number increases, the viscous forces will dominate causing the occurrence of instabilities at many scales. Large capillary numbers results in a chaotic system where the fingering dynamics is very complex. Low capillary numbers, however, results in very few or a single finger. The development of these fingers can be described by a process of shielding, spreading and splitting [8].

During the shielding process a finger lying ahead runs faster than those fingers lying behind. This is due to the instability condition. The spreading process is when the interfacial tension acts to spread a dominant finger till it reaches a preferable width. If viscous fingers grow broader than the preferred width, they grow unstable causing splitting at the tip of the finger. For this type of fingering behavior to occur, the interfacial tension should be high enough to allow for the finger tip to become unstable, but low enough to cause spreading.

The purpose of a stability analysis of an immiscible displacement is to predict the onset of instability. The determination of the conditions under which small perturbations of the displacement front will grow into viscous fingers. An ideal analysis would give a universal dimensionless scaling group and the value above which instabilities occur.

Earlier literature have reported several stability analysis of immiscible displacements [11,12,49,56,62,63,86,87,88,89]. Common for all these studies are the reported relevance of the following parameters on the stability analysis, mobility ratio, capillary and gravitational forces, displacement velocity, and permeability and wettability. A combined effect of these parameters, however, were not reported.

In 1981, Peters and Flock [85] derived a dimensionless stability number for immiscible displacements in porous media presented in Eq. 2.8. The critical value for predicting the onset of instabilities were determined to be 13.56.

$$I_{SC} = \frac{(M-1)(v-v_c)\mu_w D^2}{C^* \sigma k_{wor}} \tag{2.8}$$

The critical stability number was derived from a stability theory for a cylindrical system, and can be used to classify the stability of two-phase incompressible displacements in a homogeneous porous media.

In unstable immiscible displacements the viscous fingering is rather sensitive to the displacement rate [85]. As the displacement rate increases, smaller and more numerous viscous fingers are formed.

Unstable immiscible displacements are generally less efficient than unstable miscible displacements. The lower efficiency of immiscible displacements are usually attributed to trapping due to capillary forces. Another reason for the poor efficiency in unstable immiscible displacements was proposed by Peters et al. [84]. As mentioned in section 2.1.6, an unstable miscible displacement undergo three distinct displacement mechanisms, i.e. complete sweep of initial fingers, sweep of areas originally passed by, and spreading across the full model due to dispersion. During flow visualization experiments, it was observed that an unstable immiscible displacement, however, undergoes only the first mechanism. Following breakthrough a steady-state situation occurs in which newly injected fluid is fed into the already existing fingers. This immiscible displacement experiment was performed at zero initial water saturation. The presence of an initial water saturation enhances the stability of the displacement by promoting spreading of the injected fluid.

2.2 Polymer flooding

As mentioned in the introduction, some reservoir are specially suited for polymer flooding containing high viscous oil or large degrees of heterogeneity, and the increase in recovery efficiency may justify the expenses of a polymer flood. Several polymers have been considered for polymer flooding, however the most commonly used are polyacrylamides and polysaccharides (biopolymers).

Polyacrylamides are polymers where the monomeric unit is the acrylamide molecule. When used in polymerflooding, the polyacrylamide has usually undergone partial hydrolysis, hence the name HPAM. The normal degree of hydrolysis is about 30-35%, which has been chosen to optimize properties such as viscosity, retention and water solubility. Too large degree of hydrolysis will render the polymer too sensitive to salinity and hardness [90].

The HPAM polymer molecules are large and their structures randomly coiled, as illustrated in Fig 2.4, giving good viscosifying effect in water. The elastic behavior of the polymer structure makes it subject to degradation by high shear rates. The molecular weight of HPAM is about 5 million, and the size about 0.3 µm .

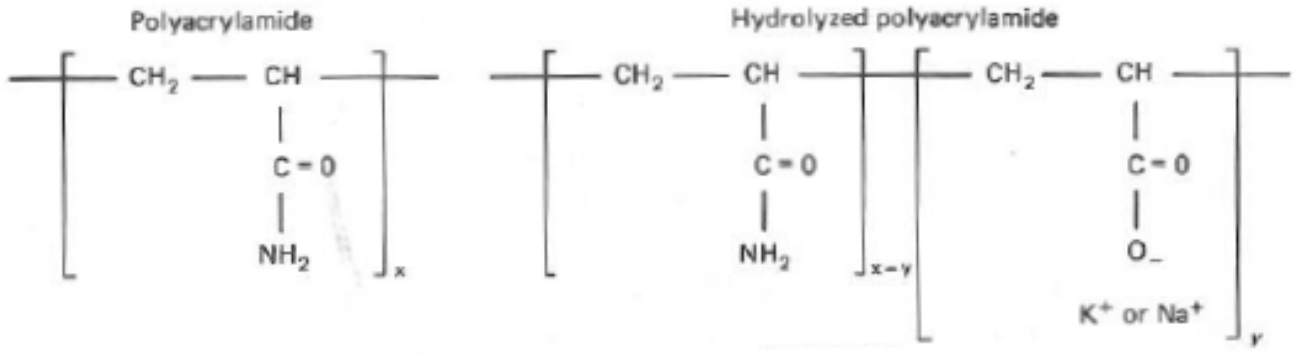

Figure 2.4: Molecular structure of partially hydrolyzed polyacrylamide [69].

The HPAM polymer is exhibits permanent permeability reduction, and is relatively resistant to bacterial attacks.

Polysaccharides are formed during a bacterial fermentation process by polymerization of saccharide molecules. The polymers are susceptible to bacterial attack in regions of the reservoir where the temperature is low. This biological degradation may be prevented by adding a biocide, like formaldehyde [91], to the injection brine. The polysaccharide Xanthan is temperature stable in the range $70\,^{\circ}C$ to above $90\,^{\circ}C$.

The structure of the biopolymer molecules is helical and rod-like, as illustrated in Fig 2.5, yielding high viscosity in water. The molecular structure is more rigid than that of HPAM, because it is highly branched. Polysaccharides have a molecular weight of about 2 million, and size about $0.4\,\mu m$.

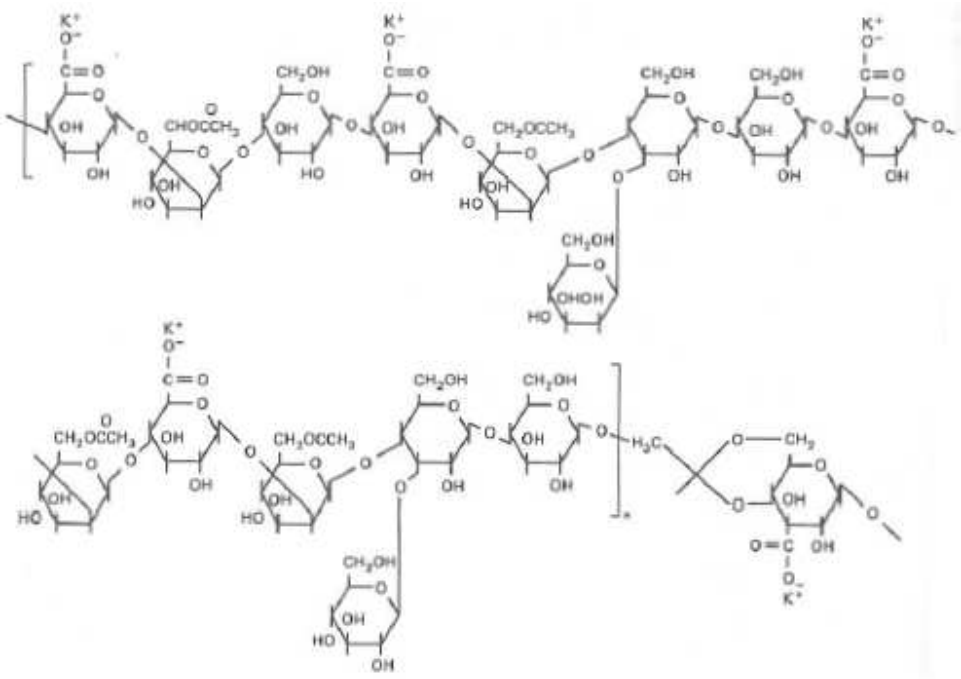

Figure 2.5: Molecular structure of polysaccharide (biopolymer) [69].

Properties of polysaccharides are insensitive to both salinity and hardness. Polysaccharides does not exhibit permanent permeability reduction.

Water containing polymer molecules have certain properties regarding the flow and the mobility of the polymer solution. The following properties are briefly discussed in this section: viscosity relations, polymer retention, permeability reduction and inaccessible pore volume.

2.2.1 Viscosity dependence on concentration:

The relationship between viscosity and polymer concentration is usually modeled by the Flory-Huggins Eq. 2.9 [92],

$$\mu_1' = \mu_1\left[1 + a_1 C_{41} + a_2 C_{41}^2 + a_3 C_{41}^3 + ... +\right] \tag{2.9}$$

where μ_1' is the viscosity of the polymer solution, μ_1 is the viscosity of the brine, C_{41} is the concentration of polymer, and a_1, a_2, and so forth are constants. The linear term of the Flory-Huggins equation accounts for the dilute range. In this range the polymer molecules act independently without entanglements. For most uses the equation may be truncated after the cubic term. Fig. 2.6 illustrates the viscosity dependence on polymer concentration for Xanthan.

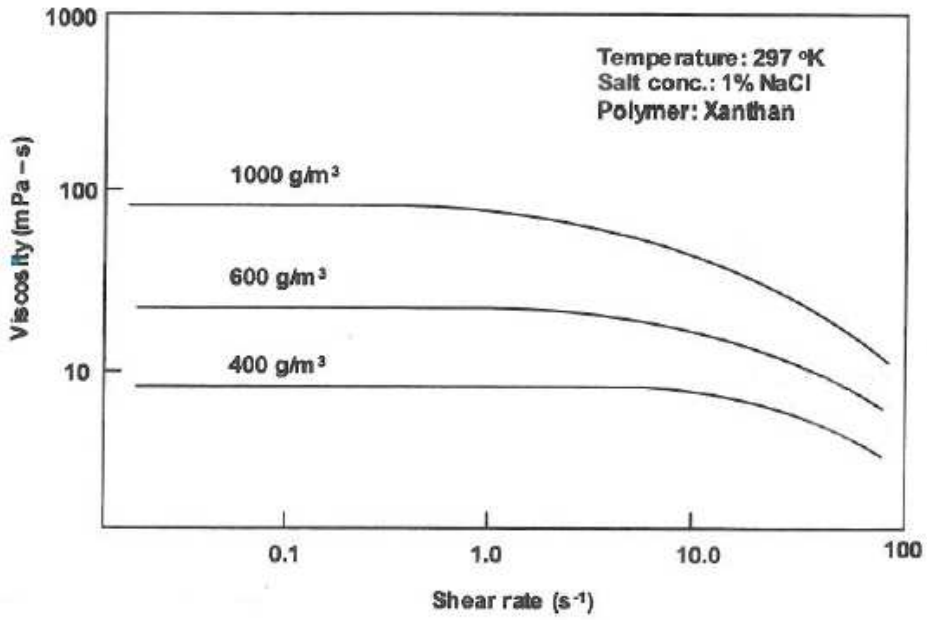

Figure 2.6: Solution viscosity of Xanthan versus shear rate, at three polymer concentrations [70].

2.2.2 Viscosity dependence on shear rate:

Newtonian fluids have shear-independent viscosity, while non-Newtonian fluids, such as polymers, have shear-dependent viscosity. Like several other non-Newtonian fluids, polymers have Newtonian regimes for low and very high shear-rates, and a pseudoplastic regime in between. Polymer viscosity decreases with

increasing shear-rate, making the polymer shear-thinning. This behavior is due to the uncoiling of polymer chains as they are elongated in shear-flow.

A power-law model may be used to describe the relationship between polymer viscosity and shear-rate [69] as presented by Eq. 2.10,

$$\mu_1^{'} = K_{pl}(\dot{\gamma})^{n_{pl}-1} \tag{2.10}$$

where K_{pl} is the power-law coefficient, n_{pl} is the power-law exponent, and $\dot{\gamma}$ is the effective shear-rate. For Newtonian fluids, $n_{pl} = 1$ and K_{pl} becomes the fluid viscosity. For shear-thinning fluids, $0 < n_{pl} < 1$. The power-law only applies over a limited range of shear-rates. For low shear-rates the viscosity is constant at μ_1^0, and above a critical shear-rate the viscosity becomes constant at μ_1^∞.

Overall behavior of a polymer solution in a wide range of shear-rates may be modeled by the Meter Eq. 2.11 [93],

$$\mu_1^{'} = \mu_1^\infty + \frac{\mu_1^0 - \mu_1^\infty}{1 + \left(\frac{\dot{\gamma}}{\dot{\gamma}_{1/2}}\right)^{n_M - 1}} \tag{2.11}$$

where $\dot{\gamma}_{1/2}$ is the shear-rate when $\mu_1^{'}$ is the average between μ_1^0 and μ_1^∞, and n_M is an empirical constant.

2.2.3 Polymer retention:

When flowing through permeable media, polymers experience retention due to adsorption to solid surfaces and trapping within small pores [69]. Retention of polymers slows down the polymer velocity and drain the polymer slug. Loss of polymers from the solution may reduce the mobility control effect. Polymer retention depends on type and molecular weight of the polymer, rock composition, brine salinity and hardness, temperature, and flow-rate.

A Langmuir-type isotherm is normally used to describe polymer adsorption, see Eq. 2.12.

$$\hat{C}_4 = \frac{a_4(C_{41})}{1 + b_4 C_{41}} \tag{2.12}$$

Where $\hat{C}_4$ and C_{41} are the polymer concentration in the aqueous phase and on the rock surface respectively. The ratio, a_4/b_4, determines the plateau value of the adsorption isotherm, and b_4 the curvature, as illustrated by Fig 2.7.

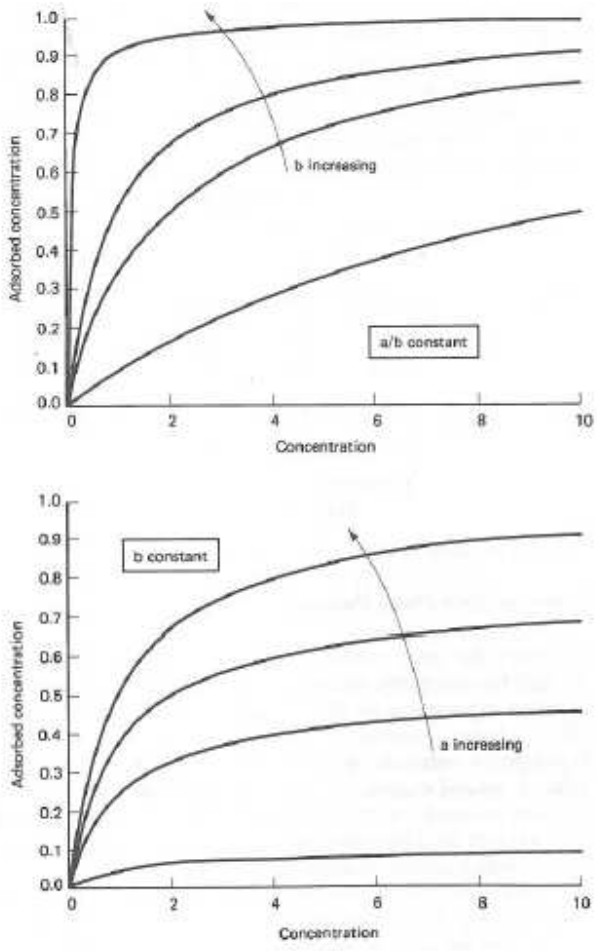

Figure 2.7: Typical shapes of Langmuir isotherms [69].

2.2.4 Permeability reduction:

As a result of polymer flooding, both mobility of displacing fluid and the effective permeability of the porous medium is reduced. The effect of permeability reduction is assumed to be irreversible. The permeability reduction is measured by a permeability reduction factor, R_k, defined as the ratio of effective permeability of water to the effective permeability of polymer.

There are two other measures in permeable media flow [94], the resistance factor and the residual resistance factor. The resistance factor, R_F, describes the change in mobility due both to increased viscosity and reduced permeability and presented by Eq. 2.13,

$$R_F = \frac{\lambda_w}{\lambda_p} = R_k \frac{\mu_p}{\mu_w} \tag{2.13}$$

The residual resistance factor, R_{RF}, which describes the lasting effect of permeability reduction as the polymer solution has passed through the medium, is presented by Eq. 2.14,

$$R_{RF} = \frac{\lambda_w}{\lambda_{w,a}} \tag{2.14}$$

where λ_w is the mobility of water prior to the polymer flood, and $\lambda_{w,a}$ is the mobility of water after a polymer flood.

2.2.5 Inaccessible pore volume:

Due to the large size of the polymer molecules, some portion of the pore space will be too small for the polymers to enter. As a result of this uninvaded or inaccessible pore volume, the flow of polymer is accelerated [69].

Inaccessible pore volume may also be explained based on a wall exclusion effect. The polymer molecules aggregate in the center of narrow channels, such that the polymer solution near the pore wall has lower viscosity than the polymer solution in the center. This results in an apparent fluid slip [95].

Inaccessible pore volume is dependent on the molecular weight of the polymer, porosity, permeability, and distribution of pore size in the permeable medium.

2.3 Observation of viscous fingering

van Meurs [86] used a glass model filled with finely powdered glass of a specific grain size representing a porous structure. If the powdered glass pack is saturated with oil having the same refracting index as the glass, the model becomes completely transparent. A linear water drive displacement was performed in a homogeneous formation. For unfavorable viscosity ratio, water invasion occurs in the form of viscous fingers as seen in Fig. 2.8.

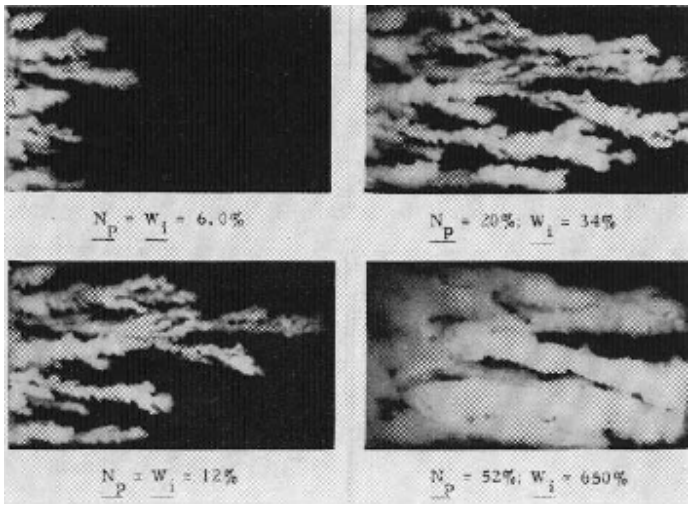

Figure 2.8: Linear water-drive process in a homogeneous formation. The viscosity ratio, between water and oil, is 80 [86].

Chuoke et al. [11] used two preferentially oil-wet glass plates to provide a uniform flow channel for displacing oil with water-glycerin solutions. The glass plates were spaced 1 mm apart. Fig. 2.9 shows a time sequence of photographs from an experiment with injection rate about twice the critical value of U_c = 198.72 m/day. Viscous fingers were clearly seen in the photographs. There were, however, dissimilarity between the form of the oil fingers and the water fingers. Fig. 2.10 shows three photographs of experiments carried out at different injection rates. An increase in injection rate results in an increase in number of fingers.

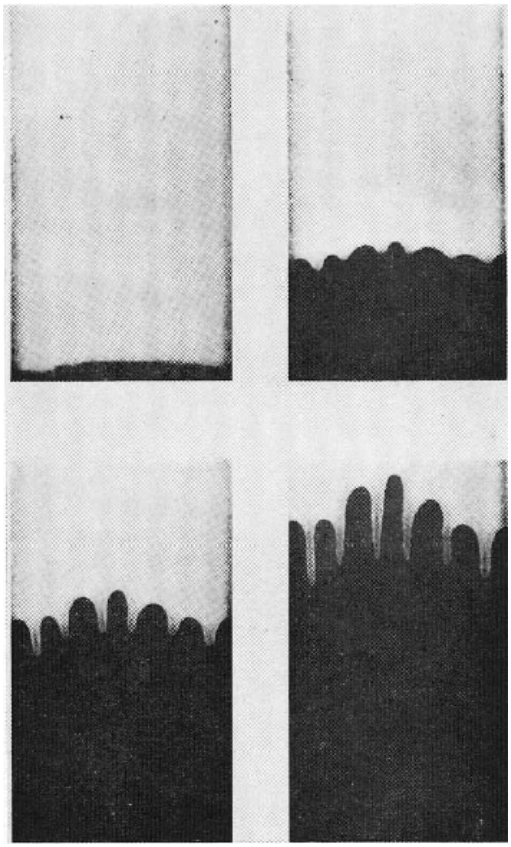

Figure 2.9: Displacement of oil by a water-glycerin solution at an injection rate of U = 354.37 m/day, at four different times. The viscosity is 0.552 mPa*s and 1.39 mPa*s for water-glycerin and oil respectively [11].

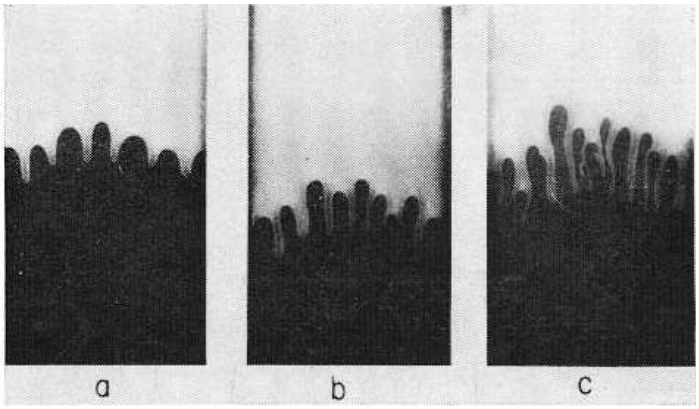

Figure 2.10: Displacement of oil by a water-glycerin solution at an injection rates (a) U = 354.37 m/day, (b) U = 751.94 m/day, and (c) U = 1434.75 m/day. The viscosity is 0.552 mPa*s and 1.39 mPa*s for water-glycerin and oil respectively [11].

Chuoke et al. [11] also used a transparent model technique to illustrate that smaller fingers are observed at higher oil viscosities, see Fig. 2.11 a) and b). Comparing Fig. 2.11 b) and c), smaller fingers are observed with a lower bulk interfacial tension. The transparent model technique was used to visualize production from oil-saturated packs containing connate water. The oil was displaced by an aqueous solution of ammonium iodide. Finger formation was observed, see Fig. 2.12.

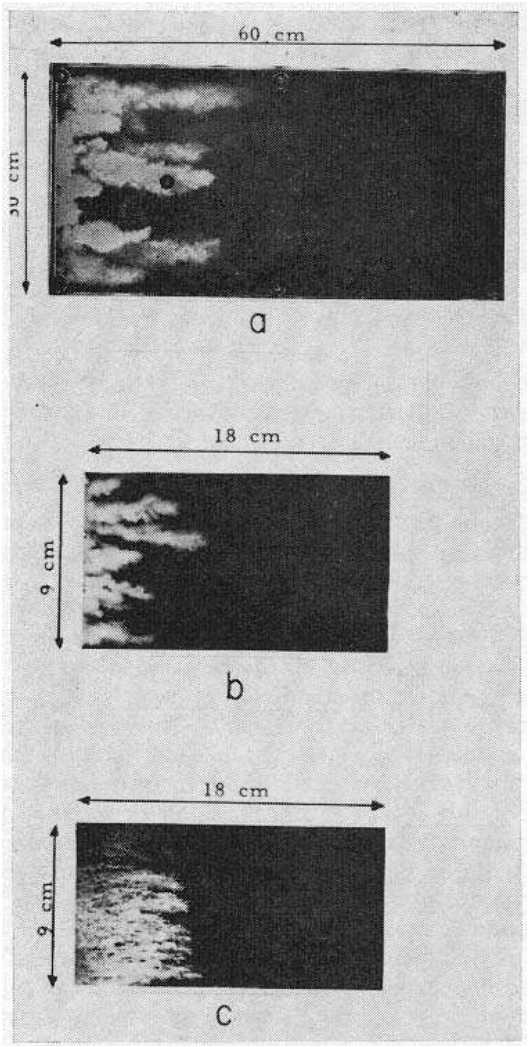

Figure 2.11: Three photographs showing the effect of oil viscosity and interfacial tension on finger size [11]. The displacing water appears white on the photograph. (a) Viscosity of water and oil is 1 mPa*s and 9.45 mPa*s, respectively. The interfacial tension is 42 mN/m. (b) Viscosity of water and oil is 1 mPa*s and 66 mPa*s, respectively. The interfacial tension is 48 mN/m. (c) Viscosity of water and oil is 1 mPa*s and 202 mPa*s, respectively. The interfacial tension is 3.5 mN/m.

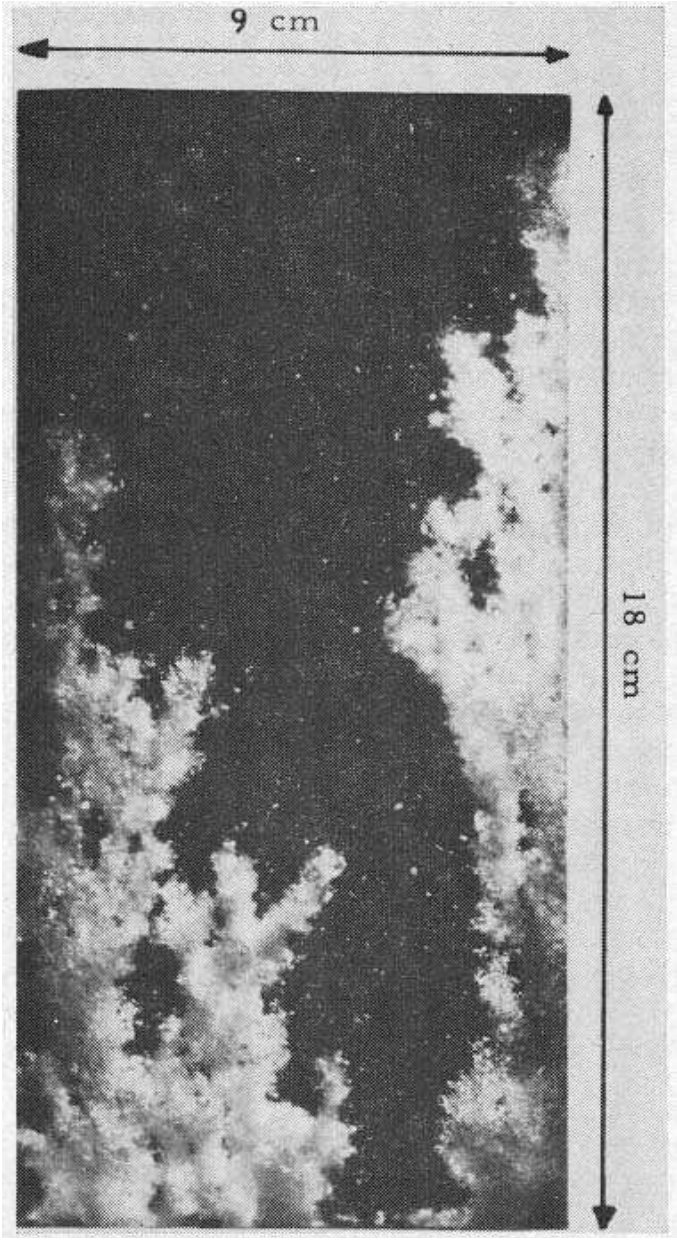

Figure 2.12: Formation of fingers in an oil-bearing porous medium with 0.15 PV of connate water. The displacing water appears white on the photograph. The viscosities of oil and water are 200 mPa*s and 1 mPa*s, respectively. The interfacial tension is 25 mN/m [11].

Blackwell et al. [15] conducted an experimental investigation of miscible displacement of oil by solvent using Lucite models. The models were uniformly packed with sand. Channeling of the less viscous solvent was observed in all experiments with fluids of equal densities. Fig. 2.13 and 2.14 show typical channeling for viscosity ratios of 20 and 383, respectively.

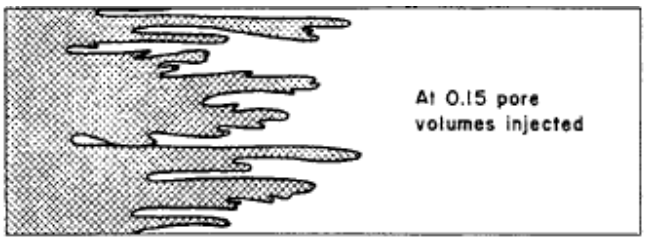

Figure 2.13: Displacement front for a mobility ratio of 20 [15].

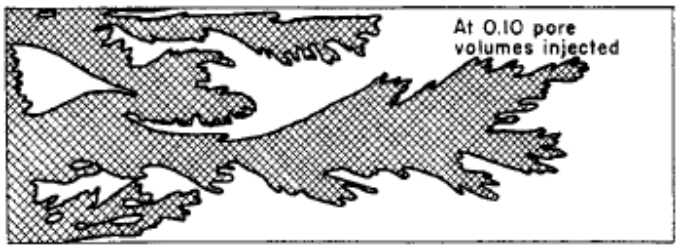

Figure 2.14: Displacement front for a mobility ratio of 383 [15].

Benham and Olson [18] used an open Hele-Shaw model make a series of miscible slug runs in order to determine the nature and degree of fingering observed during a miscible slug displacement. A series of four frames taken from a miscible slug run in an open Hele-Shaw model is shown in Fig. 2.15.

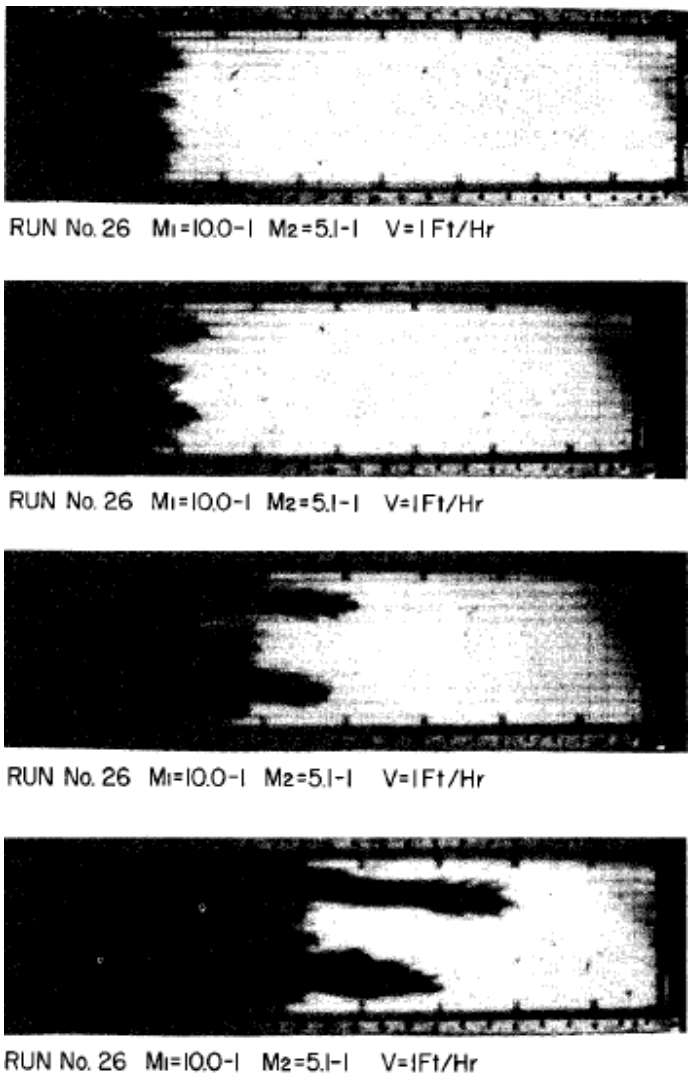

Figure 2.15: Formation of fingers for a miscible slug in an open model. The mobility ratio between the displaced fluid and the slug was 10, and the mobility ratio between slug and the displacing fluid was 5 [18].

Perkins and Johnston [49] studied viscous fingering during immiscible displacements in linear models. Experiments were performed in large Hele-Shaw models where the spacing between the glass plates was 0.000787 m. At relatively high injection rates and high mobility ratios, formation of viscous fingering was observed as illustrated in Fig 2.16. Experiments were also performed in plate glass models packed with glass beads. In the experiments where oil was displaced by water at an unfavorable mobility ratio, distinct fingers were observed as shown in Fig 2.17.

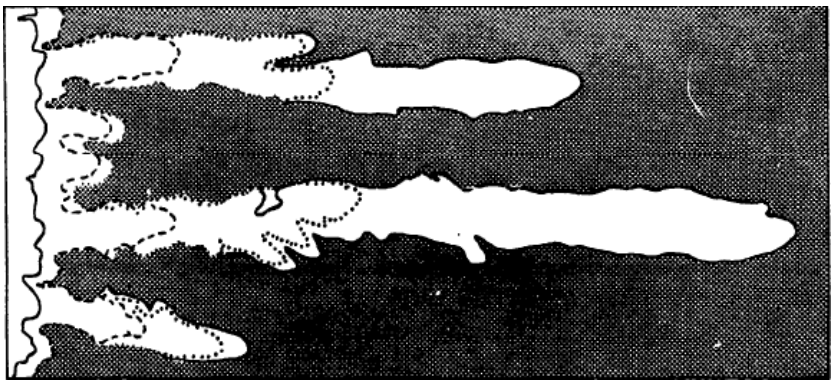

Figure 2.16: Formation of viscous fingers in a Hele-Shaw cell at different stages during an immiscible displacement. The viscosity ratio is 146 [49].

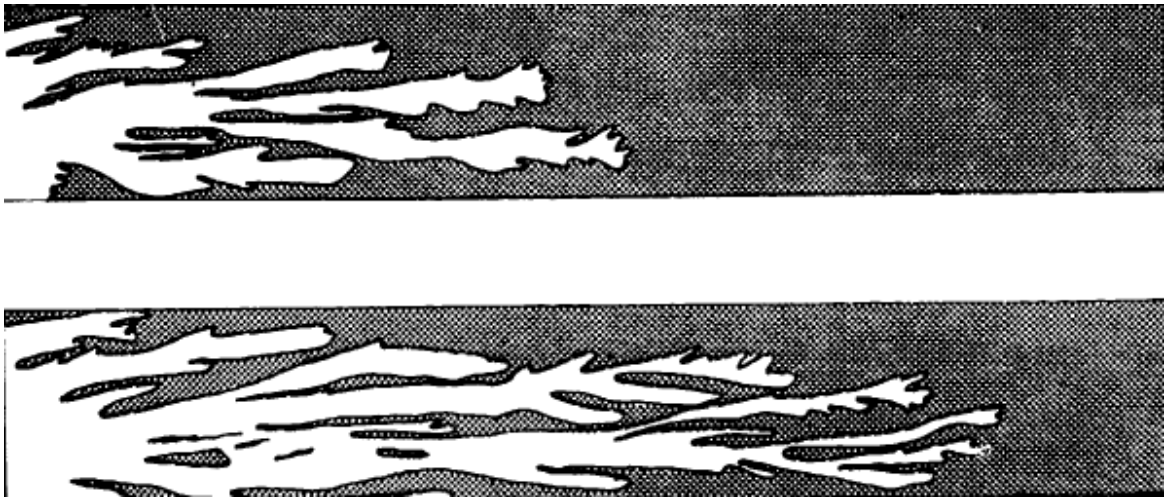

Figure 2.17: Formation of viscous fingers in a in a glass plate model packed with glass beads at two different stages during an immiscible displacement. The viscosity ratio is 146, and the initial water saturation is zero [49].

Peters and Flock [85] performed constant rate water floods on horizontal sand packs of 80 – 120 mesh Ottawa sand. During each experimental run, 18 cross sections of the cores were photographed. Fig 2.18 through 2.22 shows four out of the 18 cross sections for five different experiments. The ratio of finger wavelength to core diameter is increasing. All photographs show patterns of viscous fingers. Figure 2.18 shows numerous small fingers as the ratio between finger wavelength and core diameter is small. As this ratio increases, fewer and larger fingers are observed as in Fig 2.19 and 2.20. When the ratio between finger wavelength and core diameter is sufficiently large, only one finger is observed in the core, as in Fig 2.21 and 2.22.

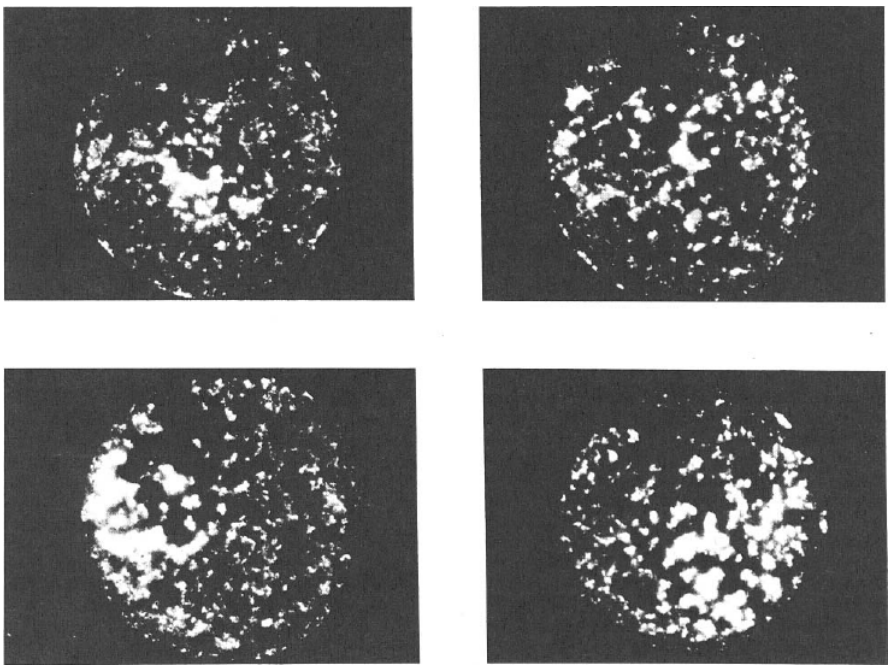

Figure 2.18: Pattern for oil-wet fingering where the ratio between finger wavelength and core diameter is 0.067 [85].

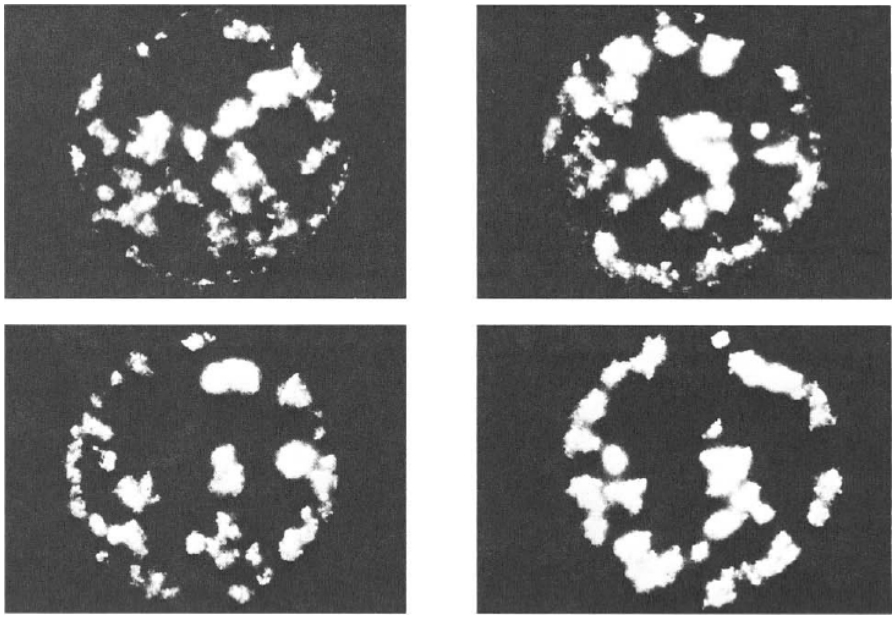

Figure 2.19: Pattern for oil-wet fingering where the ratio between finger wavelength and core diameter is 0.107 [85].

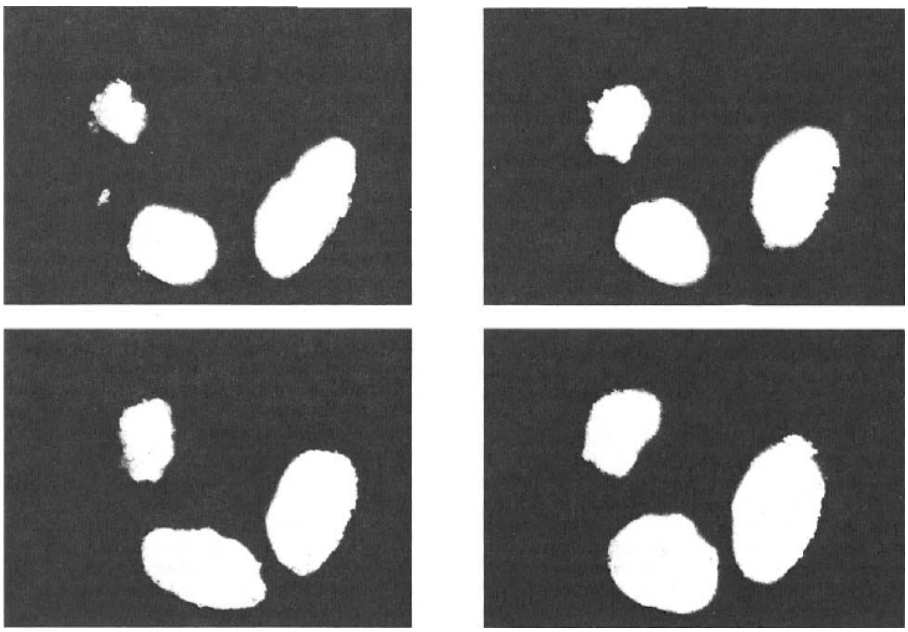

Figure 2.20: Pattern for oil-wet fingering where the ratio between finger wavelength and core diameter is 0.238 [85].

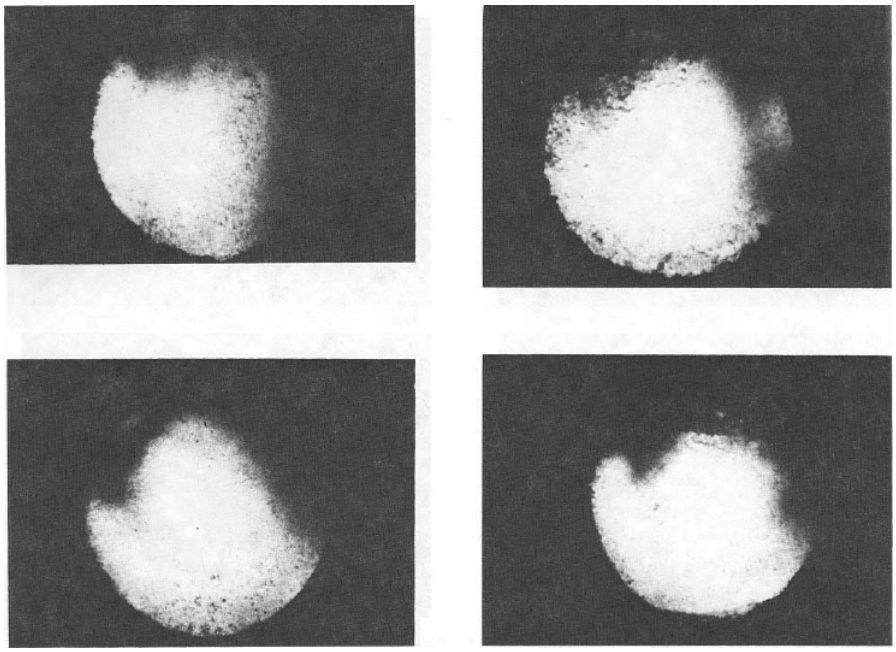

Figure 2.21: Pattern for water-wet fingering where the ratio between finger wavelength and core diameter is 0.338 [85].

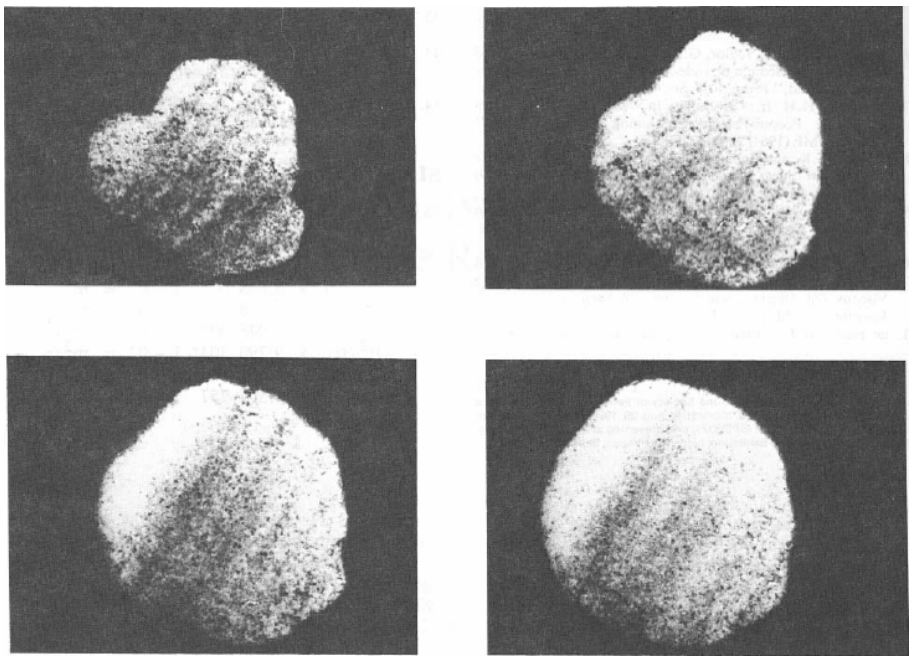

Figure 2.22: Pattern for oil-wet fingering where the ratio between finger wavelength and core diameter is 0.917 [85].

Peters and Hardham [84] used x-ray computed tomography to image core floods in time and space. Fig. 2.23 through 2.25 shows images from an unstable miscible displacement at three different time steps. Each image shows the saturation of the displacing fluid in a vertical, longitudinal slice. All images show a disorderly saturation profile where viscous fingers have penetrated the displaced fluid in an irregular manner.

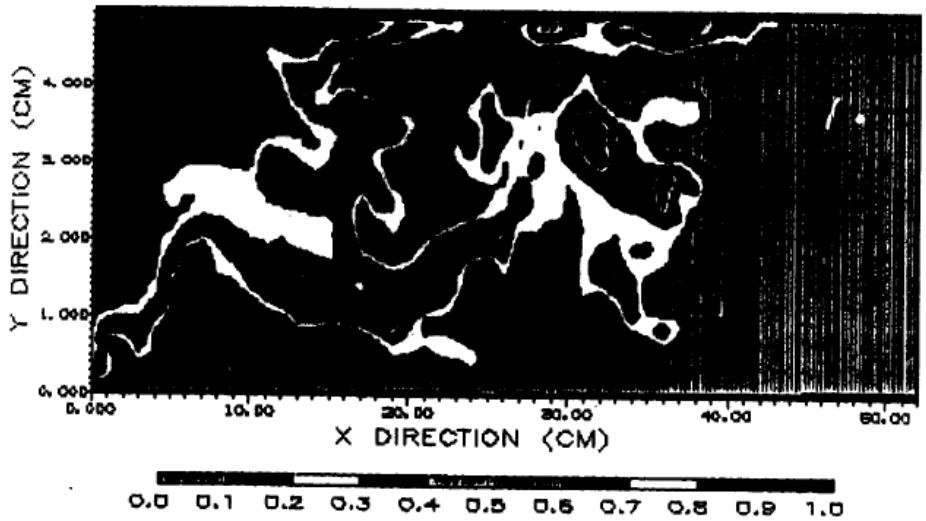

Figure 2.23: Image of saturation distribution in miscible displacement at 0.25 PV injected [84].

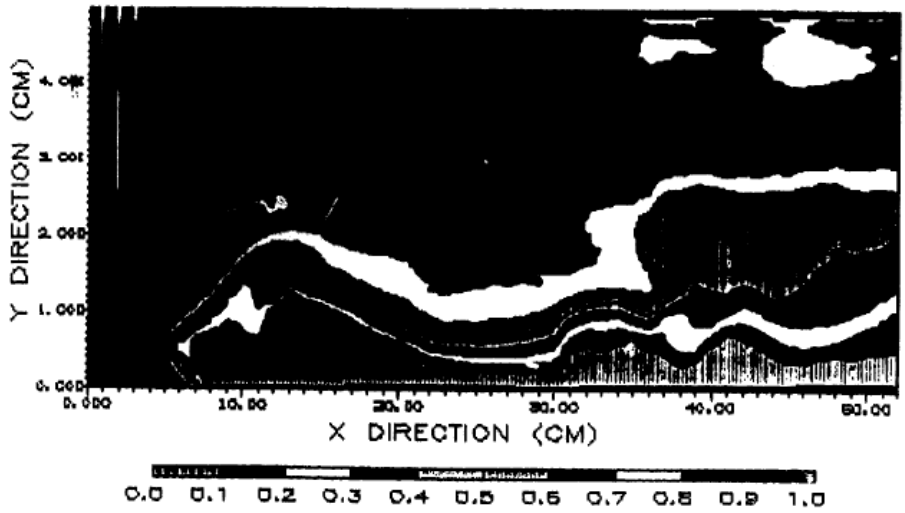

Figure 2.24: Image of saturation distribution in miscible displacement at 1.0 PV injected [84].

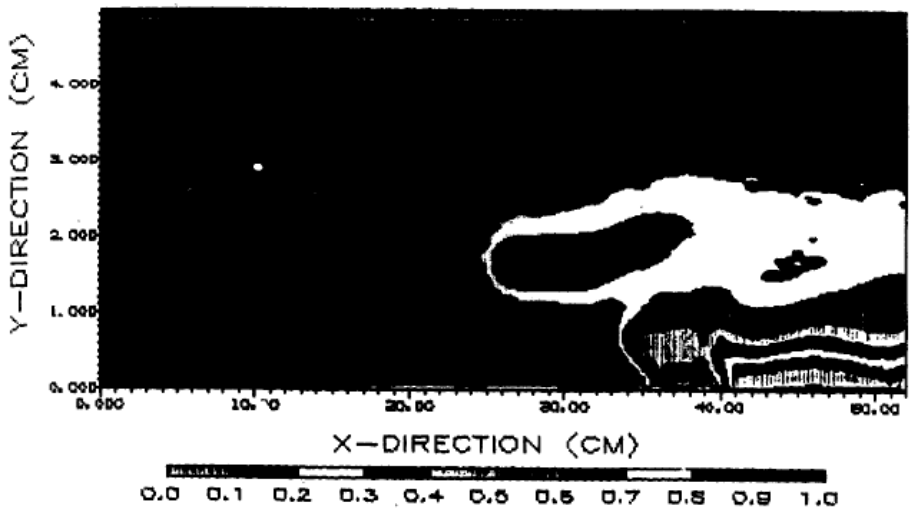

Figure 2.25: Image of saturation distribution in miscible displacement at 3.0 PV injected [84].

Fig. 2.26 through 2.28 shows images from an unstable immiscible displacement at three different time steps. Each image shows the saturation of the displacing fluid in a vertical, longitudinal slice. All images show a more disorderly saturation profile than in the miscible displacement, where viscous fingers have penetrated the displaced fluid in an irregular manner.

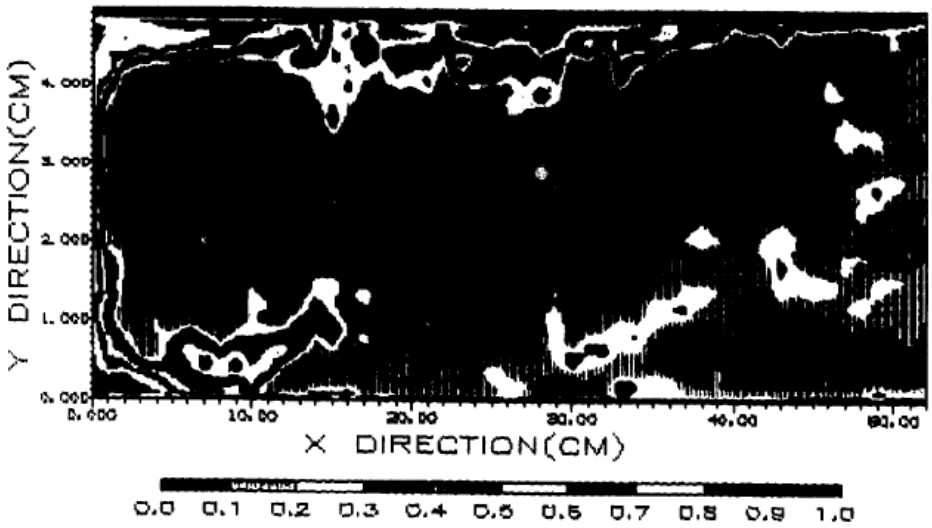

Figure 2.26: Image of saturation distribution in the immiscible displacement at 0.25 PV injected [84].

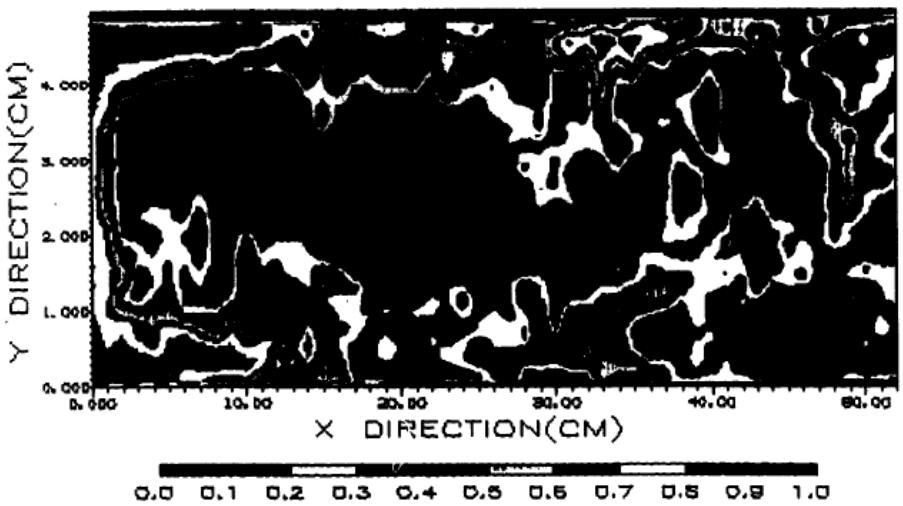

Figure 2.27: Image of saturation distribution in the immiscible displacement at 1.0 PV injected [84].

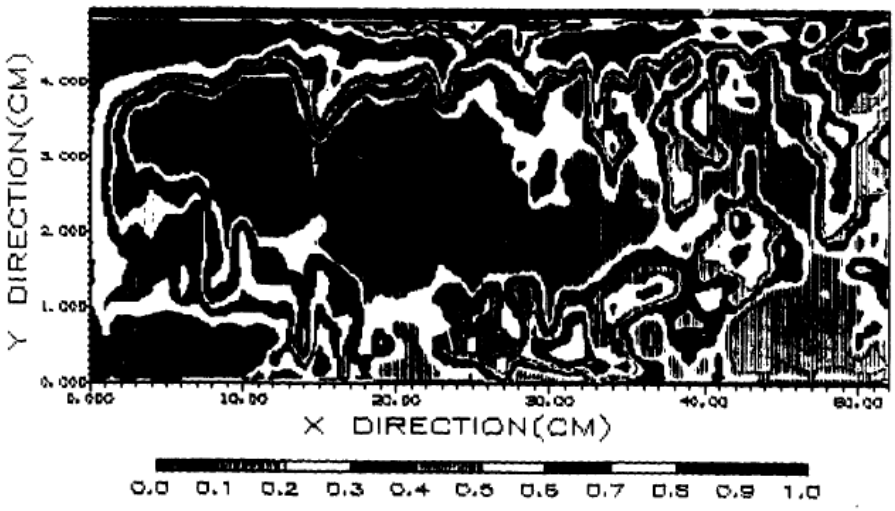

Figure 2.28: Image of saturation distribution in the immiscible displacement at 3.0 PV injected [84].

Fanchi and Christiansen [96] used a radial Hele-Shaw cell for studying miscible displacements. Several tests were performed with n-decane displacing Gloria oil at a viscosity ratio of about 90.5. Fig. 2.29 illustrates the development of viscous fingers during the displacement of Gloria oil by n-decane.

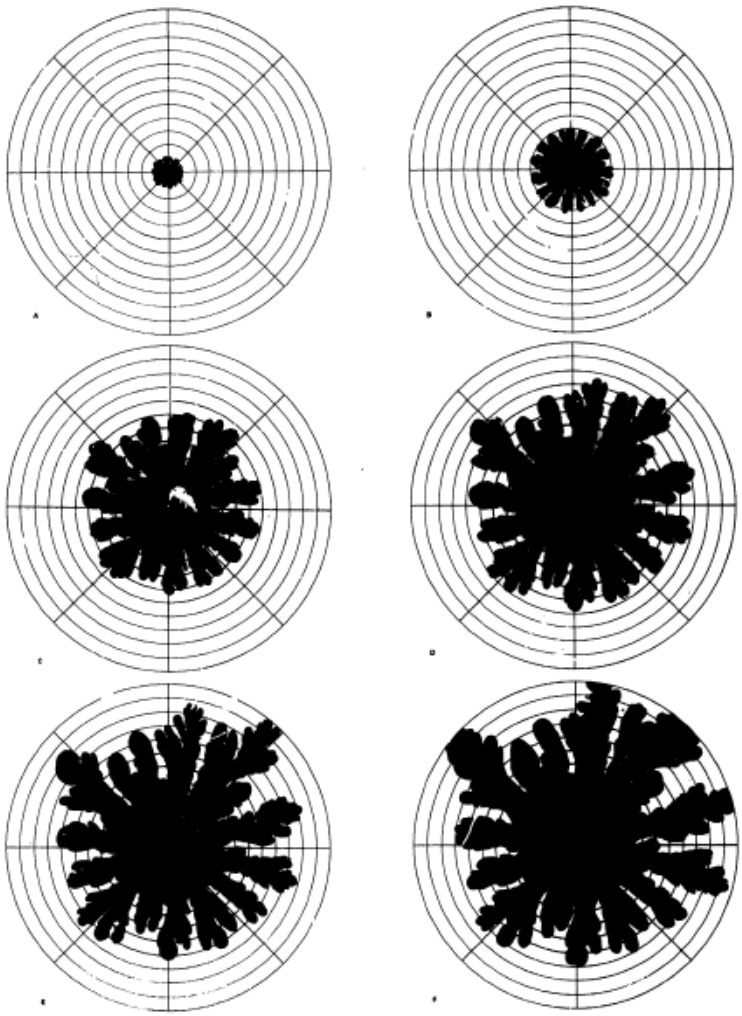

Figure 2.29: The development of viscous fingers for the miscible displacement of Gloria oil by n-decane, in a radial Hele-Shaw cell. The viscosity ratio is about 90.5 [96].

Brock and Orr [97] used a glass model filled with glass beads in visualizing viscous fingering in both homogeneous and heterogeneous systems. For both systems the displacements were performed at three different mobility ratios and flow rates. As illustrated by Fig. 2.30 and 2.31 the viscous fingers in the homogeneous model were sensitive to mobility ratio, but not to flow rate.

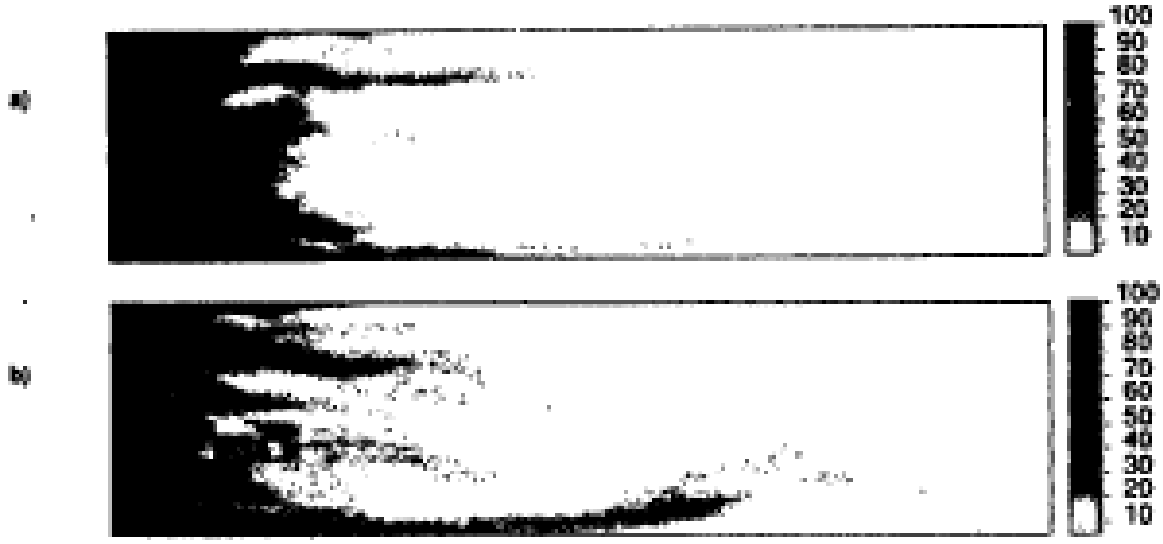

Figure 2.30: Comparison of viscous fingers at 0.15 PV injected in a homogeneous model with a mobility ratio of a) 40 and b) 80. The flow rate is 0.004323 m^3/day [97].

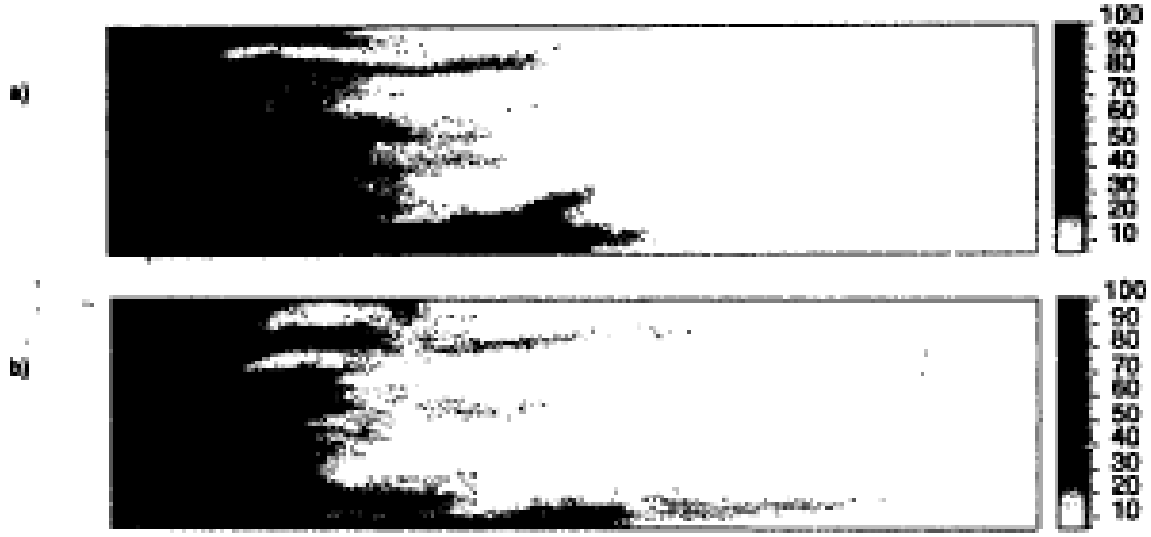

Figure 2.31: Comparison of viscous fingers at 0.20 PV injected in a homogeneous model with a flow rate of a) 0.012969 m^3/day and b) 0.004323 m^3/day. The mobility ratio is 40 [97].

Majors et al. [98] introduced a quantitative nuclear magnetic resonance imaging (NMRI) technique in studying multiple fluid systems. The authors used distilled water and a significantly more viscous silicon oil. The experiments were performed on a relatively homogeneous Berea sandstone core. Fig. 2.32 shows the NMR images of the distribution of the displacing fluid (distilled water) at 0.18 and 0.39 PV injected.

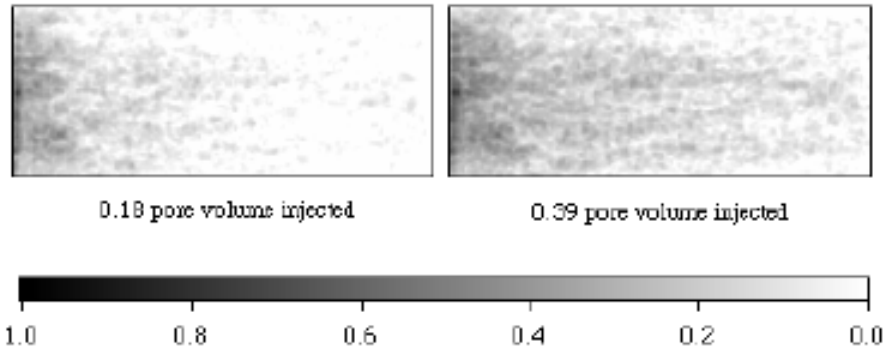

Figure 2.32: Projection spin-echo NMR images of the distribution of displacing fluid for an immiscible displacement in a Berea sandstone core. The images are at 0.18 and 0.39 PV injected, and the mobility ratio is 105 [98].

Gharbi et al. [74] used a model comprised of clear acrylic plates filled with glass beads, to visualize displacement experiments in two dimensions. The effects of mobility ratio and gravity number on unstable miscible displacements were investigated. Fig 2.33 and 2.34 illustrates the unstable displacements at viscosity ratio of 100 and 50 respectively.

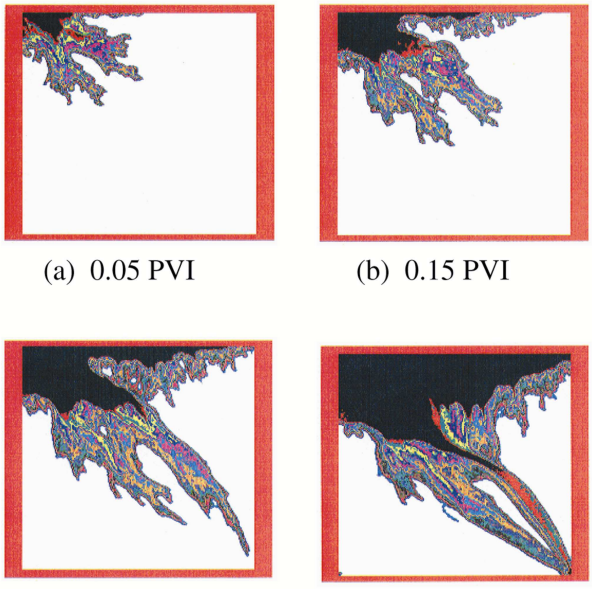

Figure 2.33: Unstable miscible displacement at 0.05, 0.15, 0.20 and 0.40 PV injected. The viscosity ratio is 100 and the gravity number is 0.00641 [74].

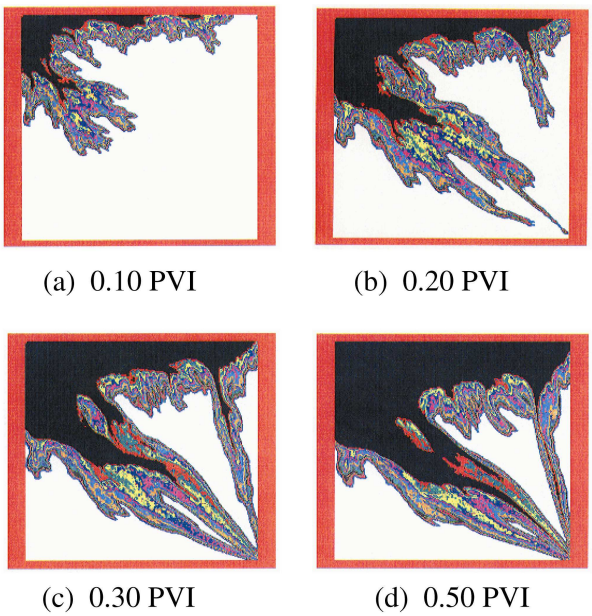

(a) 0.10 PVI (b) 0.20 PVI

(c) 0.30 PVI (d) 0.50 PVI

Figure 2.34: Unstable miscible displacement at 0.10, 0.20, 0.30 and 0.50 PV injected. The viscosity ratio is 50 and the gravity number is 0.0077 [74].

3 UTCHEM – chemical simulator

The simulations in this thesis are run with the UTCHEM simulator. Which is a three-dimensional chemical flooding simulator, developed at the University of Texas at Austin. In this section a general description of the simulator is given, together with a more detailed description of the polymer option.

3.1 General

UTCHEM is a three-dimensional, multi component, multiphase, and compositional model for chemical flooding processes [99]. The simulator accounts for complex phase behavior, properties of heterogeneous porous media, and physical and chemical transformations. Advanced concepts in high-order numerical accuracy are used, together with dispersion control, and vector and parallel processing.

The flow equations in UTCHEM are solved using a block-centered finite-difference scheme. It is an Implicit Pressure and Explicit Concentration (IPEC) solution method. Concentrations and saturations are solved in a flash routine. Balance equations include an energy balance equation, including heat flow between reservoir and under- and over-burden rocks, explicitly solved for reservoir temperature, and mass conservation equations, determining the pressure for up to four fluid phases.

The UTCHEM simulator is unique in that it allows for flow and transport of multiple phases containing multiple species and multiple biological and chemical reactions. Flow and mass-transport equations, in UTCHEM, may be solved for any number of chemical components. Such chemical components include water, organic contaminants, surfactant, polymer, alcohol, etc., and are specified by the user. The chemical components may form up to four fluid phases, aqueous, oleic, microemulsion and gas. A number of solid minerals may form as well, dependent overall composition.

The UTCHEM simulator allows for variation in capillary pressure and relative permeability throughout the porous medium.

Limitations in the usage of the UTCHEM simulator lie in the number of grid blocks. Due to small time step restrictions and insufficient memory, the amount of grid blocks of, for example, a realistic polymer flood is limited to about 100 000 [100]. Other limitations are related to the description of hydrocarbon-phase properties. In UTCHEM the hydrocarbon-phase generally consists of a single component, and oil and water viscosities and compressibilities are given as constants.

In this thesis all models contain a total amount of 22 500 grid blocks. Due to the size of the models, problems occurred in post processing of simulation results. The software accompanying UTCHEM, UTSURF, proved to be inadequate when processing files of such magnitude. An Excel spread-sheet application was developed in order to visualize saturation data. The amount of saturation data made it necessary to use the 2007 version of Excel.

3.2 Polymer option

When modeling a polymer flood in UTCHEM, several polymer properties have to be described in the model. These polymer properties include the viscosity dependence on concentration and shear-rate, polymer retention, permeability reduction, and inaccessible pore volume. This section contain brief descriptions of how these properties are modeled in UTCHEM.

3.2.1 Viscosity dependence on concentration:

The viscosity of a polymer solution is dependent on both polymer concentration and salinity. UTCHEM uses a modified Flory-Huggins equation, which in addition accounts for variation in salinity as presented in Eq. 3.1,

$$\mu_1^{'} = \mu_1\left[1 + (A_{P1}C_{41} + A_{P2}C_{41}^2 + A_{P3}C_{41}^3)C_{SEP}^{Sp}\right] \tag{3.1}$$

where A_{P1}, A_{P2}, and A_{P3} are parameters for calculating polymer viscosity at zero shear rate as a function of both polymer and electrolyte concentrations. C_{SEP} is the effective salinity for polymer [101], and Sp is the slope of viscosity versus effective salinity on a log-log plot.

3.2.2 Viscosity dependence on shear rate:

The overall behavior of a polymer solution in a wide range of shear-rates may be modeled by the Meter Eq. 3.2 [93],

$$\mu_1^{'} = \mu_1^{\infty} + \frac{\mu_1^0 - \mu_1^{\infty}}{1 + \left(\frac{\dot{\gamma}}{\dot{\gamma}_{1/2}}\right)^{n_M - 1}} \tag{3.2}$$

where $\dot{\gamma}_{1/2}$ is the shear-rate when μ_l' is the average between μ_l^0 and μ_l^∞, and n_M is an empirical constant. UTCHEM uses the Meter equation. When applied to a permeable media the shear-rate is an equivalent shear-rate $\dot{\gamma}_{eq}$, and μ_l' is normally called the apparent viscosity. In such a case the shear-rate is modeled by a modified Blaze-Kozeny capillary bundle equation for multiphase flow, Eq. 3.3, [102,103],

$$\dot{\gamma}_{eq} = \frac{\dot{\gamma}_c |u_l|}{\sqrt{\bar{k} k_{rl} \phi S_l}} \tag{3.3}$$

Where $\dot{\gamma}_c$ is $3.97C\ \sec^{-1}$, and C is a shear-rate coefficient accounting for non-ideal effects [103,104]. The average permeability, $\bar{k}$, is given by Eq. 3.4,

$$\bar{k} = \left[\frac{1}{k_x} \left(\frac{u_{xl}}{u_l} \right)^2 + \frac{1}{k_y} \left(\frac{u_{yl}}{u_l} \right)^2 + \frac{1}{k_z} \left(\frac{u_{zl}}{u_l} \right)^2 \right]^{-1} \tag{3.4}$$

3.2.3 Polymer retention:

A Langmuir-type isotherm is normally used to describe polymer adsorption. The Langmuir-type isotherm used by UTCHEM takes into consideration salinity, polymer concentration and permeability [105], and is given by Eq. 3.5,

$$\hat{C}_4 = \frac{a_4 (C_{41})}{1 + b_4 C_{41}} \tag{3.5}$$

Where $\hat{C}_4$ and C_{41} are the polymer concentration in the aqueous phase and on the rock surface respectively. As mentioned in section 2.2.3 the ratio, a_4/b_4, determines the plateau value of the adsorption isotherm, and b_4 the curvature.

In UTCHEM the parameter, a_4, is defined by Eq. 3.6,

$$a_4 = (a_{41} + a_{42} C_{SEP}) \left(\frac{k_{ref}}{k} \right)^{0.5} \tag{3.6}$$

The reference permeability, k_{ref}, is the permeability at which the input parameters are specified.

3.2.4 Permeability reduction:

In UTCHEM the permeability reduction factor is modeled by Eq. 3.7 [101],

$$R_k = 1 + \frac{(R_{k,max} - 1) b_{rk} C_{41}}{1 + b_{rk} C_{41}} \tag{3.7}$$

where the maximum permeability reduction factor is given by Eq. 3.8,

$$R_{k,max} = \max \left\{ \left[1 - \frac{c_{rk} \left(A_{pl} C_{SEP}^{Sp} \right)^{1/3}}{\left(\frac{\sqrt{k_x k_y}}{\phi} \right)^{1/2}} \right]^{-4}, 10 \right\} \tag{3.8}$$

and 1is the phase with the highest polymer concentrations. b_{rk} and c_{rk} are input parameters in UTCHEM.

3.2.5 Inaccessible pore volume:

In UTCHEM the effect of inaccessible pore volume is modeled by multiplying the porosity in the conservation equation of polymer by the input parameter of effective pore volume.

4 Experimental input

A 2D X-ray photon counting scanner for estimation of in-situ saturations has been developed by CIPR. The instrumentation also allows for x-ray imaging, which has been applied to detect and visualize fast changes in flow patterns.

Experiments [6] have been performed on four different Bentheimer samples, each 0.3x0.3x0.02 m. Amongst these, a number of miscible displacements using oils of different viscosities. Water flooding experiments were run at different rates and with different oil water interfacial tensions. The experimental study also included one case of polymer injection following a water flood.

The input data from the experiment [6] used in this thesis, are presented in Table 4.1, 4.2, and 4.3,

Sample #	Dim [m x m x m]	PV	ϕ
1	0.30 x 0.30 x 0.0205	401	0.223
4	0.30 x 0.297 x 0.0197	422	0.241

Table 4.1: Dimensions, pore volume and porosity for sample 1 and 4.

Exact values of permeabilities were not given in the report, but according to tests performed at Reslab, a permeability of about $2.5\mu m^2$ is reasonable. Both samples had three tubing connectors attached at the inlet side, and two at the outlet side. Figure 4.1 shows a photo of the prepared sample, fitted in the x-ray cabinet.

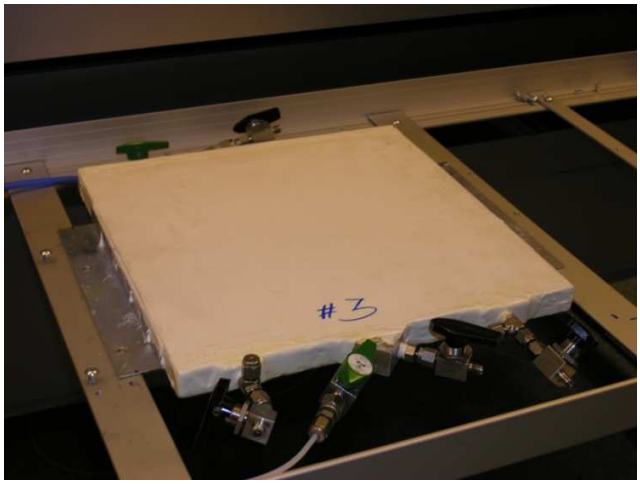

Figure 4.1: Photo of a prepared sample placed in the x-ray cabinet [6].

NaI was added to the brine in order to visualize the displacement using the x-ray scanner.

Test #	Oil	Brine	μ [mPa*s]	ρ [g/cm^3]	IFT o-w [mN/m]
1	n-decane iododecane		0.92 ~1	0.73 1.25	
2	"paraffinum liquidum" iododecane		~200 ~1	0.862 1.25	
3	"paraffinum liquidum"	15% NaI	~1	1.111	25
4	"paraffinum liquidum"	15% NaI	~1	1.111	25
5	"paraffinum liquidum"	10% NaI 0.5% Xanthan	24 – 100 (shear dep.)	~1.07	~25

Table 4.2: Oil, brine and polymer solution properties, including viscosity, density and interfacial tension.

Test #	Filling sequence	# of inj. ports	Q_w [m^3/day]	S_{wi}	S_{or}	Total PV inj.	Fingering observed
1	ndecane iododecane	3	~0.0001441 – 0.0007205	0	0.49	2.35	No
2	"paraffinum liquidum" iododecane	3	~0.00007205- 0.002882	0	0.49		Yes
3	"paraffinum liquidum" Water	3	~0.00007205 – 0.001441	0	0.49		1st part
4	"paraffinum liquidum" Water	3	~0.00007205 – 0.004323	0.12	0.53	0.7	No
5	"paraffinum liquidum" Polymer	2	~0.002882- 0.001441	0.53	0.31	3	No

Table 4.3: The table consists of filling sequence, the number of injection ports, injection rates in all tests, residual oil saturation, total amount of pore volumes injected, and whether or not fingering was observed.

No fingering was observed for miscible displacement with low mobility contrast. The displacement did, however, yield an indifferent spreading process as illustrated by figure 4.2. For a miscible displacement, using low viscous displacing oil and a high viscous displaced oil, the development of viscous fingering was observed. The observed sharpening fingers grow from the tip of the finger and are reinforced through established fingers. Some amount of fingering could also be observed for immiscible displacements of high viscous oil by water, at 100% initial oil saturation. Due to capillary forces and spontaneous imbibitions these fingers developed differently in both shape and form. Instead of a sharpening of the fingers, the fronts continue to grow wider and more diffuse until joined together. The fingers developed are spreading. No frontal instabilities were observed for immiscible displacement of highly viscous oil by water at initial water saturation of 0.12, an indifferent process is observed.

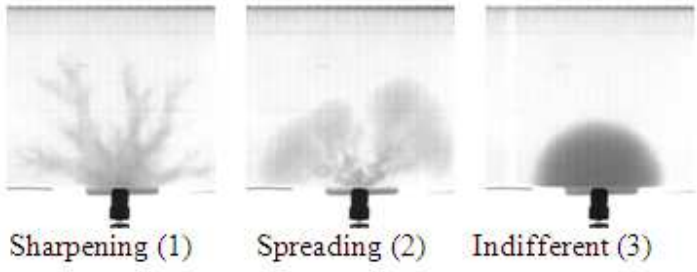

Figure 4.2: The different types of fingering observed during unstable displacement, sharpening (miscible M>>1), spreading (immiscible M>>1, S_{wi}=0), and indifferent (miscible M~1) [6].

By performing a polymer flood after the water flood the oil recovery increased considerable. Oil recovery after the water flood was 45.3% HCPV, increasing to 64.0% HCPV after the polymer flood. The displacement appeared stable, even at such unfavorable mobility ratio. No viscous fingers were observed in the water flood, due to an initial water saturation of 0.14. If microscopic displacement is assumed equal for water and polymer flooding, the additional oil recovered indicates that the residual oil saturation was not reached during the water flood. Both X-ray profiles and saturation measurements confirm the formation of an oil bank in front of the polymer.

5 Viscous fingering evaluation

In the theoretical description of viscous fingering in section 2.1.1, the process of finger initiation is normally attributed to permeability heterogeneities. In order for viscous fingering to initiate in the numerical models, variation in local grid block permeability was introduced.

Prior to creating the simulation models for history matching the experimental data presented in section 4, an evaluation of the effect of both numerical dispersion and degree of heterogeneity was performed. Description of the models used in this evaluation, together with the results, are presented in this section.

5.1 Effect of numerical dispersion

In order to study the effect of numerical dispersion on the shape of the displacement front, a fairly simple 0.30m x 0.30m x 0.02m homogeneous model was created in UTCHEM. The porosity of the model was 0.22 and the permeability constant at $3\mu m^2$. Water was injected in the upper left hand corner at 0.001441 m^3/day. The ratio between water and oil viscosity were 10 to 1 mPa*s, and capillary pressure was disregarded. The model was run with the following number of grid blocks: 5x5x1, 10x10x1, 20x20x1, 30x30x1, 60x60x1 and 100x100x1.

The results are presented in the figures below. The complete picture series is presented in Appendix 1.

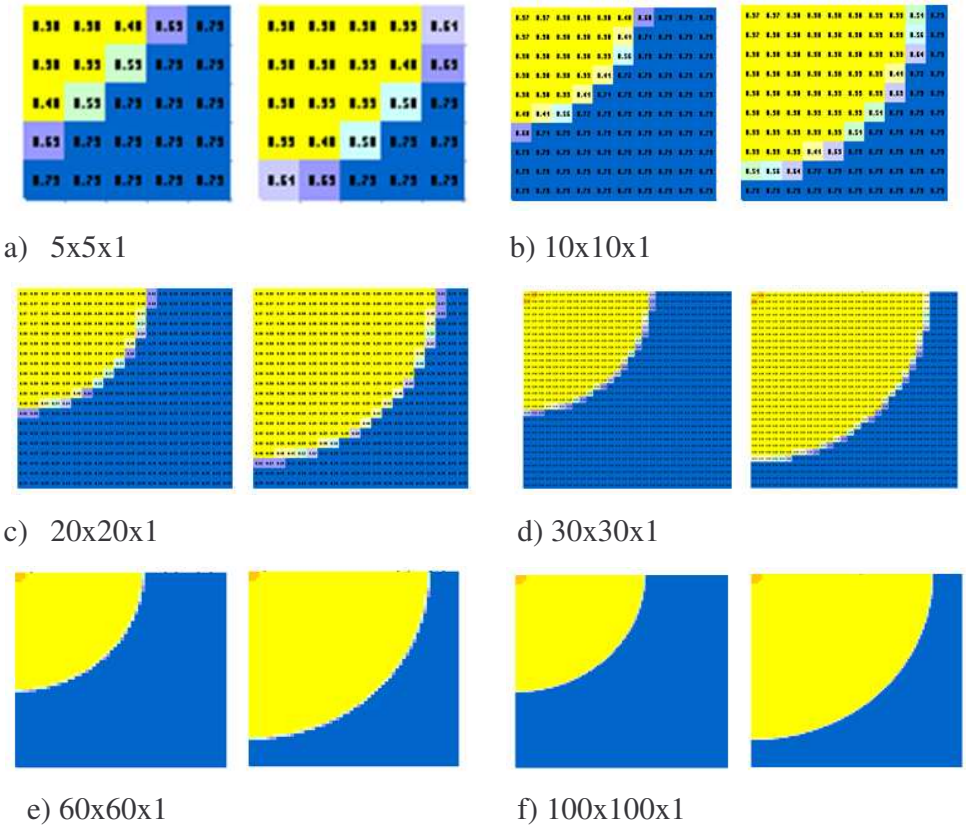

a) 5x5x1 b) 10x10x1

c) 20x20x1 d) 30x30x1

e) 60x60x1 f) 100x100x1

Figure 5.1: The effect of amount and size of grid blocks, a) through f), on the shape of the displacement front. The yellow and blue colors in the figure represents the water and oil respectively. The left-hand figures are at 1 PV injected, and the right-hand figures are at 2 PV injected.

As illustrated by Fig 5.1, the shape and smoothness of the waterfront is greatly affected by the numerical dispersion. The effect, however, is less substantial for models greater than 60x60x1 grid blocks. Still, the finest and smoothest shape of the front was obtained by 100x100x1 grid blocks. In order to get the best possible results, the remainder of models designed in this thesis all have 150 x 150 x 1 grid blocks.

5.2 Effect of heterogeneities

Investigating the effect of heterogeneity on the form and development of viscous fingering a similar 0.30m x 0.30m x 0.02m model was created in UTCHEM. This model, however, contained 150x150x1 grid blocks. The porosity was still 0.22, and capillary pressure not included. Water viscosity was 1 mPa*s while the oil viscosity was 200 mPa*s, yielding an unfavorable mobility ratio.

Water was injected from two ports at 0.0007205 m^3/day. The model was run with several different degrees of heterogeneity, but all with the same average value of $2.5\mu m^2$. This was done to determine how large the

permeability differences have to be in order for viscous fingers to form. The model was also run with residual saturations and relative permeability both dependent and independent on capillary number. The relative permeability data used when independent on capillary number and at low capillary numbers is presented in Table 5.1, and the relative permeability curves in Fig. 5.2,

S_{wi}	0.0001	S_{or}	0.0001
k'_{rw}	1	k'_{ro}	1
Corey exponent, w	2	Corey exponent, o	2

Table 5.1: Residual saturations, relative permeability endpoints, and Corey exponents for water and oil used when independent on capillary number and at low capillary numbers.

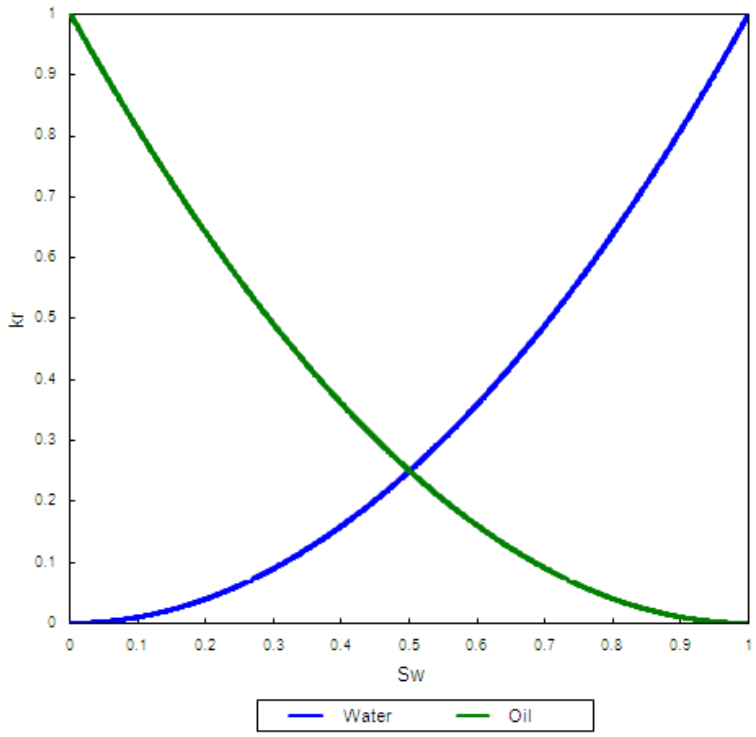

Figure 5.2: Relative permeability curves for water and oil used when independent on capillary number and at low capillary numbers.

When residual saturations and relative permeability was set to be dependent on capillary number, the data presented in Table 5.1 and Figure 5.2 was used for low capillary number. For high capillary number the following data, presented in table 5.2 and figure 5.3, was used,

S_{wi}	0	S_{or}	0
k'_{rw}	1	k'_{ro}	1
Corey exponent, w	1	Corey exponent, o	1

Table 5.2: Residual saturations, relative permeability endpoints, and Corey exponents for water and oil used at high capillary numbers.

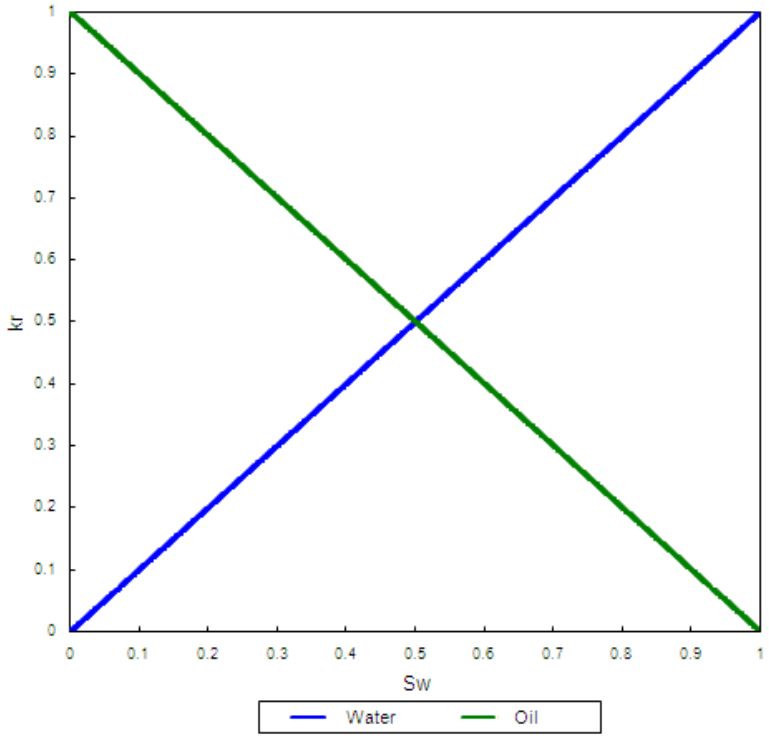

Figure 5.3: Relative permeability curves for water and oil used at high capillary numbers.

The results are presented in Fig. 5.5 and 5.6. Complete picture series are presented in Appendix 2. The color scale of the saturation profiles is presented in Fig. 5.4.

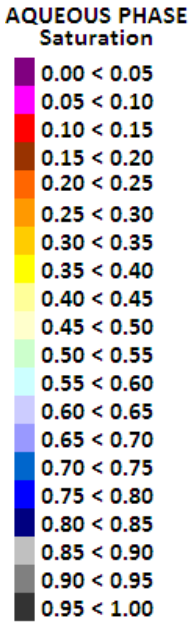

Figure 5.4: The color scale for aqueous phase used in the saturation profiles in Fig. 5.5 and 5.6.

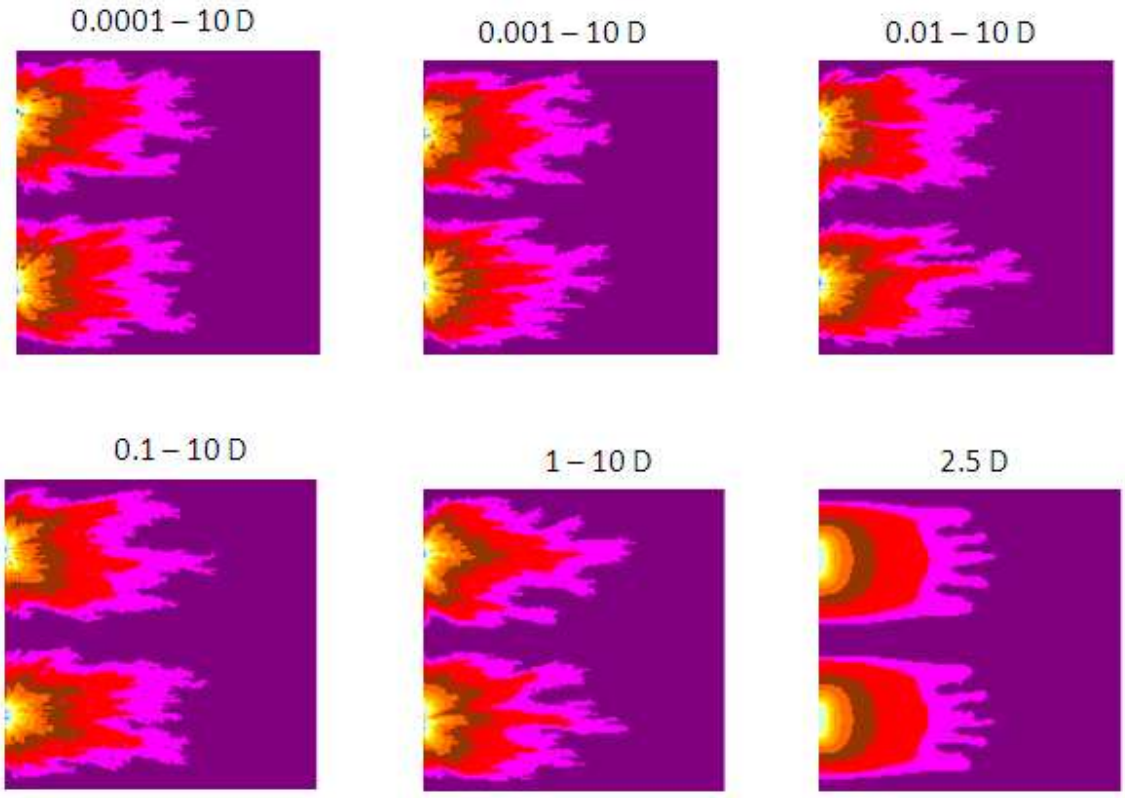

Figure 5.5: Simulated saturation profiles at different degrees of heterogeneity, at 0.05 PV injected. Residual saturations and relative permeability curves are independent on capillary number.

Saturation profiles where residual saturations and relative permeability curves are independent on capillary number, clearly shows viscous fingering. In this case the relative permeability curves in Fig. 5.2 are used throughout the simulation. Viscous fingers are even observed in the homogeneous model ($2.5\mu m^2$) in Fig 5.5. The fingering in this model, however, is contained to the lowest saturations (the light purple color in the saturation profiles). At all heterogeneity distributions viscous fingering appear to be fairly similar, but there is an increase in the amount of fingering as the degree of heterogeneity increases.

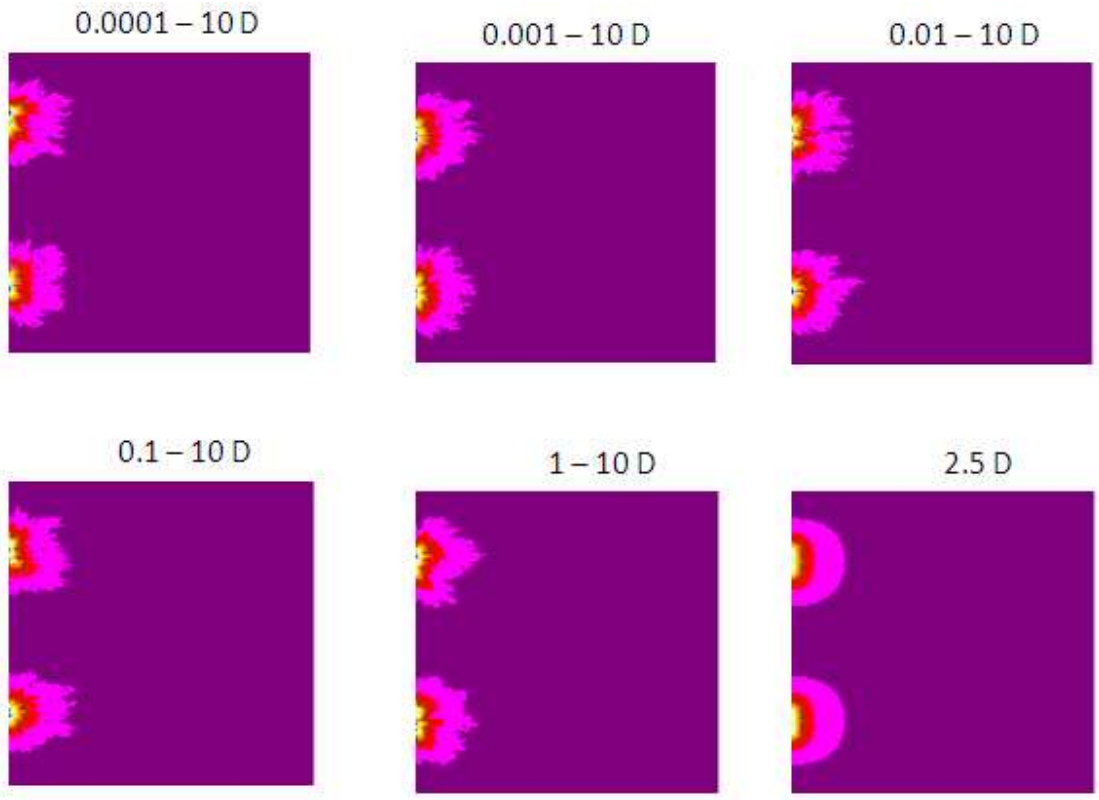

Figure 5.6: Simulated saturation profiles at different degrees of heterogeneity, at 0.005 PV injected. Residual saturations and relative permeability curves are dependent on capillary number.

Saturation profiles where residual saturations and relative permeability curves are dependent on capillary number, clearly shows some amount of viscous fingering. In this case the relative permeability curves in Fig. 5.2 are used for low capillary number, and the relative permeability curves in Fig. 5.3 are used for high capillary number. Viscous fingers are not observed in the homogeneous model ($2.5\mu m^2$) in Fig. 5.6. At all heterogeneity distributions viscous fingering appear to be somewhat similar, still there is an increase in the amount of fingering as the degree of heterogeneity increases. The amount of fingering in these

models, however, are largely contained to the lowest saturations (the light purple color in the saturation profiles). A very little amount of fingering is observed in the higher saturation steps.

Both Fig 5.5 and 5.6 show that the degree of heterogeneity did not have a very large effect on the viscous fingering. Increasing the degree of heterogeneity increases the amount of viscous fingering. Thus the largest degree of heterogeneity was chosen for use in later models in this thesis. The dependence of residual saturations and relative permeability on capillary number did, however, have a large effect on the observed fingering. In the model where this dependence was included, the residual saturations, and thus the relative permeability curves, are changed as the capillary number increases. The relative permeability curves in the model will change from those presented in Fig. 5.2, towards the relative permeability curves presented in Fig. 5.3. The only difference in relative permeability in between Fig. 5.2 and 5.3, is the Corey exponent. Thus, a change in Corey exponent from 2 to 1.4 give a significant reduction in fingering. The effect of the Corey exponent on amount of fingering observed might be worth taking a further look at, but was not included in this thesis.

Theory regarding the dependence of residual saturations on capillary number is presented in more detail in Appendix 3.

6 Numerical models

Several numerical models were created in order to history match the experimental data presented in section 4. The description of the different simulation models are presented in this section. First a basic model is described , from which all other models are derived. Two simulation models each, were created for the miscible and immiscible displacements. At last follows a description of the model for the polymer flood. The description of the different simulation models are presented in this section.

6.1 The numerical model used as a basis for all other numerical models - BASIC

The BASIC model is a square model with horizontal measures of 0.30m x 0.30m. The height of the model is 0.02 m. It is a simple Cartesian model, holding 150 cells in both x- and y-direction, and 1 cell in the z-direction. The cells are 2 mm in the x- and y-direction, and 2 cm in the z-direction. Metric units are used throughout the model.

The model contains no heterogeneities. The porosity is 0.22 throughout the entire model. The permeability is $2.5\mu m^2$ in the x-and y-direction and 50 % lower in the z-direction. Residual saturations are taken from the experimental data presented in section 4. In the BASIC model the capillary pressure is set to be zero.

The initial water saturation in the model is set to 0.0001. Relative permeability is modeled based on a Corey type function using Eq. 6.1,

$$k_{r\ell} = k^0_{r\ell} \left(S_{n\ell}\right)^{n_\ell} \tag{6.1}$$

where the normalized saturations are defined in Eq. 6.2,

$$S_{n\ell} = \frac{S_\ell - S_{\ell r}}{1 - S_{wi} - S_{or}} \tag{6.2}$$

$k^0_{r\ell}$, n_ℓ, and $S_{\ell r}$ are respectively the relative permeability endpoint, exponent, and saturation for phase ℓ. Phase ℓ is either aqueous or oleic.

The relative permeability curve in BASIC is independent on both capillary and trapping number, and modeled as close to miscible as possible. Due to the large size of the model, the Corey exponents could not bet set to zero. Both residual saturations and relative permeability curves are set to be independent of

capillary number. The input data for relative permeability are presented in Table 6.1, and the relative permeability curves are presented in Fig. 6.1,

S_{wi}	0.0001	S_{or}	0.0001
k'_{rw}	1	k'_{ro}	1
Corey exponent, w	1.4	Corey exponent, o	1.4

Table 6.1: Residual saturations, relative permeability endpoints and Corey exponents for water and oil used in the BASIC model.

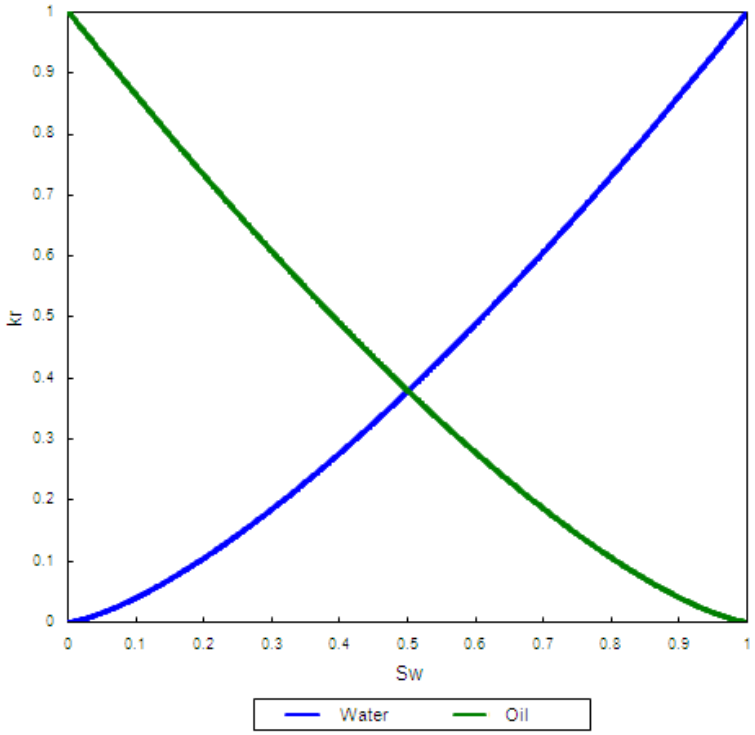

Figure 6.1: Relative permeability curves for water and oil used in the BASIC model.

UTCHEM allows for only one oleic phase. In order to model a miscible displacement the second oil is modeled as the aqueous phase. This is made possible by giving aqueous phase all properties of second oil, and using the miscible relative permeability curves, and interfacial tension of zero.

The viscosity of water and oil is set to 1 mPa*s and 200 mPa*s, respectively. The density for water is set to be 1.25 g/cm^3, and oil density is set to be 0.73 g/cm^3. Compressibility of water, oil and rock is set to be zero

throughout the model. The depth of the top layer in the model is set at zero, and the initial pressure in the BASIC model is 101 kPa.

The BASIC model contains a total of five wells. Fig. 6.2 illustrates the placement of the wells. Well 1, 2, and 3 are the injection wells set to inject at 0.001441 m^3/day. All three injection wells are rate constrained. Well 4 and 5 are producers, set to produce with a minimum flowing bottomhole pressure of 0 kPa and a maximum flowing bottomhole pressure of 1251. The minimal total flow rate is set to 0 m^3/day, and the maximum total flow rate is set to 4000 m^3/day. Both producing wells are pressure constrained. All five wells are horizontal, and fully completed over 10 cells. The well radius is set to be 0.001 m for all five wells. The exact positioning of the well are listed in Table 6.2,

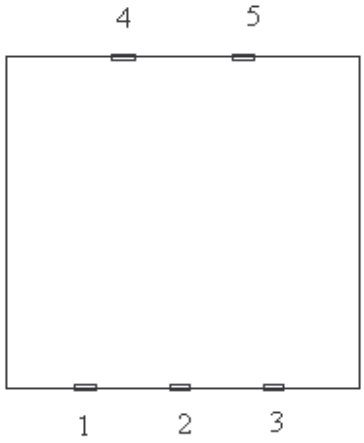

Figure 6.2: Illustration of the placement of the five wells.

Well #	Well name	j	k	i-first	i-last
1	INJE1	150	1	20	30
2	INJE2	150	1	70	80
3	INJE3	150	1	120	130
4	PROD1	1	1	45	55
5	PROD2	1	1	95	105

Table 6.2: Name, number, and (i, j, k) components for each well.

The output parameters wanted from the simulation are given in the OUTPUT OPTIONS in the input file. For the simulations the main output parameter is the IPSAT – profiles for phase saturations.

In the BASIC model the simulation is set to run for 0.1166 days. The maximum time step length is set at 0.5 days, and the minimum time step length is set at 0.005 days. These lengths are defined in order to prevent convergence failure in the simulations.

The tuning parameters in the BASIC model were set to the following values presented in Table 6.3,

DT – initial time step size	0.000001
DCLIM – tolerance for concentration changes for first three components	0.002
CNMAX – maximum courant number	0.5
CNMIN – minimum courant number	0.005

Table 6.3: Tuning parameters for the BASIC model

Theory regarding the tuning parameters is presented in more detail in Appendix 4.

The input file for the Basic model is presented in Appendix 5.

6.2 Numerical model of the first miscible process - MISC1, Test 1 in Table 4.3

In order to model the miscible process of iododecane displacing n-decane, a few changes had to be made in the BASIC model. n-decane was modeled as the oleic phase, and iododecane was modeled using the aqueous phase.

The first miscible model, MISC1, included permeability heterogeneities. Thus IPERMX was changed from constant permeability for the entire model, to variable permeability over the whole model. A permeability field varying from 0.0001 to 10 μm^2, with a mean value of $2.5 \mu m^2$ was included in the model. This permeability field was used for all heterogeneous models in this thesis. Porosity, saturations and relative permeability are kept as in the BASIC model, as are the densities and compressibilities. The viscosity for oil phase was set to 0.92 mPa*s.

The only other changes from the BASIC model are the time and rates of injection. Injection starts from INJE2 at the rate 0.000578 m^3/day. After 0.0014 days the injection rate is changed to 0.000693 m^3/day. At 0.0049 days of injection the rate in INJE2 is increased to 0.000743 m^3/day. Injection is stopped in INJE2 after 0.208 days. The reporting times in the MISC1 model are presented in Table 6.4,

Time step #	Reporting time [days]
1	0.0014
2	0.0049
3	0.2080
4	0.8330

Table 6.4: Number of time step and the reporting time in days used in MISC1.

6.3 Numerical model of the second miscible process - MISC2, Test 2 in Table 4.3

In order to model the miscible process of iododecane displacing “paraffinum liquidum”, some changes had to be made in the BASIC model. As in the model for the first miscible process, iododecane was modeled using the aqueous phase.

The second miscible model, MISC2, also included permeability heterogeneities. Again IPERMX was changed from constant permeability for the entire model, to variable permeability over the whole model. Porosity and saturations are kept as in the BASIC model, as are the viscosities, densities and compressibilities. The relative permeability curve in MISC2 is a little different from that of the basic model. The relative permeability exponent has set to 2 for both oil and water. The result of this is the relative permeability curve presented in Fig. 6.3,

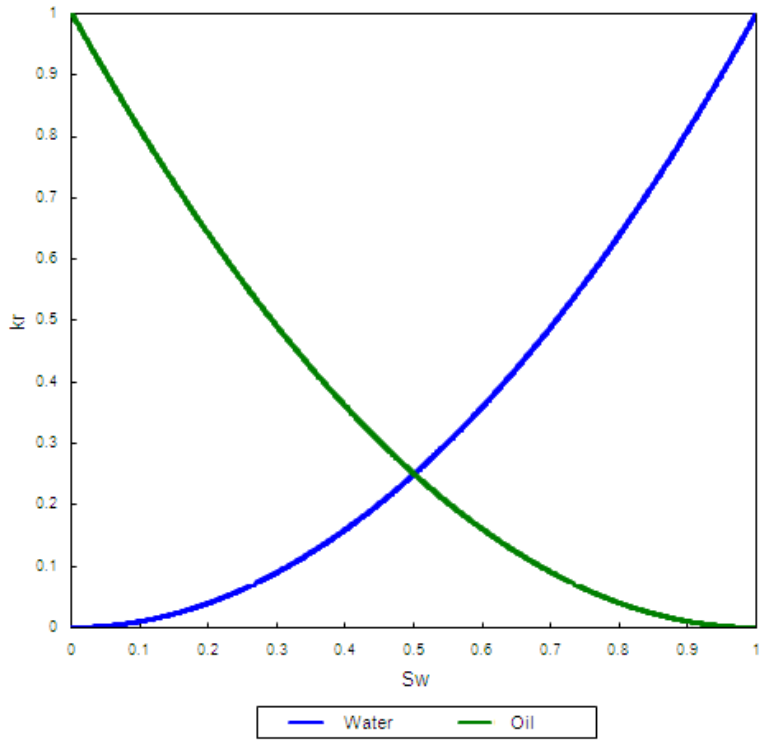

Figure 6.3: Relative permeability curves for water and oil used in the MISC2 model.

The reason for this increase in the relative permeability exponent is that it resulted in a greater amount of fingering. Other changes from the Basic model are concerning time and length of injection, and injection rates. Also injection well 1 were used. The injection starts from INJE2 at the rate 0.000721 m^3/day. 0.0035 days after injection start the injection rate in INJE2 is changed to 0.0007211 m^3/day. After 0.0104 days the injection in INJE2 is stopped, and nothing is injected into the reservoir until after 0.0207 days from injection start. After this INJE1 is set to inject at 0.0000245 m^3/day. At 0.0208 days the injection rate in INJE1 is increased to 0.00245 m^3/day. This injection rate is kept until 0.0417 days after injection start, when INJE1 is closed. The model was set to run for a total of 0.1 days, with reporting times as presented in Table 6.5,

Time step #	Reporting time [days]
1	0.0035
2	0.0104
3	0.0208
4	0.0278
5	0.0417

Table 6.5: Number of time step and the reporting time in days used in MISC2.

6.4 Numerical model of the first immiscible process - IMMIS1, Test 3 in Table 4.3

When modeling the immiscible processes of water displacing "paraffinum liquidum" at zero initial water saturation, several changes had to be made to the BASIC model. Water was now modeled using the aqueous phase in UTCHEM.

The first immiscible process was modeled with 50 x 50 x 1 grid blocks, as opposed to the 150 x 150 x 1 grid blocks in the BASIC model. One of the limitations of the UTCHEM simulator is in the amount of grid blocks used in a model. Introducing capillary pressure increases the complexity of the model, thus it was decided to reduce the number of grid blocks in order to minimize simulation problems. This decision was supported by the fact that x-ray images, displaying an area 0.11 x 0.11 m of the original 0.30 x 0.30 m slab, were available from the laboratory experiment. The size of each grid block was kept the same as in the BASIC model.

In order to include a variable permeability field, IPERMX was changed from constant permeability for the entire model, to variable permeability over the whole model. The porosity was kept as in the BASIC model.

To ensure an immiscible process the interfacial tension between oil and water was set to be 25 mN/m. The viscosity was set to 1 mPa*s and at 200 mPa*s, for the water and oil respectively. In IMMIS1 the initial water saturation was kept as in the BASIC model. The relative permeability curves had to be altered to describe an immiscible process. The input data for the relative permeability curve for IMMIS1 are presented in the Table 6.6, and the relative permeability curves are presented in Fig. 6.4,

S_{wi}	0.0001	S_{or}	0.49
k'_{rw}	0.1	k'_{ro}	1
Corey exponent, w	1.4	Corey exponent, o	4

Table 6.6: Residual saturations, relative permeability endpoints and Corey exponents for water and oil used in the IMMIS1 model.

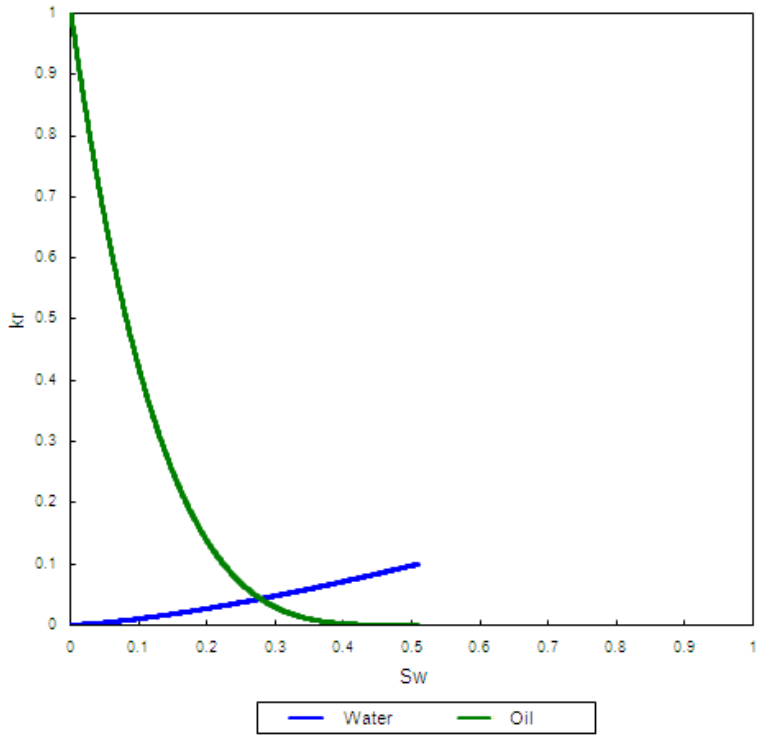

Figure 6.4: Relative permeability curves for water and oil used in IMMIS1.

In the models for immiscible processes capillary pressure was included. Capillary pressure was modeled as the imbibition Corey option in UTCHEM. In Brooks and Corey capillary pressure-saturation relationship [106], the capillary pressure is scaled for interfacial tension, porosity, and permeability [107] as shown in Eq. 6.3,

$$P_{cow} = C_{pci}\sqrt{\frac{\phi}{k}}\frac{\sigma_{ow}}{\sigma_{ow}}\left(1-S_n\right)^{-1/\lambda i} \tag{6.3}$$

C_{pci} and $EPC_i = -1/\lambda_i$ are positive input parameters in UTCHEM. The normalized saturations, S_n, for water displacing oil are defined in Eq. 6.4,

$$S_{nw} = \frac{S_w - S_{wi}}{1 - S_{wi} - S_{or}} \tag{6.4}$$

The capillary pressure parameters used in IMMIS1 are presented in Table 6.7, and the capillary pressure curve is presented in Fig. 6.5. Due to the large variation in permeability throughout the model, the capillary

pressure were modeled individually for each grid block, ensuring the same initial capillary pressure for all grid blocks. Thus separate C_{pci} values had to be given for every grid block. This is done in UTCHEM by setting the ICPC value to 2.

ICPC	2
C_{pci} average	700
EPC_i	3

Table 6.7: Input parameters for capillary pressure in IMMIS1.

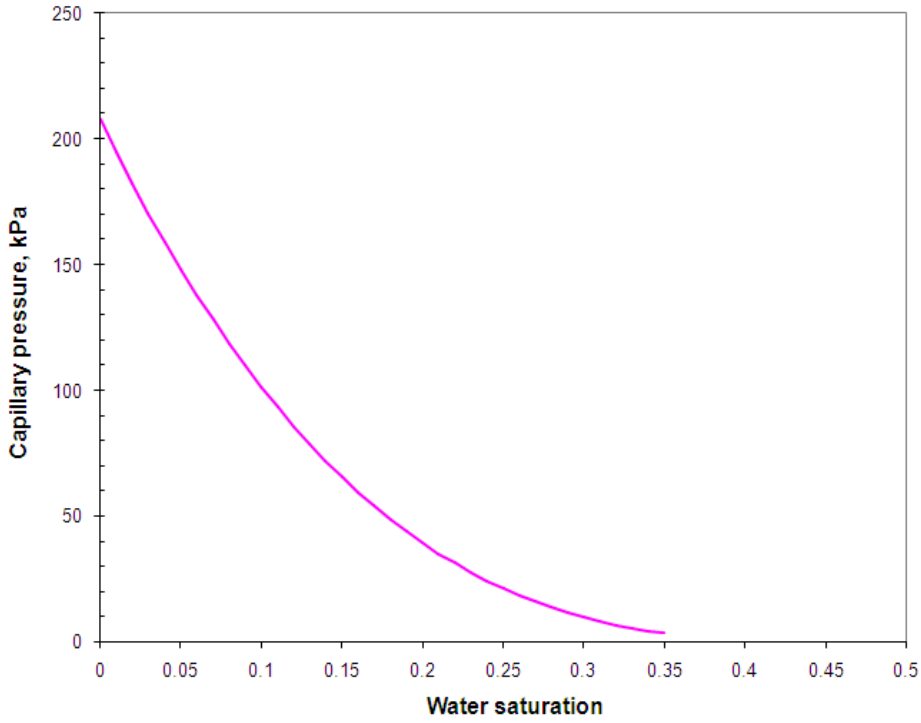

Figure 6.5: Capillary pressure curve used in the IMMIS1 model.

In the IMMIS1 model injection starts from INJE2 at a rate of 0.0000721 m^3/day. After 0.0125 days the rate is increased to 0.00036 m^3/day. At 0.0292 days injection is switched from INJE2 to INJE1, still at the same rate. After 0.354 days injection is started from INJE3 as well, at a rate of 0.0001442 m^3/day. The rate in INJE3 is increased to 0.000360 m^3/day after 0.0597 days. After 0.0951 days injection in INJE2 is started up again at a rate of 0.00036 m^3/day. The rates in both INJE1 and INJE3 are increased to 0.0007205 m^3/day. After 0.2333 days the rate in all three injection wells are increased to 0.001441 m^3/day. Injection is stopped

after 0.4583 days. The model was set to run for a total of 0.5 days, with reporting times as presented in Table 6.8,

Time step #	Reporting time [days]
1	0.0125
2	0.0208
3	0.0292
4	0.0354
5	0.0597
6	0.0951
7	0.2333
8	0.4583

Table 6.8: Number of time step, and the reporting time in days used in IMMIS1.

Input file for the first immiscible process, IMMISC1, is presented in Appendix 6.

6.5 Numerical model of the second immiscible process - IMMIS2, Test 4 in Table 4.3

When modeling the immiscible processes of water displacing "paraffinum liquidum" at an initial water saturation of 0.12, several changes had to be made to the BASIC model. As in the model for the first immiscible process the water was now modeled using the aqueous phase in UTCHEM.

The IMMIS2 model is very similar to the IMMIS1 model. The model for the second immiscible process were also modeled with 50 x 50 grid blocks. The only differences between IMMISC1 and IMMISC2 lie in the initial saturation of water, and thus the relative permeability and the capillary pressure curves. The input data for the relative permeability curve for IMMIS2 are presented in the Tables 6.9, and the relative permeability curves are presented in Fig. 6.6,

S_{wi}	0.12	S_{or}	0.49
k'_{rw}	0.1	k'_{ro}	1
Corey exponent, w	1.4	Corey exponent, o	4

Table 6.9: Residual saturations, relative permeability endpoints and Corey exponents for water and oil used in the IMMIS2 model.

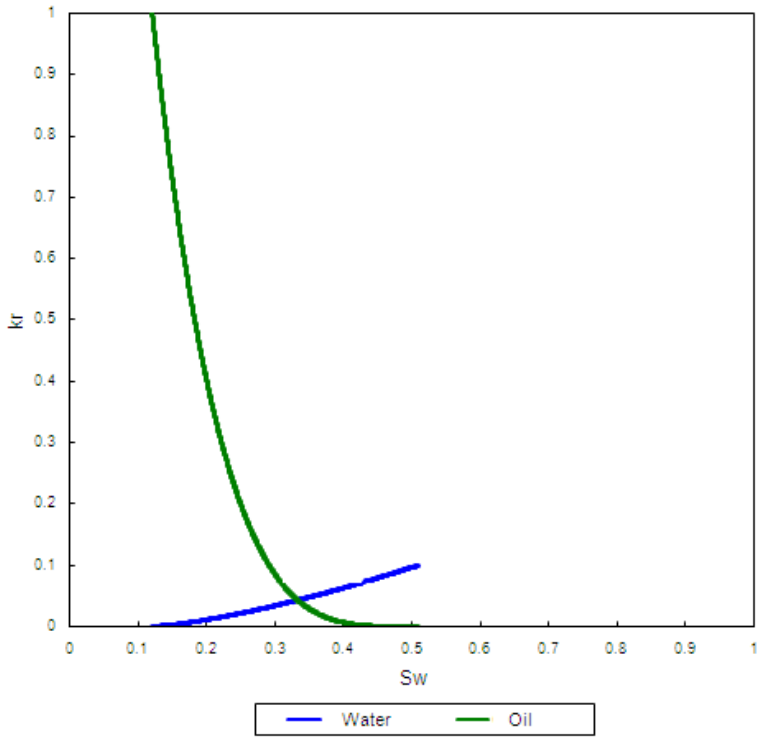

Figure 6.6: Relative permeability curves for water and oil used in IMMIS2.

The capillary pressure parameters used in IMMIS2 are presented in Table 6.10, and the capillary pressure curve is presented in Fig. 6.7. The capillary pressure in IMMISC2 were modeled in the same way as in IMMISC1, by giving separate C_{pci} for all grid blocks.

C_{pci} average	700
EPC_i	3

Table 6.10: Capillary pressure input parameters in IMMIS2.

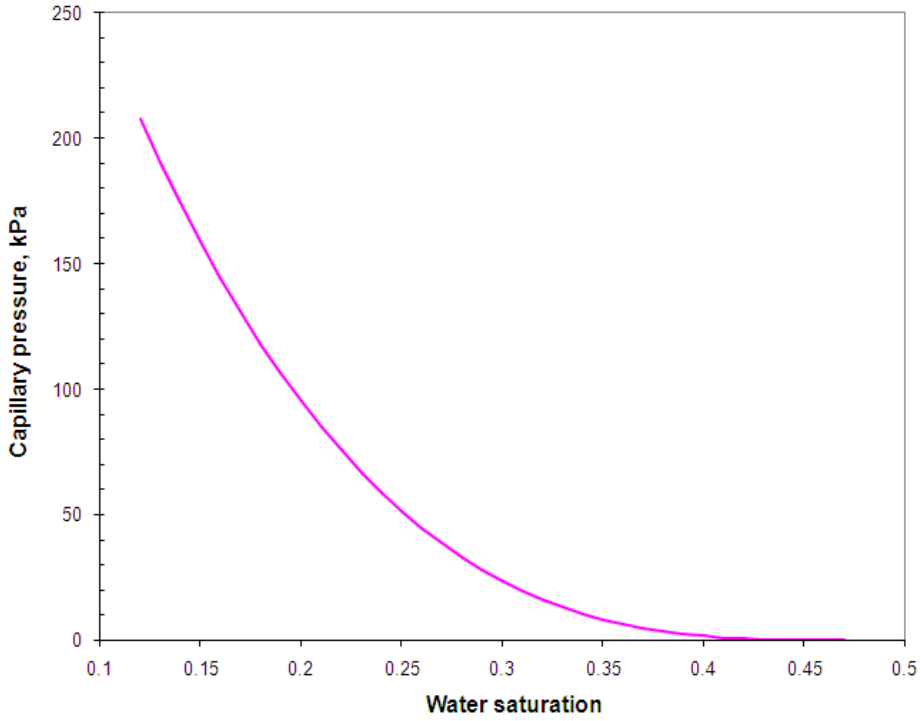

Figure 6.7: Capillary pressure curve for IMMIS2.

In IMMIS2 the injection starts of with INJE2 at the rate 0.0000721 m^3/day. After 0.0222 days the injection rate is increased to 0.00036 m^3/day. The injection is switched to INJE1 after 0.0347 days. At 0.0528 days the injection was switched to INJE3, and the rate increased to 0.001441 m^3/day. After 0.0694 days the injection was moved back to INJE1 and the rate increased to 0.004323 m^3/day. The model was set to run for a total of 0.1 days, with reporting times as presented in Table 6.11,

Time step #	Reporting time [days]
1	0.0097
2	0.0368
3	0.0542
4	0.0792

Table 6.11: Number of time step and the reporting time in days used in IMMIS2.

6.6 Numerical model of polymer flood following a water flood - POLY, Test 5 in Table 4.3

When modeling the polymer flood following a water flood, several changes had to be made to the BASIC model. As in the models for the immiscible displacements, the water was now modeled using the aqueous phase in UTCHEM. The polymers were added to the aqueous phase as a component.

In order to turn the Basic model into a model for polymer flow, POLY, the PERMX was changed to include a variable permeability field. Then all flags indicating the use of polymers were changed to include polymers in the simulation. These flags are,

- icf(kc) – flag indicating which components are included in the simulation
- IPRFLF – flag indicating which component profiles should be written

The initial water saturation in the polymer model, POLY, was set to be 0.53 representing a polymer flood following a water flood. The residual oil saturation after the water flood was 0.47. During a polymer flood in UTCHEM the input residual oil saturation is not lowered. Therefore the input value for S_{or} had to be set to the residual saturation obtained after the polymer flood. Thus the residual oil saturation in POLY was set to be 0.31. Relative permeability curves had to be altered to fit an immiscible process. The input data for relative permeability are presented in Table 6.12, and the relative permeability curves are presented in Fig. 6.8,

S_{wi}	0.14	S_{or}	0.31
k'_{rw}	0.1	k'_{ro}	1
Corey exponent, w	1.4	Corey exponent, o	4

Table 6.12: Residual saturations, relative permeability endpoints and Corey exponents for water and oil used in the POLY model.

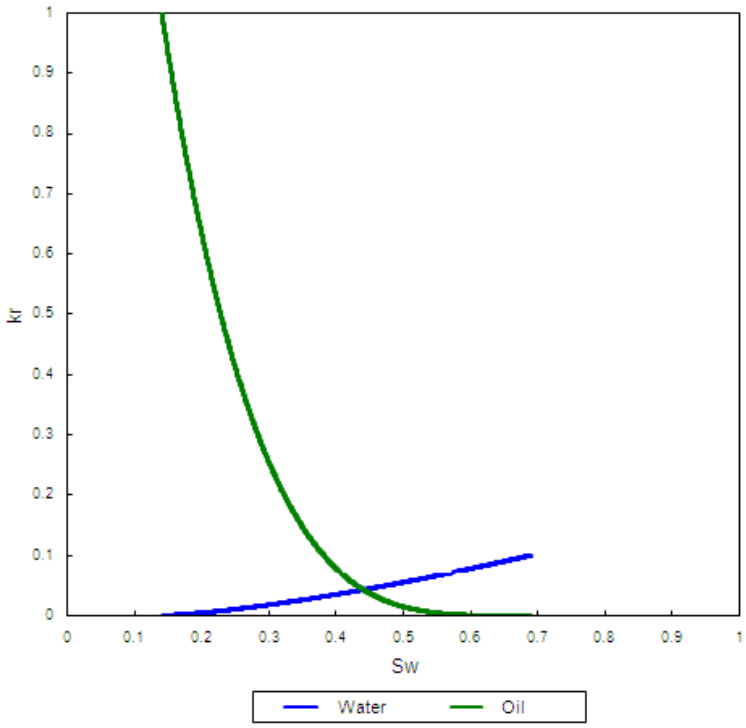

Figure 6.8: Relative permeability curves for water and oil, used in POLY.

In POLY the injection is started from INJE1 and INJE3 at the respective rates 0.002882 m^3/day, and 0.001441 m^3/day. After 0.06 PV the injection rate in INJE1 is reduced to 0.001441 m^3/day. The injection is stopped after a total injection of 3 PV. The model was set to run for a total of 3 PV, with reporting times as presented in Table 6.13,

Time step #	Reporting time [PV]
1	0.06
2	0. 4
3	0.66
4	2

Table 6.13: Number of time step and the reporting time in days used in POLY.

In UTCHEM there are several input parameters describing the properties of polymers as presented in section 3.2. The following sections include a description of the input parameters that have been used in the POLY model.

6.6.1 Viscosity dependence on concentration

The values of A_{P1}, A_{P2}, and A_{P3} used in POLY, are presented in table 6.14. Viscosity dependence on polymer concentration is presented in Fig. 6.9,

A_{P1}	200
A_{P2}	2000
A_{P3}	1000

Table 6.14: Input parameters describing viscosity dependence on polymer concentration.

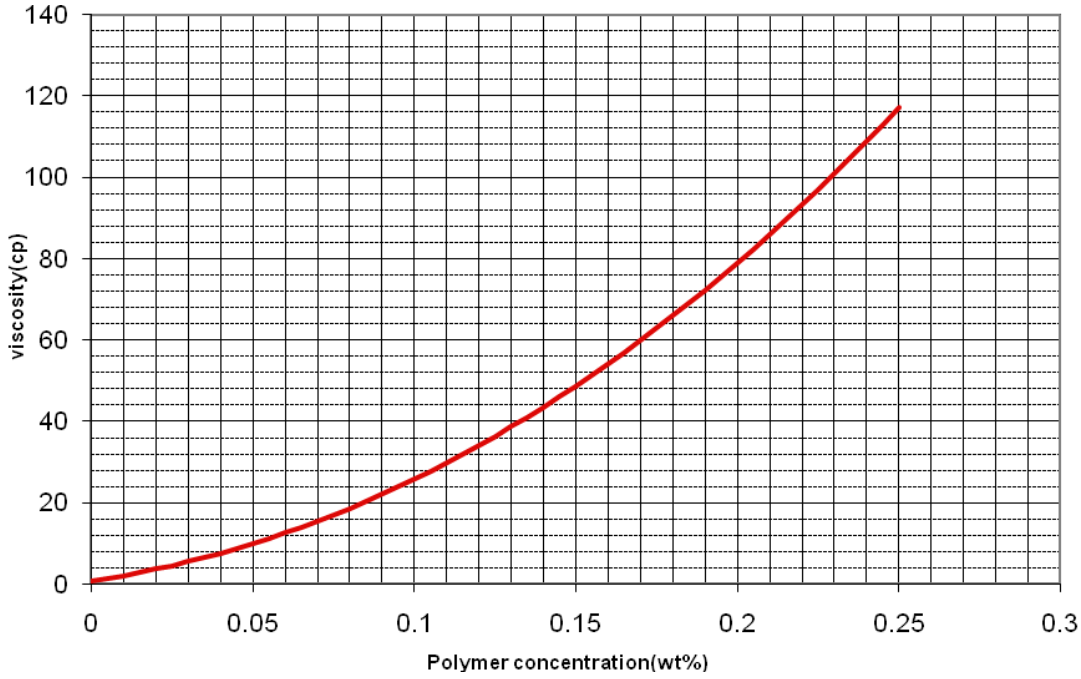

Figure 6.9: Viscosity dependence on polymer concentration.

The values of Sp and C_{SEP} used in POLY are presented in Table 6.15, and the plot of viscosity dependence on effective salinity is presented in Fig. 6.10,

Sp	0
C_{SEP}	0.01

Table 6.15: The value below which polymer viscosity is considered to be independent on salinity, C_{SEP}, and the slope of the viscosity versus effective salinity on a log-log plot, Sp.

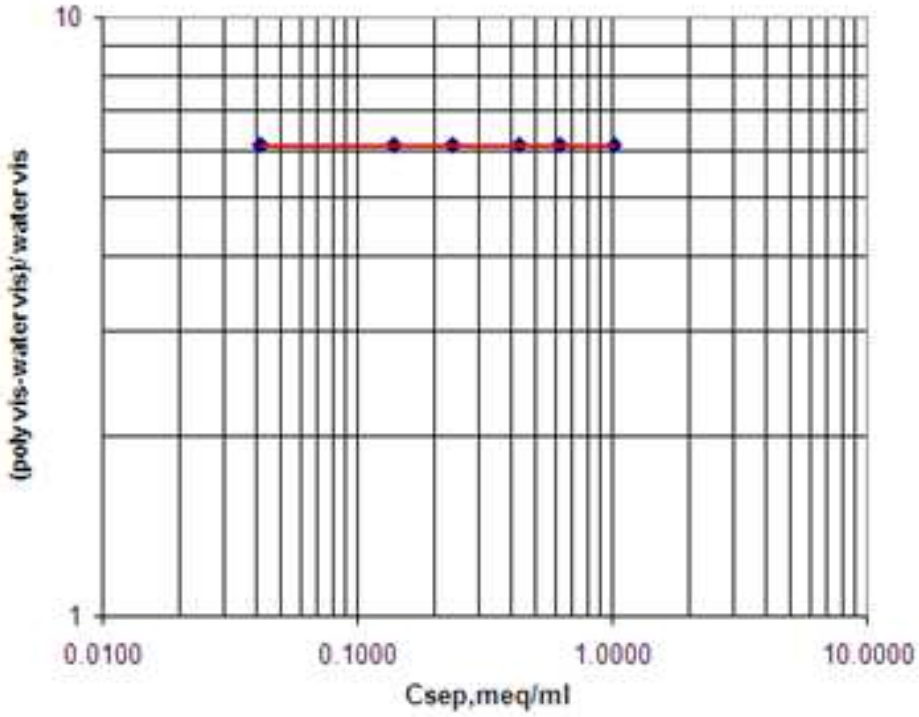

Figure 6.10: Viscosity dependence on effective salinity.

6.6.2 Viscosity dependence on shear rate

The values of $\dot{\gamma}_c$, $\dot{\gamma}_{1/2}$,and n_M used in POLY are presented in Table 6.16, and the viscosity dependence on shear rate is presented in Fig. 6.11,

GAMMAC, $\dot{\gamma}_c$	0
GAMHF, $\dot{\gamma}_{1/2}$	0.01
POWN, n_M	1.8

Table 6.16: Shear rate coefficient, GAMMAC, the shear rate at which polymer viscosity is half the viscosity at zero shear rate.

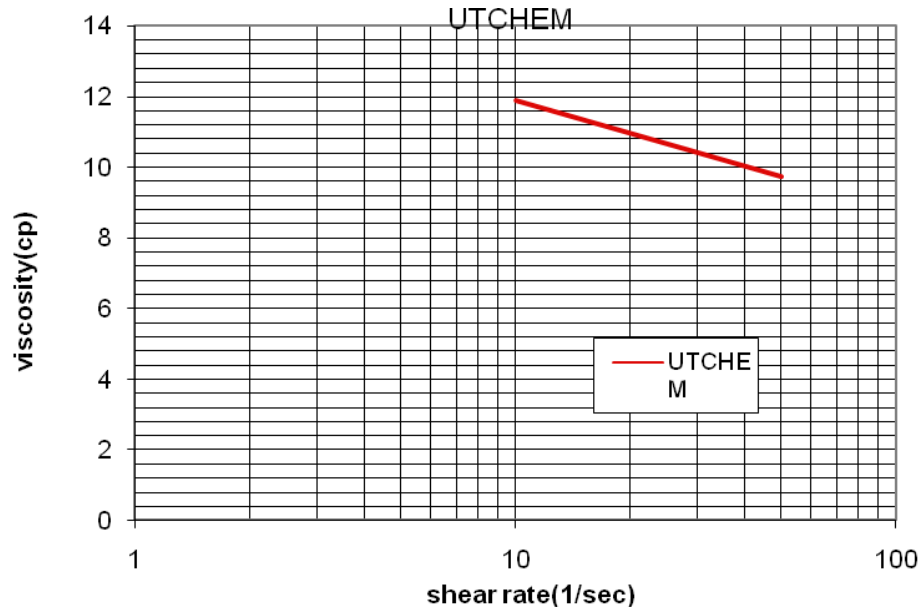

Figure 6.11: Viscosity dependence on shear rate.

6.6.3 Polymer retention

The values for a_{41}, a_{42}, and b_4 used in the POLY model are presented in Table 6.17, and polymer adsorption dependence on concentration is presented in Fig. 6.12,

a_{41}	4.8
a_{42}	0
b_4	100

Table 6.17: Polymer adsorption parameters used in POLY.

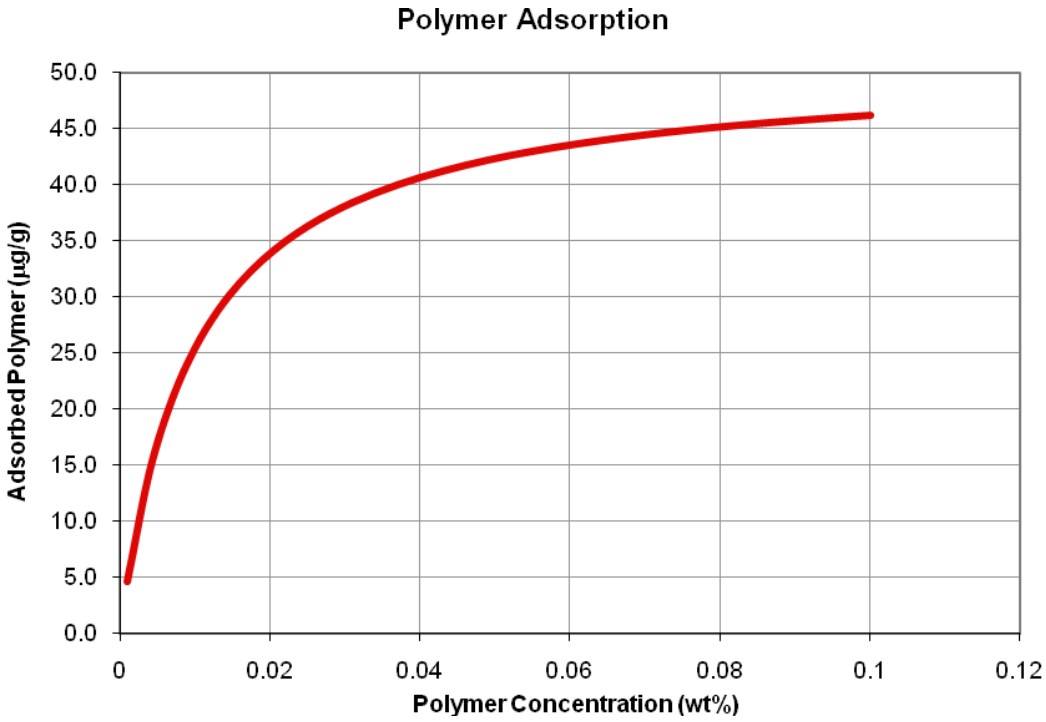

Figure 6.12: Polymer adsorption dependence on polymer concentration.

6.6.4 Permeability reduction

The values for b_{rk} and c_{rk} used in POLY are listed in Table 6.18, and permeability reduction factor dependence on permeability is presented in Fig. 6.13,

b_{rk}	100
c_{rk}	0

Table 6.18: Parameters for calculating permeability reduction factor.

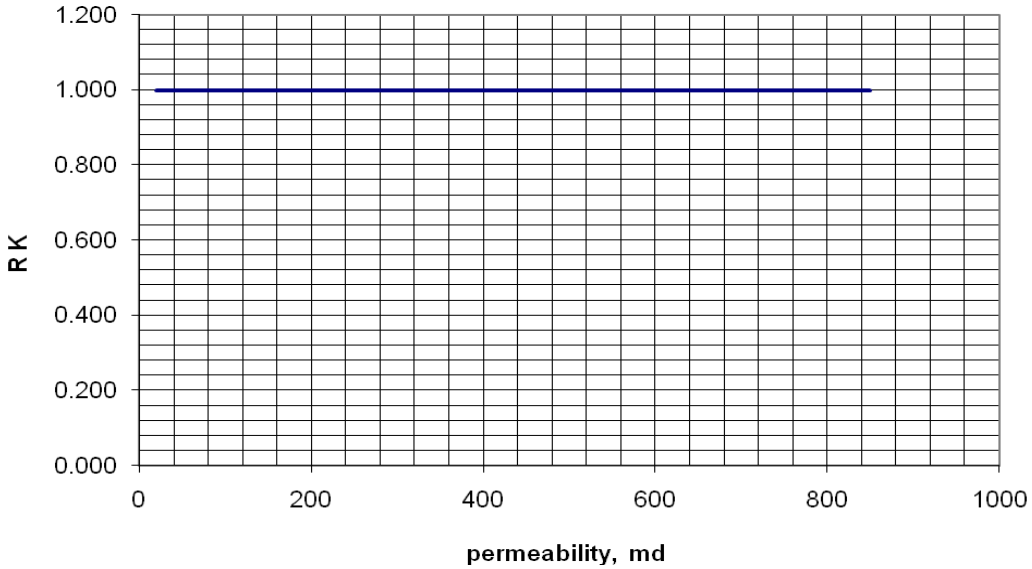

Figure 6.13: Permeability reduction factor dependence on permeability.

6.6.5 Inaccessible pore volume

In POLY the effective porosity for polymer, which is the ratio of apparent porosity for polymer to actual porosity, is set to be EPHI4 = 1.

7 Results and discussion

The results of all simulations are presented and compared to the corresponding experiments. Saturation data from the simulations were reported at the same moments in time as the x-ray photos were taken. The results from the simulation and experimental study are therefore comparable regarding the time schedule.

In all the x-ray images the dark areas mean low x-ray intensities, doped fluid (water with NaI or iododecane). The light areas mean high x-ray intensities, oil without dope. Only qualitative evaluation of the saturation is available from the x-ray images.

The simulated saturation variations are given according to the color scale on Fig. 7.1-23, and clearly show the evolution of the injected fluid with time.

7.1 Simulation results from the first miscible process - MISC1, Test 1 in Table 4.3

For the miscible displacement of n-decane by iododecane an indifferent type of spherical spreading (see Fig. 4.2) was observed in the experimental study. The mobility ratio for this process was approximately 1. The results of the simulation of this process, together with x-ray images from the experimental study [6], are presented in Fig. 7.1-3.

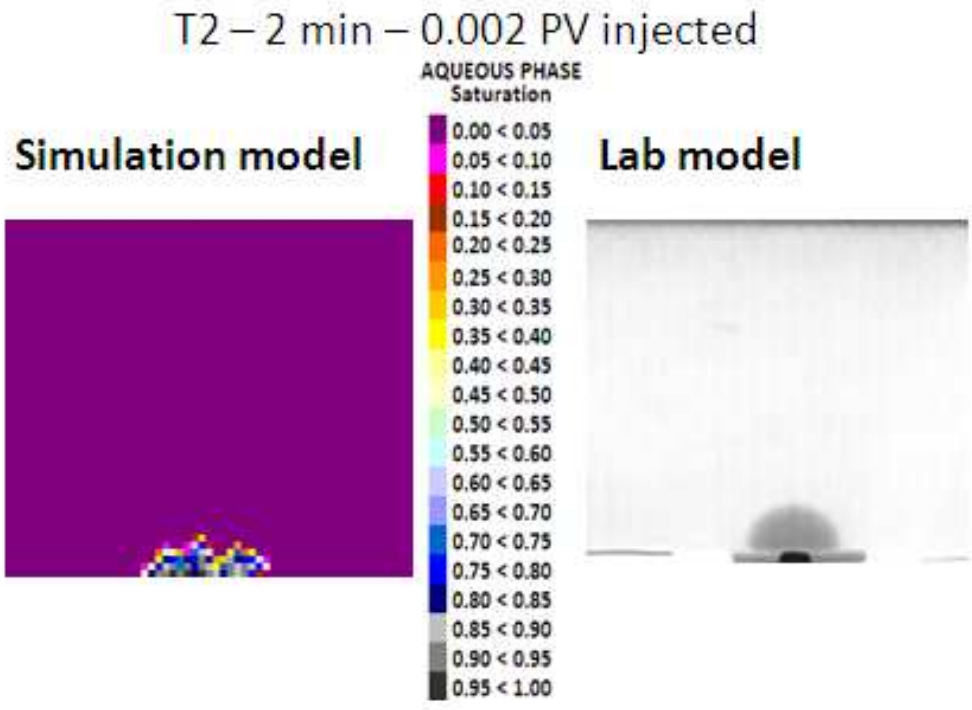

Figure 7.1: Simulated saturation profiles and x-ray images at 2 minutes, 0.002 PV injected.

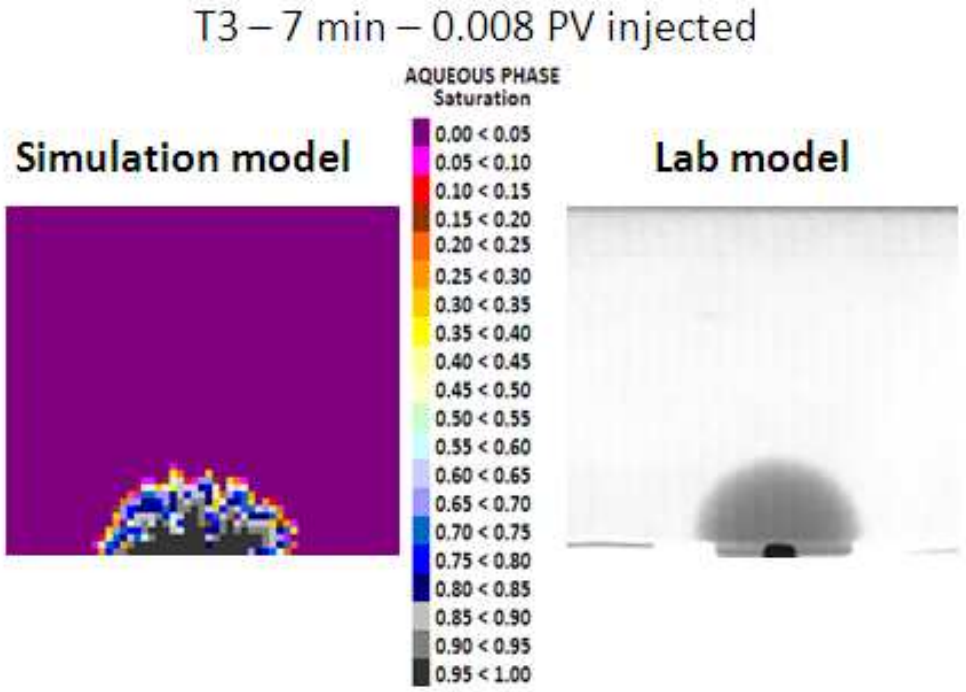

Figure 7.2: Simulated saturation profiles and x-ray images at 7 minutes, 0.008 PV injected.

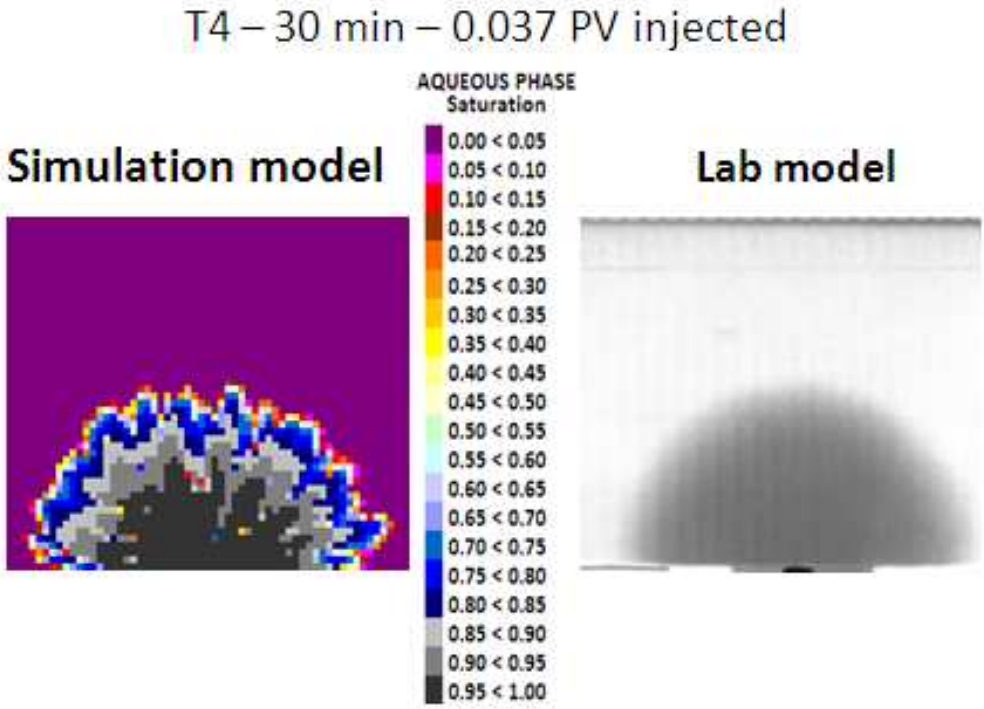

Figure 7.3: Simulated saturation profiles and x-ray images at 30 minutes, 0.037 PV injected.

The x-ray images in Fig. 7.1 through 7.3 displays an 0.11 x 0.11 m part of the Bentheimer block close to the second injection well. Consequently, the simulated saturations are presented by a similar 0.11 x 0.11 m area close to the injector INJE2. The simulated images show a good match with the x-ray images, with an overall spherical spreading of the displacement front. There are, however, small instabilities or fingers along the front in the simulated saturation profiles. A decrease in iododecane saturation towards the front of the displacement is observed in the x-ray images, and may indicate dispersion along the front. This decrease in saturation is also observed in the simulated saturation profiles, but again there is a difference in the smoothness of the front.

The reason for the small instabilities occurring at the displacement front in the simulated saturation profiles may be due to the large degree of heterogeneity. In the experimental report the permeability is given at about $2.5\mu m^2$. This, however, is merely an average value, and there is no knowledge of the exact distribution of permeability. In the UTCHEM model the permeability varies randomly between 0.0001 – 10 μm^2, with an average of $2.5\mu m^2$. This wide distribution may give very large permeability contrasts in neighboring cells, causing small perturbations and therefore instabilities along the front.

In a miscible system dispersive mixing would normally cause the transition zone to grow laterally, preventing the growth of fingers [9]. Dispersivity, however, is dependent on the modeling of heterogeneities. When a random permeability field is used with a very fine grid, the heterogeneity will dominate over dispersion [101]. In a less heterogeneous model perhaps the dispersion would be of greater significance.

In modeling the first miscible process, the UTCHEM simulator gave satisfactory results. The overall saturation profiles gave a good match to the experimental x-ray images. Some small instabilities were observed in the simulated saturation profiles. In MISC1 the longitudinal and transverse dispersivity were given at 0.001 and 0.0001 respectively. Decreasing the degree of heterogeneity and altering the dispersivity parameters in the model, might diminish the instabilities observed in the simulated saturation profiles.

7.2 Simulation results from the second miscible process - MISC2, Test 2 in Table 4.3

For the miscible displacement of high viscous paraffin by iododecane, viscous fingers were clearly observed. The observed fingers were sharpening (see Fig. 4.2), growing from the tip of the finger, and reinforcing already established fingers. The mobility ratio in this process was very unfavorable. The results

of the simulation of this process, together with x-ray images from the experimental study [6], are presented in Fig. 7.4-7.

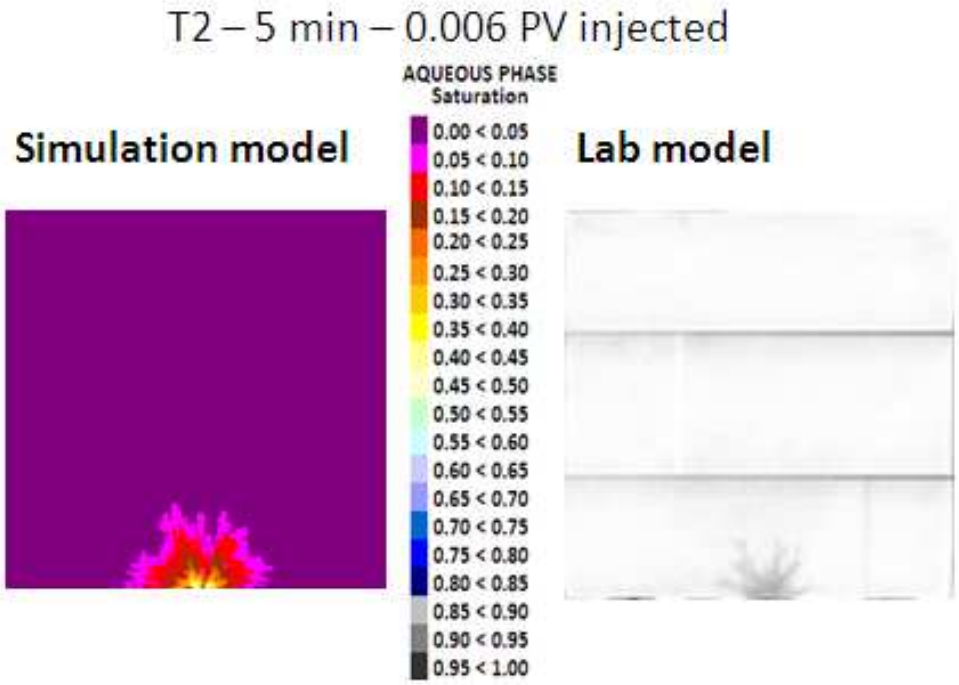

Figure 7.4: Simulated saturation profiles and x-ray images at 5 minutes, 0.006 PV injected.

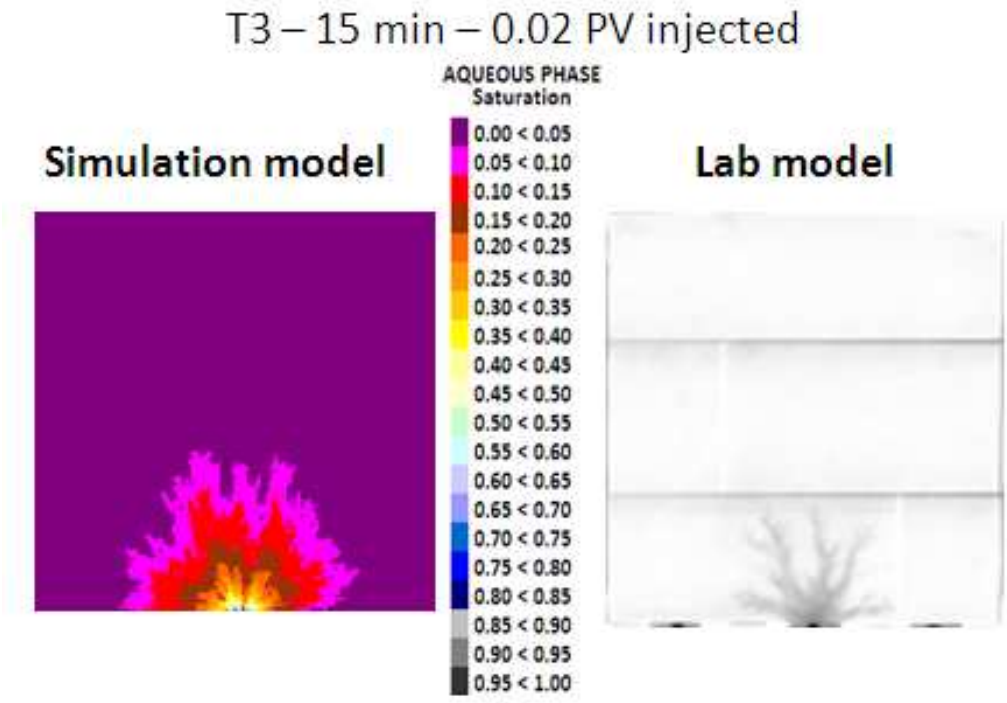

Figure 7.5: Simulated saturation profiles and x-ray images at 15 minutes, 0.02 PV injected.

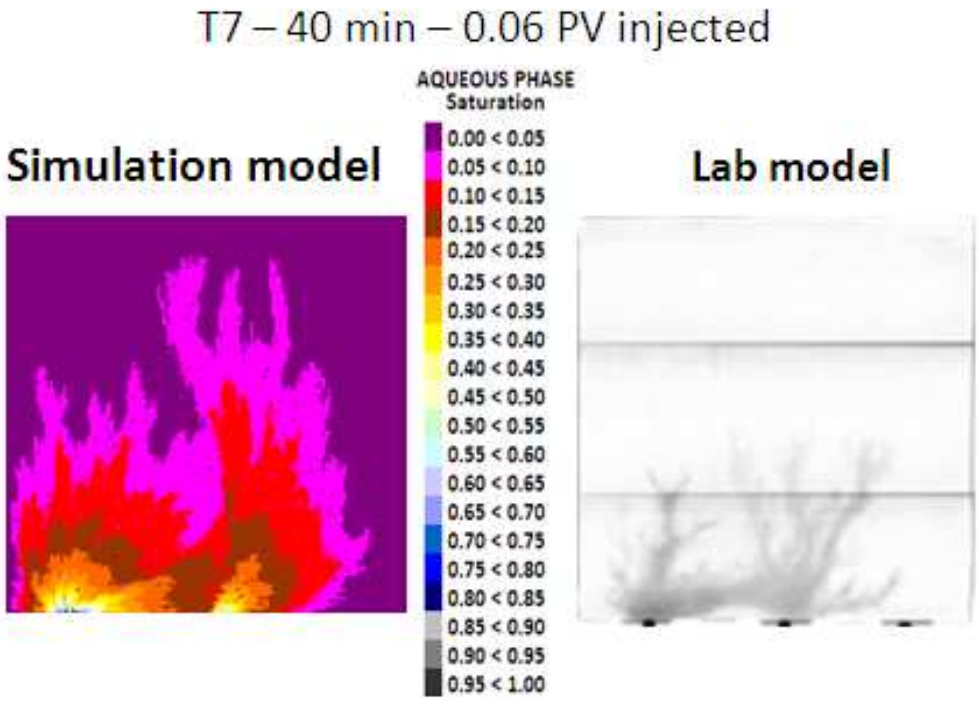

Figure 7.6: Simulated saturation profiles and x-ray images at 40 minutes, 0.06 PV injected.

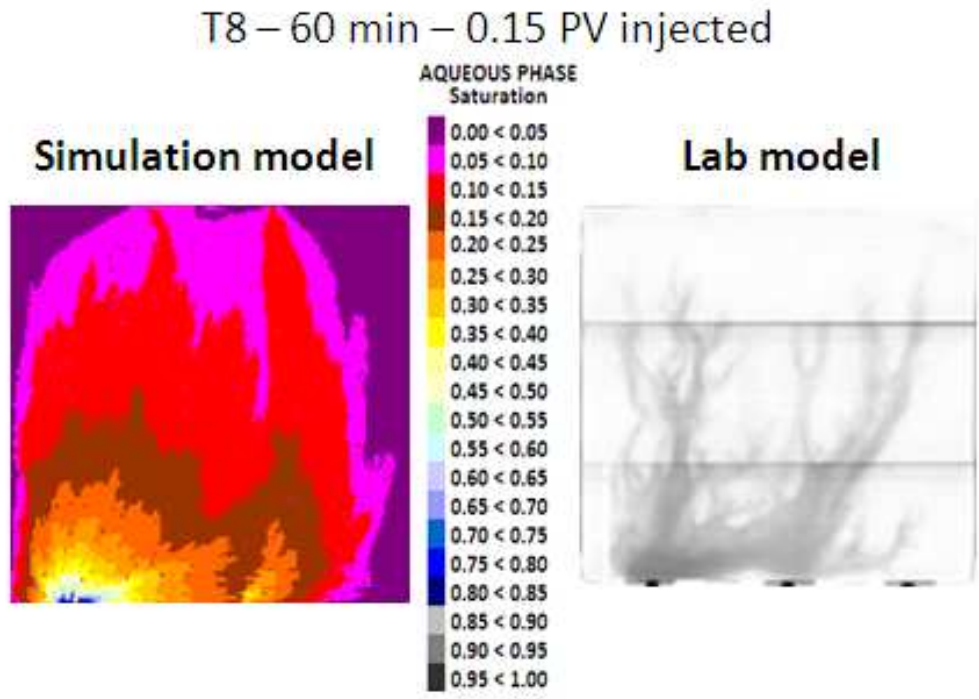

Figure 7.7: Simulated saturation profiles and x-ray images at 60 minutes, 0.15 PV injected.

Viscous fingers are clearly observed in simulated saturation profiles, but they are not a complete match to those in the laboratory model. As the flow in the x-ray images seem to mainly go through the initially developed fingers, ensuring growth from the tip of the fingers. Each finger in the simulated images seems to grow more in width during the displacement, and thus giving a better sweep. Both the simulated and experimental images are each at the exact same point in time. However, it looks like the viscous fingers in the simulated model advance faster than in laboratory model. This seems to be limited only to the lowest water saturations, between 0.05 and 0.1 (the light purple color in the saturation profiles). The decrease in saturation along the viscous fingers appears to be significantly less steep in the simulated model.

The relative permeability exponent should be close to 1 for a miscible process [9]. Unfortunately UTCHEM comprises convergence troubles with exponents lower than 1.4. An exponent of 1.4, however, gave very little fingering. Increasing the exponent to 2, also increased the amount of fingering. As discussed in section 5.2, this value for Corey exponent also gave an amount of fingering in a homogeneous model. Still it gave simulated results closest to the experimental results.

Finger growth in width is caused by transverse dispersion and merging of smaller fingers. The transverse dispersivity in MISC2 was kept constant at 0.0001. Changing the transverse dispersion might give less growth in the width of the fingers in the simulated saturation profiles. An alteration in the dispersion parameters may also change the steepness of the simulated saturation profiles.

The UTHEM simulator has proven very useful in modeling viscous fingering in a miscible process. The simulated saturation profiles showed viscous fingering very similar to that observed in the experimental x-ray images. Effects of transverse dispersion on the widths of the fingers is something which might be worth looking further into.

7.3 Simulation results from the first immiscible process - IMMISC1, Test 3 in Table 4.3

For the immiscible displacement of highly viscous paraffin by water at zero initial water saturation, spreading fingers (see Fig. 4.2) were observed in the experimental x-ray images. Fingers first appeared, but then grew increasingly diffuse especially in the front of the fingers. After a while the fingers were completely smeared out, and an apparent stable displacement front was observed. The mobility ratio in this process was very unfavorable. Capillary pressure was included in the model.

The simulation result from the first immiscible process did not give an exact match of the experimental results at the time steps given in the report. In order to observe the initiation of the displacement in the simulated results, time steps in the order of seconds were reported. The experimental x-ray images for the first immiscible displacement are presented in Appendix 7. The results of the simulation of this process are presented in Fig. 7.8-10.

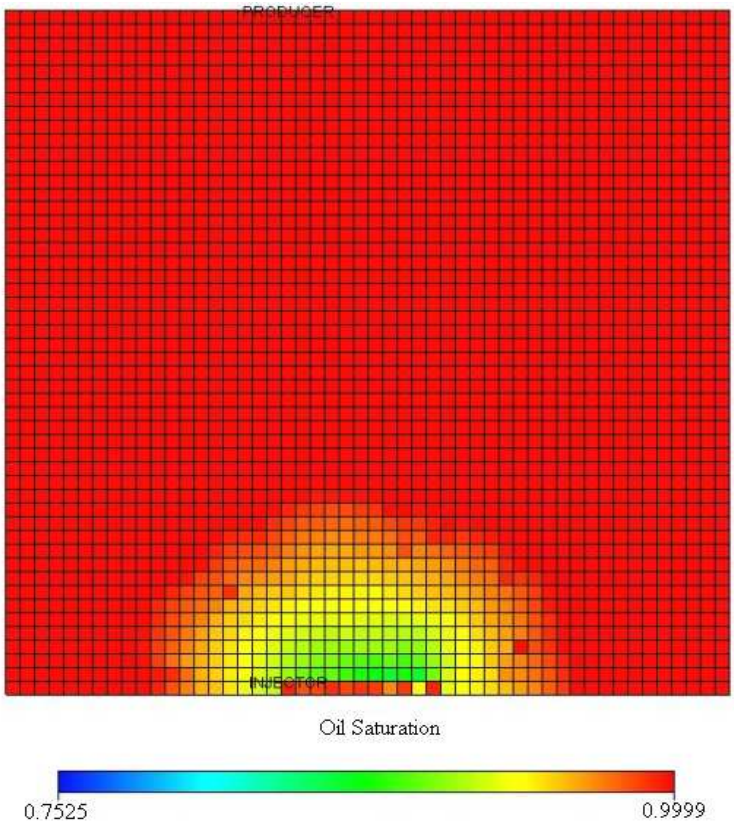

Figure 7.8: Simulated oil saturation profile at 5 seconds.

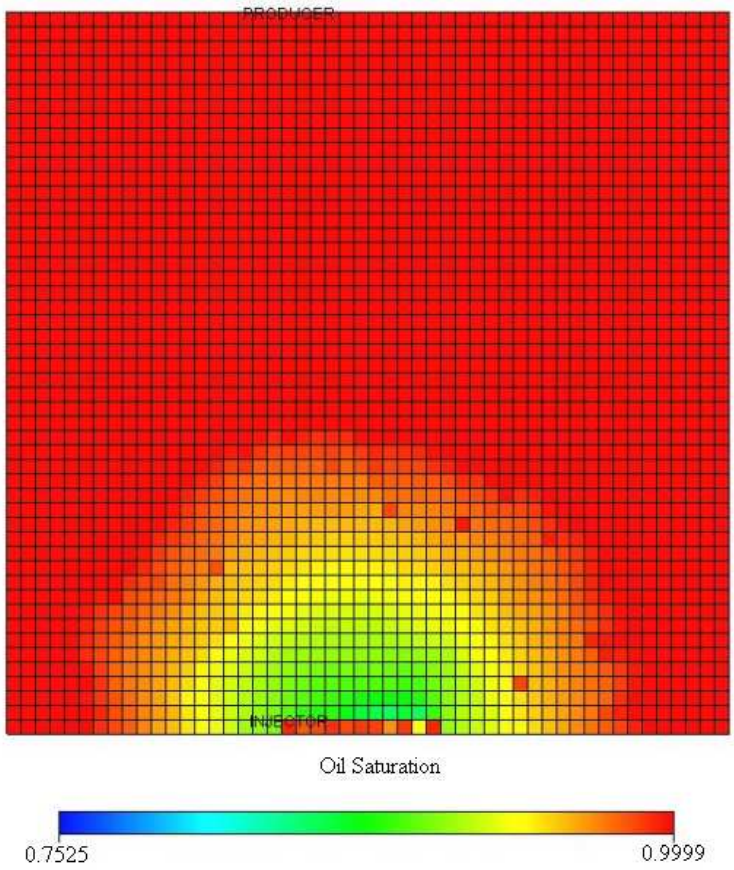

Figure 7.9: Simulated oil saturation profile at 10 seconds.

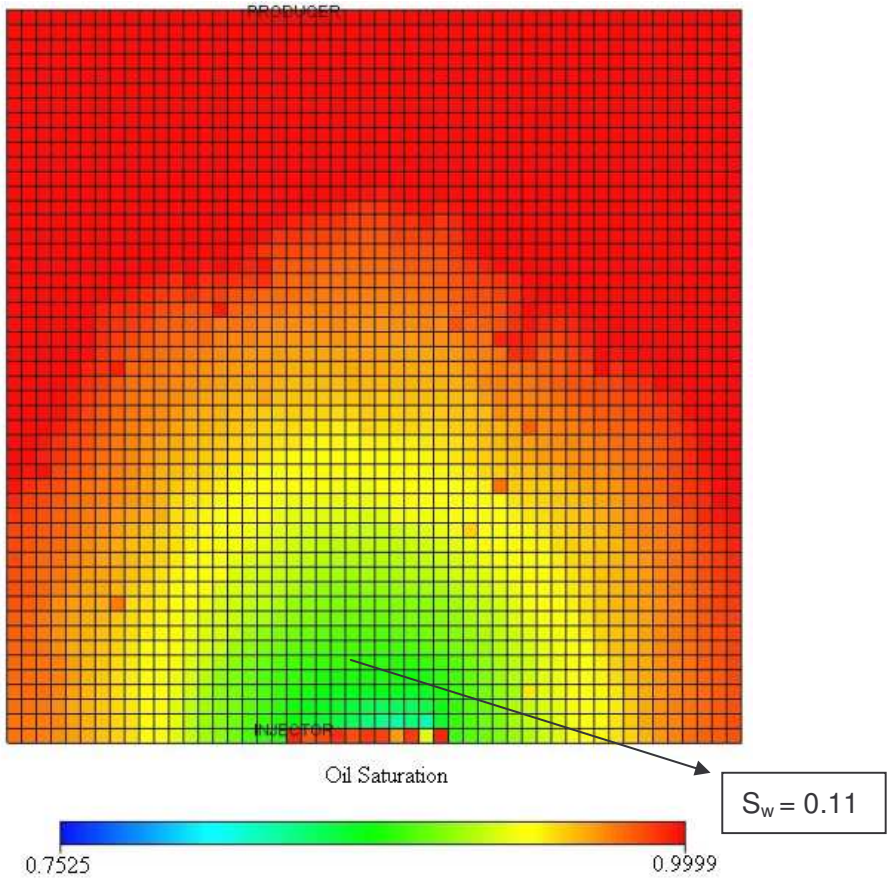

Figure 7.10: Simulated oil saturation profile at 25 seconds.

In order to avoid trouble with negative block pressure, the grid blocks perforated by the wells were modeled with zero capillary pressure. This results in somewhat higher saturations in these grid blocks, which is observed in the simulated saturation profiles.

When implementing capillary pressure in a UTCHEM model, tuning of the time stepping control becomes very important. For the simulation to run smoothly, DT (initial time step size) was reduced by a factor of 100, CNMAX (maximum courant number) by a factor of 500, and CNMIN (minimum courant number) by a factor of 100 000.

Simulated results of the immiscible displacement at zero initial water saturation, showed no initial fingering as was observed in the experiment. Fig. 7. 8-10 shows that an indifferent type displacement front is developed, which is a result of the capillary effect. In Fig. 7.10, the saturation of block (i=6, j=45) is given as S_w=0.11. Thus during the first 25 seconds of displacement, the water saturation in this block is increased by 11.2%.

The UTHEM simulator was unable to model the spreading process (see Fig. 4.2) observed during the laboratory immiscible displacement. The simulated saturation profiles showed an indifferent type displacement process. The initial displacement occurred much sooner for the simulated model, thus simulated saturation profiles were not comparable with the x-ray images from the experiment.

7.4 Simulation results from the second immiscible process - IMMISC2, Test 4 in Table 4.3

For the immiscible displacement of highly viscous paraffin by water at an initial water saturation of 0.12, no viscous fingering was observed in the experimental x-ray images. The mobility ratio in this process was very unfavorable. Capillary pressure was included in the model.

The simulation result from the second immiscible process gave a good match of the experimental results, but at earlier time steps than reported in the laboratory experiment. In order to observe the initiation of the displacement in the simulated results, time steps in the order of seconds were reported. The experimental x-ray images for the second immiscible displacement, is presented in Appendix 8. The results of the simulation of this process are presented in Fig. 7.11-13.

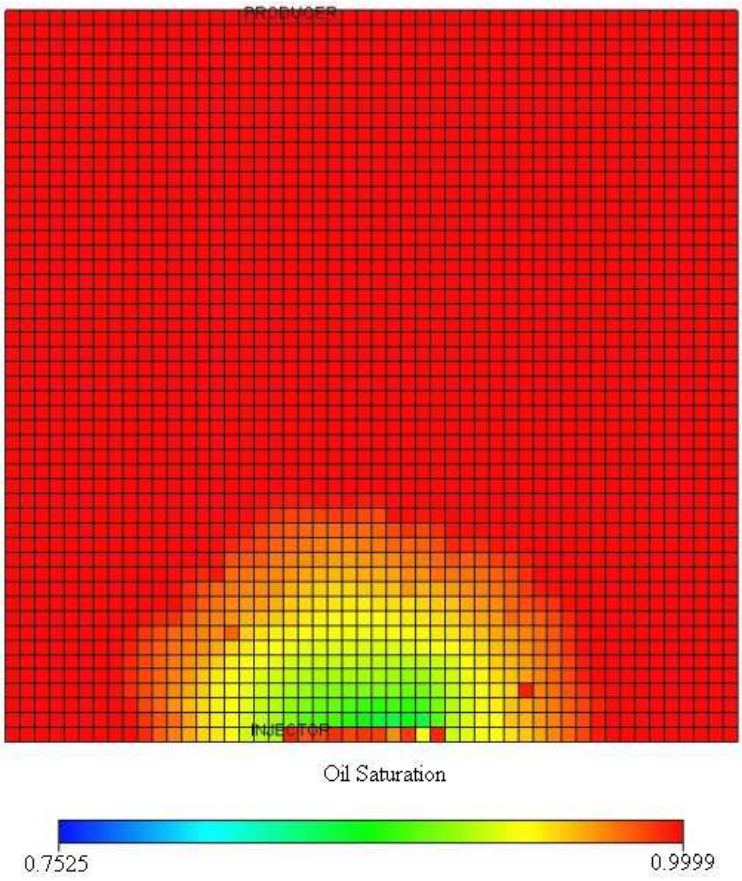

Figure 7.11: Simulated oil saturation profile at 5 seconds.

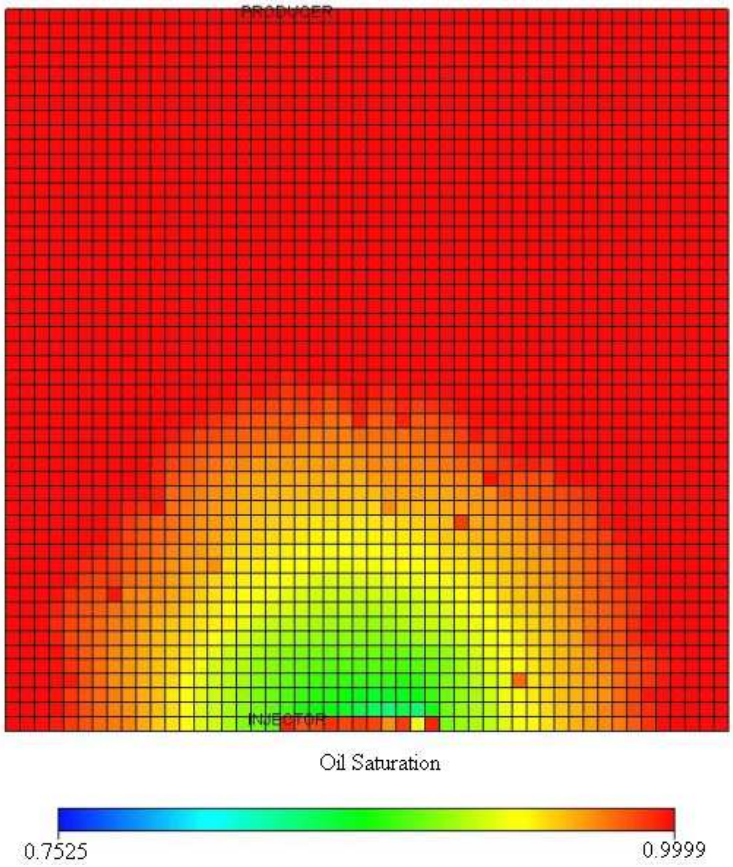

Figure 7.12: Simulated oil saturation profile at10 seconds.

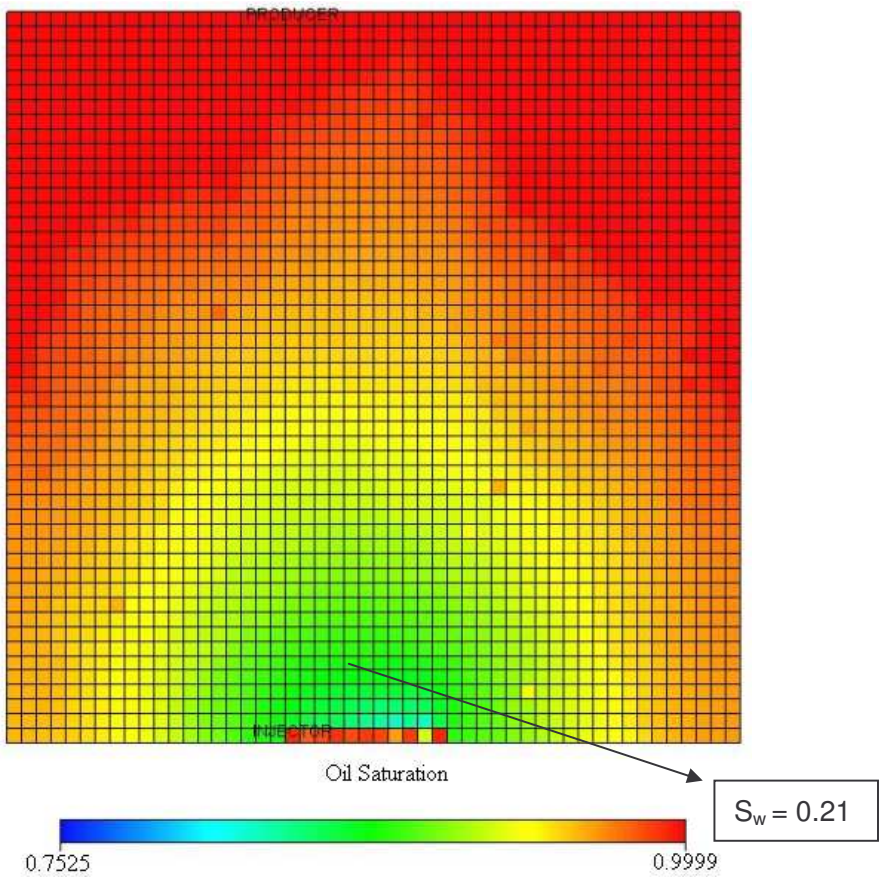

Figure 7.13: Simulated oil saturation profile at 25 seconds.

The grid blocks perforated by wells were also modeled with zero capillary pressure for the second immiscible process. The tuning parameters were set to be equal that of the first immiscible process, to avoid problems during the simulation.

Simulated results of the immiscible displacement at S_{wi}=0.12 , showed no initial fingering an indifferent type displacement front similar to that observed for the laboratory experiment. In Fig. 7.13, the saturation of block (i=6, j=45) is given as S_w=0.21. Thus during the first 25 seconds of displacement, the water saturation in this block is increased by 9.97%. Compared to section 7.3, the increase in water saturation after 25 seconds is nearly the same for immiscible displacements with or without the presence of initial water saturation.

The UTHEM simulator was able to model the indifferent process (see Fig. 4.2) observed during the laboratory immiscible displacement. Including capillary pressure dampens out the fingers observed in the miscible cases at similar unfavorable mobility ratio. The initial displacement occurred much sooner for the

simulated model, thus simulated saturation profiles were not comparable with the x-ray images from the experiment. The water relative permeability could be increased and oil relative permeability decreased to better history match the frontal displacement. The simulated results did, however, show that in the presence of initial water saturation and capillary pressure, an immiscible displacement at unfavorable mobility ratio is displaced in an indifferent manner.

7.5 Simulation results of the polymer flood following a water flood - POLY, Test 5 in Table 4.3

In the experimental study a polymer flood was performed after a water flood. The water flood gave a recovery of 45.3 %, and left the residual oil saturation at 0.47. After the polymer flood the recovery had increased to 64.0 %, and the residual oil saturation reduced to 0.31. The formation of an oil bank was easily observed on the x-ray images. The results of the simulation of the polymer flood, together with x-ray images from the experimental study [6], are presented in Fig. 7.14-17.

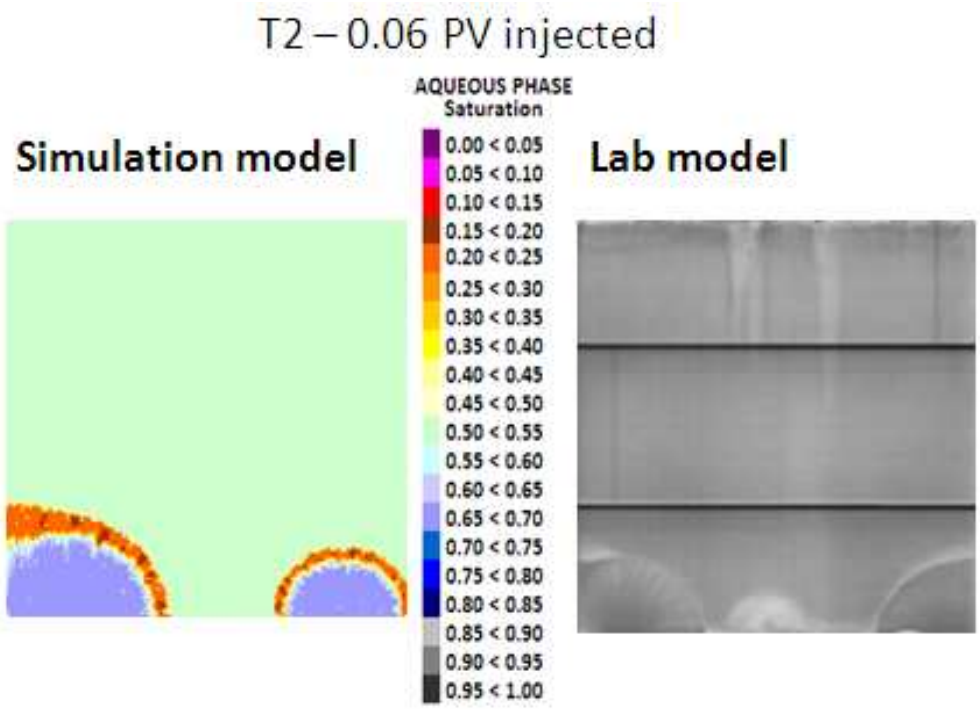

Figure 7.14: Simulated saturation profiles from the POLY model, and x-ray images at 0.06 PV injected.

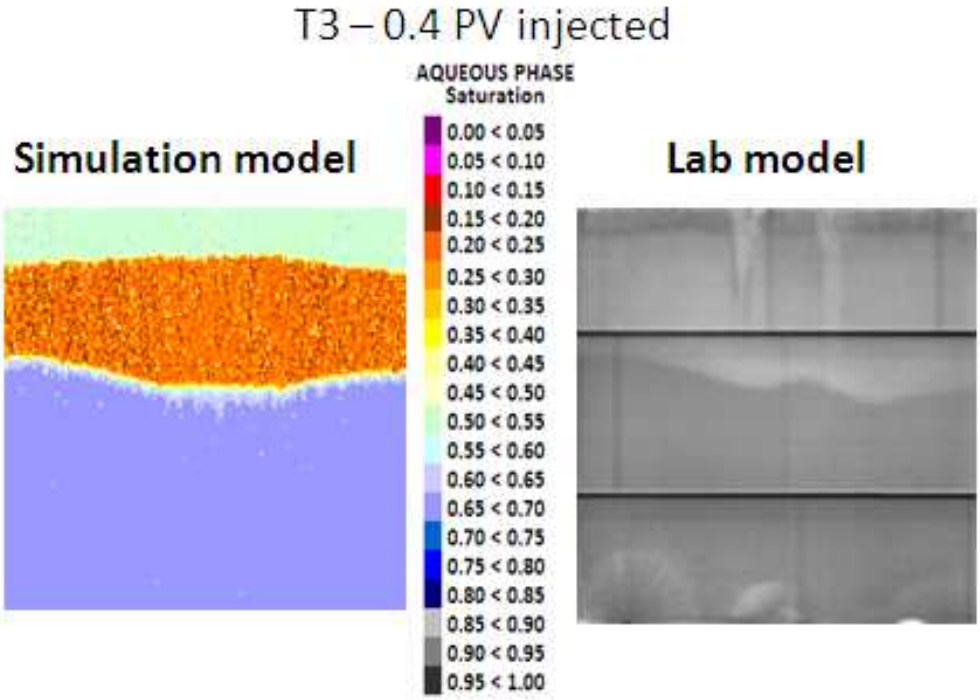

Figure 7.15: Simulated saturation profiles from the POLY model, and x-ray images at 0.4 PV injected.

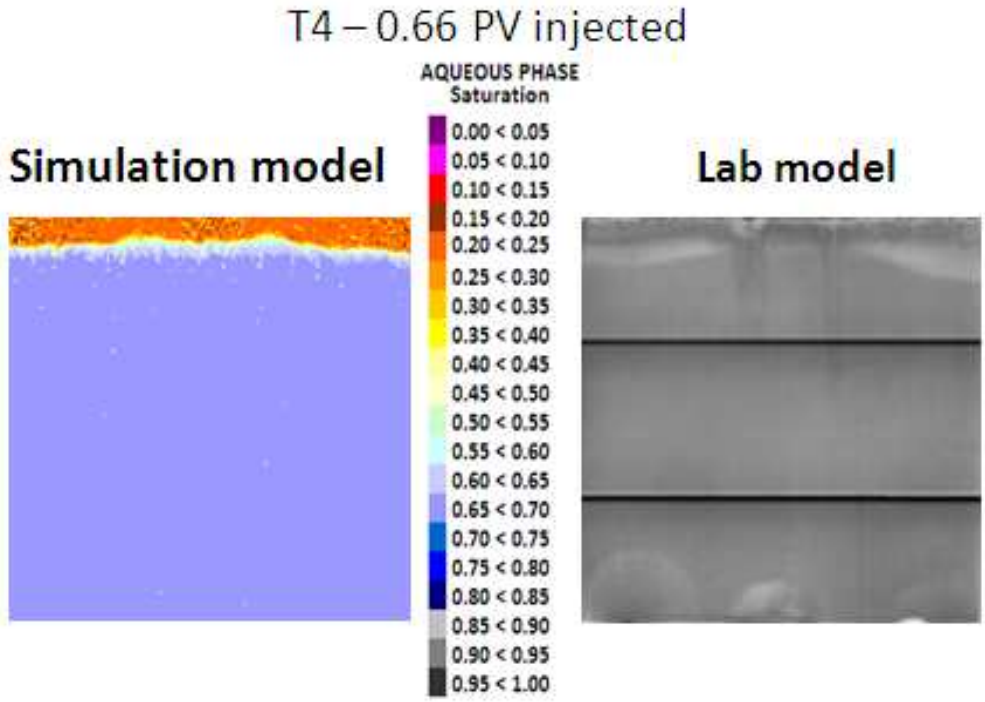

Figure 7.16: Simulated saturation profiles from the POLY model, and x-ray images at 0.66 PV injected.

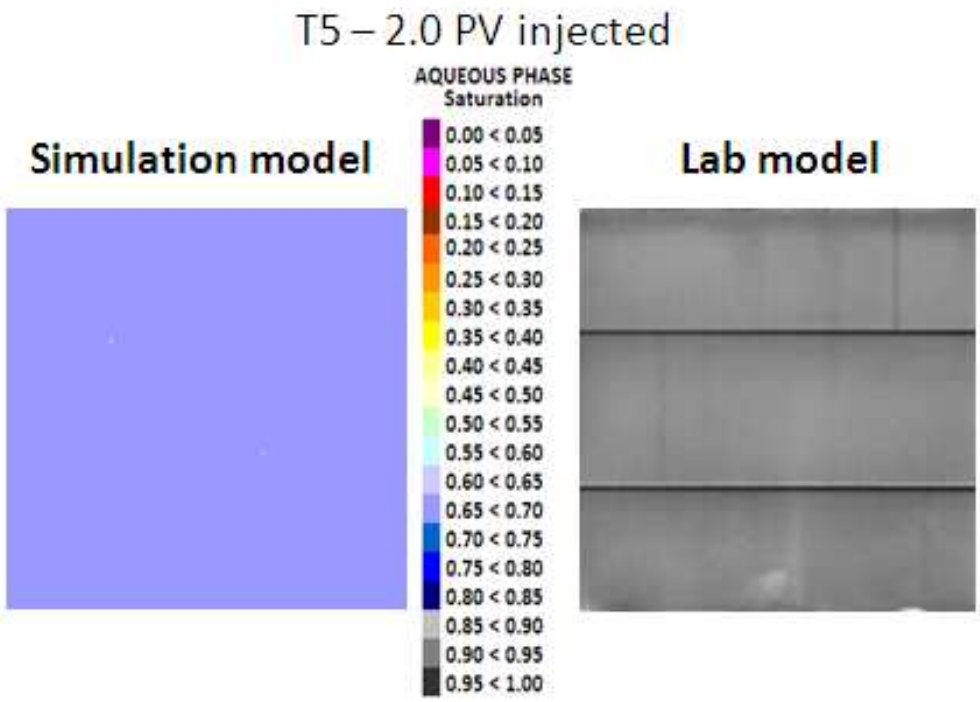

Figure 7.17: Simulated saturation profiles from the POLY model, and x-ray images at 2.0 PV injected.

The accumulation of an oil bank is observed in the simulated images. Already after 0.06 PV injection, the oil bank has formed in front of the polymer. After 0.4 PV of injection the oil bank has grown considerable in size. Compared to the x-ray image at this time step, the back of the oil bank is at about the same position. The front, however, has advanced further than in the simulated image. The images in Fig. 7.16 and 7.17 are very similar. An increase in water saturation throughout the model is easily observed at the end of the simulated polymer flood.

If the microscopic displacement efficiency for water and polymer is assumed to be equal, then $S_{or,w}$ is equal to $S_{or,p}$. The additional oil recovery during the polymer flood may come from locally spread higher oil saturation, or small oil pockets appearing homogeneous on the scale of the x-ray averaging. As the x-ray imaging show the accumulation of an oil bank in front of the polymer, it indicates areas locally unswept after the water flood. Alternatively, the mobilization of oil may be due to aerial variation in the saturation indicating that some areas may have not been completely flooded to S_{or} by the injection of water. As the injection of polymer may give an improvement in sweep, the early poorly contacted areas may be flooded down to residual oil saturation.

As mentioned earlier the experimental S_{or} after water flooding was 0.47. This, however, was just the measured residual oil saturation at the end of the experiment. After the polymer flood the measured S_{or} was 0.31. Polymer flooding normally does not cause a reduction in residual oil saturation. The same S_{or} could have been obtained by the water flood, had it been continued. As a result the residual oil saturation in the UTCHEM model for polymer flood, were set to be 0.31. This change in S_{or} was necessary in order to observe the formation of an oil bank.

The permeability field in the POLY model includes a wide distribution of permeabilities from 0.0001 μm^2 and all the way up to 10 μm^2. Since the initial water saturation in POLY were set to be 0.53 in the input file, this saturation will be uniformly distributed throughout the model. In order to test if this heterogeneity caused the accumulation of the oil bank, two new models were created from the POLY model. One model, POLY1, with the same heterogeneity distribution as in the POLY model, the other model, POLY2, was made homogeneous. Both POLY1 and POLY2 were first run with 9 PV water injection prior to the polymer flood. The results of the simulation of POLY1, together with x-ray images from the experimental study [6], are presented in Fig. 7.18-20.

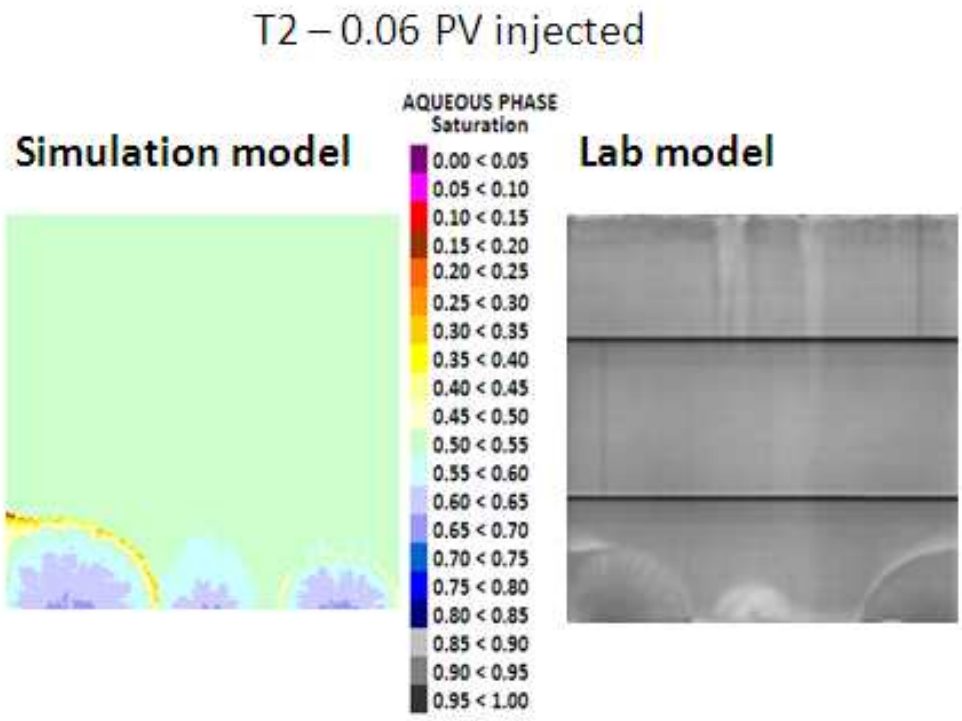

Figure 7.18: Simulated saturation profiles from the POLY1 model, and x-ray images at 0.06 PV injected.

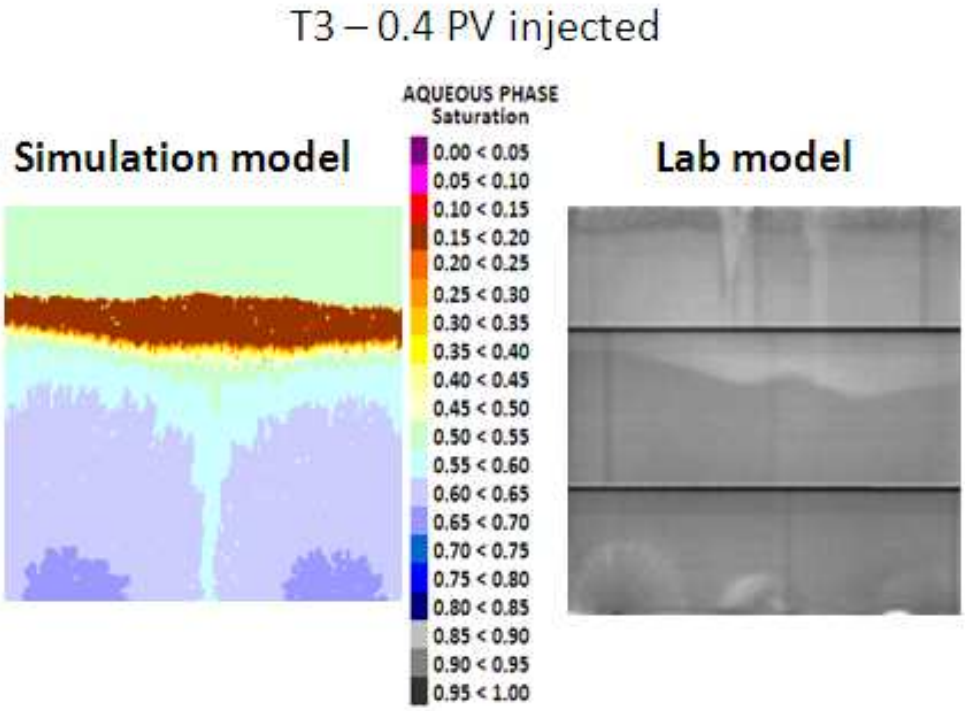

Figure 7.19: Simulated saturation profiles from the POLY1 model, and x-ray images at 0.4 PV injected.

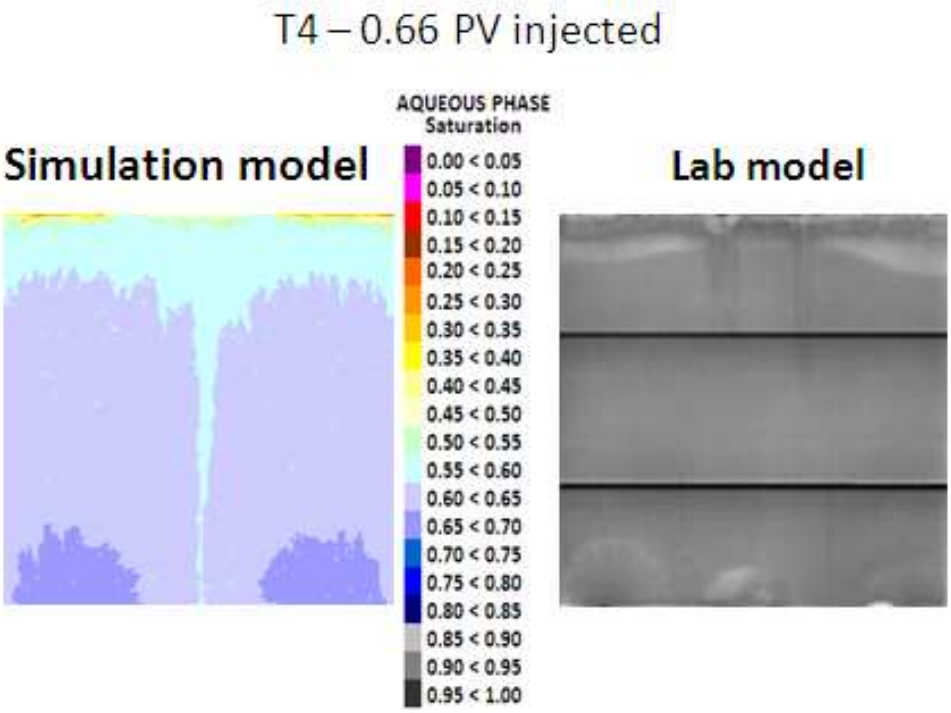

Figure 7.20: Simulated saturation profiles from the POLY1 model, and x-ray images at 2.0 PV injected.

The results of the simulation of POLY2, together with x-ray images from the experimental study [6], are presented in Fig. 7.21-23.

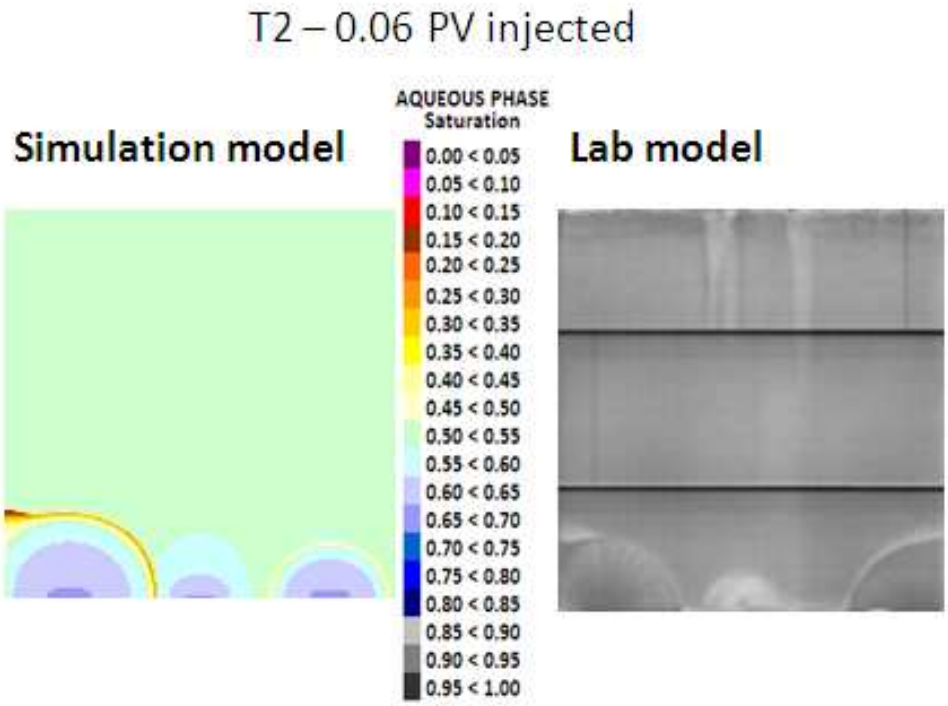

Figure 7.21: Simulated saturation profiles from the POLY2 model, and x-ray images at 0.06 PV injected.

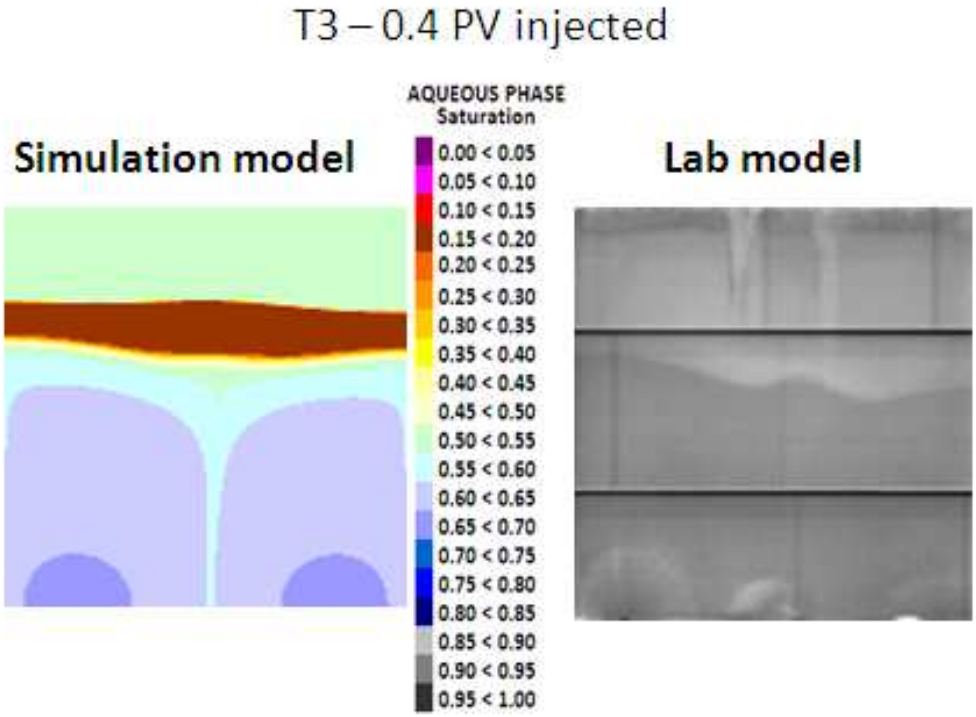

Figure 7.22: Simulated saturation profiles from the POLY2 model, and x-ray images at 0.4 PV injected.

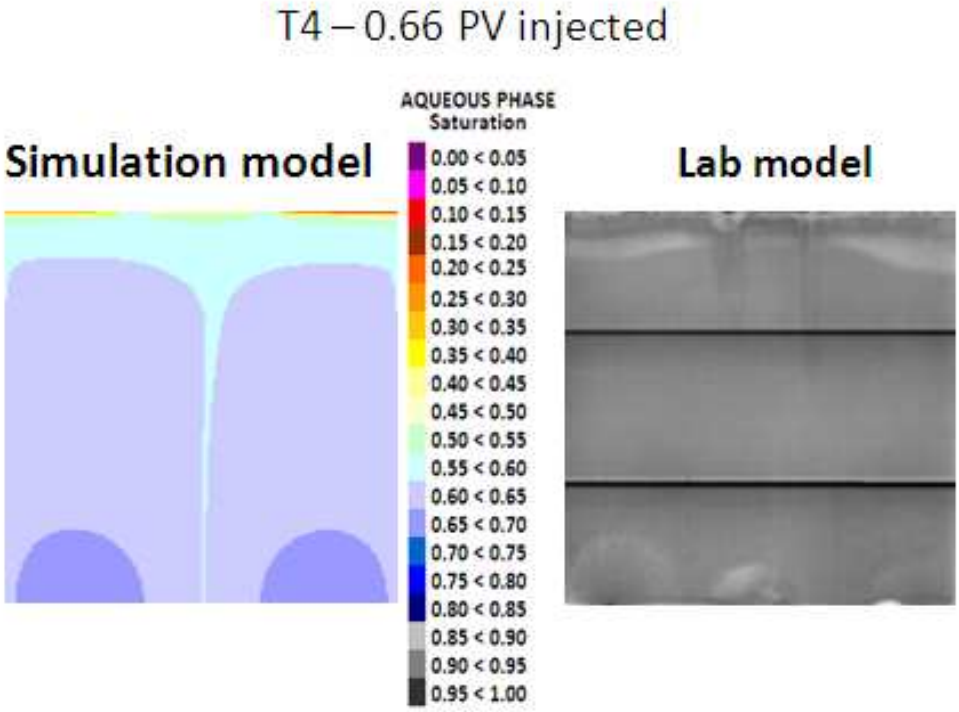

Figure 7.23: Simulated saturation profiles from the POLY2 model, and x-ray images at 2.0 PV injected.

From Fig. 7.18-7.23 the accumulation of an oil bank is observed. The formation and development of the oil bank is very similar in heterogeneous and the homogeneous model. The difference lie in the smoothness of the displacement fronts between water and oil bank, and between oil bank and polymer solution. As a very similar oil bank was formed in both models, the cause of the oil bank accumulation in the UTCHEM model was due to the change in residual oil saturation.

In comparing Fig. 7.18-7.20 to Fig. 7.14-7.16 it is observed that the accumulated oil bank is slightly different. In the results from POLY1 the oil bank appear more concentrated, than in the saturation profiles from POLY. The difference in the two models, POLY and POLY1, is in the distribution of the initial water saturation. In POLY the initial saturation is evenly distributed, but in POLY1 the initial water saturation increase towards the injector. This uneven distribution of initial water saturation may be the cause of the different appearance of the accumulated oil bank in POLY1. The input file for POLY2 is presented in Appendix 9.

The UTHEM simulator has proven very useful in modeling polymer flood after a water flood. The simulated saturation profiles showed the accumulation of an oil bank very similar to that observed in the

experimental x-ray images. An even distribution of initial water saturation of 0.53 gave results closes to experimental results. Heterogeneity did not seem to have an effect on the accumulation of an oil bank.

8 Conclusions

The UTCHEM chemical simulator was used in order to history match 2-D laboratory slab experiments of miscible displacements, immiscible displacements, and a polymer flood following after a water flood.

Variation in local grid block permeability was introduced to initiate viscous fingers. The average permeability was always equal to the permeability of the rock used in the experiments. A larger variation in the permeability field increased the fingering for miscible displacement.

Numerical dispersion has the effect of smearing out fronts during a displacement of fluids. Reducing the grid block size reduces the numerical dispersion. Therefore the grid block size for miscible displacement was set very low (0.002 m x 0.002 m). The grid block size could not be set to lower values due to limitation in stability of the UTCHEM simulator.

The UTCHEM simulator proved to be a useful tool in modeling miscible processes. Simulated saturation profiles, matching the experimental saturation profiles, were obtained for the miscible process at favorable mobility ratio. Some small instabilities were observed along the front of the displacement simulated saturation profile, probably due to the permeability variations between neighboring grid blocks.

Viscous fingering, very similar to that observed in the laboratory experiment, were obtained when modeling a miscible displacement at unfavorable mobility ratio in UTCHEM. The finger growth, in both length and width, seem to be somewhat more pronounced in the simulated results, thus giving a somewhat better sweep compared to the experiments. This could be due to limitation in the variations in the applied permeability field, or non-straight line relative permeability curves.

For the laboratory experiment of the immiscible displacement at S_{wi}=0, some initial fingers were generated, but water seemed to be strongly imbibed forming water films on the solid surface. The effect of capillarity on the frontal displacement was to smear out the front. This was not observed in the simulated results, which showed an indifferent type displacement. The establishment of water films is a kinetic reaction that is not included in the simulators and the experimental fast film formation was not observed in UTCHEM, thus initial fingering was not observed. In order to take a look at this establishing effect, the kinetics of spontaneous imbibitions would have to be involved. From a practical point of view, matching the immiscible displacement at S_{wi}=0 is of less importance, as all reservoirs contain an irreducible water saturation.

The experimental results of the immiscible displacement at S_{wi}=0.12 showed an indifferent type displacement process completely capillary dominated, even at unfavorable mobility ratio. These results were modeled successfully in UTCHEM.

The polymer option available in UTCHEM gave very satisfactory results compared to the laboratory experiment carried out at CIPR. An oil bank, very similar to what was observed in the experiment, was generated as seen in the simulated saturation profiles. A necessary condition for the accumulation of the oil bank was that the residual oil saturation was reduced from 0.53 (after the experimental water flood) to 0.31 (after the experimental polymer flood). No change of the relative permeability was necessary. The best match to the experimental results was obtained with an evenly distributed water saturation of 0.53. By injecting 9 PV of water into the model prior to the polymer flood, thus achieving an average water saturation of 0.53, the accumulated oil bank appeared more concentrated. In this case, the oil bank appeared a little different from that in the experimental results. Heterogeneity in the model had little if any affect on the accumulation of the oil bank.

9 Recommendations

During this thesis several areas emerged where further work is needed. These areas include the following:

- Increasing the Corey exponent, for both water and oil, from 1.4 to 2 resulted in increased amount of fingering, see section 5.2. Investigating the effect of the Corey exponent on the amount of fingering obtained by the UTCHEM simulator, could be interesting in order to see if other values for Corey exponents would give even a better match to experimental results.
- During miscible displacements, dispersion effects the displacement fronts. In the UTCHEM simulator, a severely heterogeneity field that is randomly distributed, may dominate the effect of dispersion. Investigating the effect of heterogeneity on dispersion in fine-grid UTCHEM models of miscible displacements, may provide answers to whether dispersion had any effect on the displacement fronts in the models presented in this thesis .
- Finger growth in both length and width are affected by dispersion. Both longitudinal and transverse dispersion may be represented by several models. The best choice for dispersion model should therefore be analyzed.
- Capillary pressure was applied to the numerical models of immiscible displacement. The simulated saturation profiles did not match the experimental images according to the time step. Thus a sensitivity study of the shape of the capillary pressure curve, and the absolute value of capillary pressure, would be interesting.
- All models presented in this thesis contained gird blocks of 0.002 m x 0.002 m x 0.02 m. Investigation of expanded grid sensitivity could done by looking at part of the model using even finer grid blocks.

10 Symbols and abbreviations

w	Water
o	Oil
M	Mobility ratio
M^o	Endpoint mobility ratio
k_{rw}, k_{r1}	Relative water permeability
k^o_{rw}	Endpoint relative water permeability
k_{ro}	Relative oil permeability
k^o_{ro}	Endpoint relative oil permeability
μ_w	Viscosity of water, mPa*s
μ_o	Viscosity of oil, mPa*s
NCS	Norwegian Continental Shelf
x_f	Distance from inlet to the undisturbed, see Fig. 2.1 page 10
ε	Distance from undisturbed front to the front in the high permeable region, see Fig. 2.1 page 10
k	Absolute permeability, cm^2
Δp	Pressure difference
ϕ	Porosity
λ_c	Finger width, cm
K_t	Transverse dispersion coefficient, cm^2/s
v	average interstitial velocity, cm/s
PV	Pore volume
PVI	Pore volume injected
c	Solvent concentration
u	Constant darcy velocity, cm/s
ρ	Density, gm/cm^3
g	Gravitational acceleration, cm/s^2
L_x	Length in the x-direction, cm
L_y	Length in the y-direction, cm
δ	Length of transition zone, cm
N_c	Capillary number

σ	Interfacial tension, mN/m
I_{SC}	Dimentionless number for cylindricalsystem
v_c	Characteristic velocity, m/s
D	Core diameter, m
C	Chuoke's constant
k_{wor}	Permeability to water at residual oil saturation, m^2
C^*	Wettability number
R_k	Permeability reduction factor
$R_{k,max}$	Maximum permeability reduction factor
R_F	Resistance factor
R_{RF}	Residual resistance factor
λ_w	Mobility of water
$\lambda_{w,A}$	Mobility of water after a polymer flood
λ_p	Mobility of polymer
K_{pl}	Power-law coefficient
n_{pl}	Power-law exponent
$\dot{\gamma}$	Effective shear rate
μ_1^0	Constant viscosity at low shear-rate
μ_1^∞	Constant viscosity above critical shear rate
$\dot{\gamma}_{1/2}$	Shear-rate when μ_1' is the average between μ_1^0 and μ_1^∞
$\hat{C}_4$	Polymer concentration in aqueous phase
C_{41}	Polymer concentration on rock surface
a_4, b_4	Constants
NMR	Nuclear magnetic resonance
NMRI	Nuclear magnetic resonance imaging
IPEC	Implicit pressure and Explicit Concentration
C_{SEP}	Effective salinity for polymer
A_{P1}, A_{P2}, A_{P3}	Constants
Sp	Slope of viscosity versus effective salinity on a log-log plot.
n_M	Empirical constant

$\dot{\gamma}_{eq}$	Equivalent shear-rate
$\dot{\gamma}_c$	$3.97C\ sec^{-1}$
$\bar{k}$	Average permeability
S_w, S_1	Saturation of water
S_{wi}	Initial water saturation
S_o	Saturation of oil
S_{or}	Residual oil saturation
S_n	Normalized saturation
K_{ref}	Reference permeability
c_{rk}, b_{rk}	Input parameters in UTCHEM
Dim	Dimension
IFT o-w	Interfacial tension between oil and water, mN/m
Q_w	Injection rate, m^3/day
HCPV	Hydro carbon pore volume
D	Darcy (permeability), $D=1.0132\ \mu m^2$
P_{cow}	Capillary pressure between oil and water
C_{pci}, EPC_i	Positive input parameters in UTCHEM
wt%	Weight percent
cp	centipoice, 1 cp = 1 mPa*s

11 References

1. Dake, L.P., "The Practice of Reservoir Engineering", Elsevier Science B. V., Amsterdam (1994)
2. Craig, F.F.Jr., "The Reservoir Engineering Aspects of Waterflooding", American Institute of Mining, Metallurgical, and Petroleum Engineers Inc., Texas (1971)
3. Skjæveland, S.M. and Kleppe, J., "Recent Advances in Improved Oil Recovery Methods for North Sea Sandstone Reservoirs", Norwegian Petroleum Directorate, Stavanger (1992)
4. Pye, D.J., "Improved Secondary Recovery by Control of Water Mobility", JPT (Aug. 1964) 911-6; Trans., AIME, 321
5. Sandiford, B.B., "Laboratory and Field Studies of Waterflood using Polymer Solution to Increase the Oil Recovery", JPT (Aug. 1964) 917-22; Trans., AIME, 322
6. Ormehaug, P.A. and Skauge, A., "Experimental Study of Increased Recovery in Adverse Mobility Reservoirs", Unifob AS – Avdeling for Petroleumsforskning, Bergen (2007)
7. Collins, R.E., "Flow of Fluids through Porous Media", Reinhold Publishing Co., New York City (1961) 201.
8. Homsy, G.M., "Viscous Fingering in Porous Medium", Ann. Rev. Fluid. Mech. 19, 271-311 (1987)
9. Stalkup, F.I.Jr, "Miscible Displacement", SPE Monograph Series, American Institute of Mining, Metallurgical, and Petroleum Engineers Inc., United States of America (1983)
10. Perrine, R.L., "The Development of Stability Theory for Miscible Liquid-Liquid Displacement", Soc. Pet. Eng. J. (1961) 17-25
11. Chuoke, R.L., van Meurs, P., and van der Poel, C., "The Instability of Slow, Immiscible Viscous Liquid-Liquid Displacements in Permeable Media", Trans., AIME (1959) 216, 188-94
12. Outmans, H.D., "Nonlinear Theory for Frontal Stability and Viscous Fingering in Porous Media", Soc. Pet. Eng. J. (1962) 165-76
13. Chandrasekhar, S., "Hydrodynamic and Hydromagnetic Stability", Oxford Clarendon Press, London (1961)
14. Gardner, J.W. and Ypma, J.G.J, "An Investigation of Phase Behavior – Macroscopic Bypassing Interaction in CO_2 Flooding", paper SPE 10686 presented at the 1982 SPE Enhanced Oil Recovery Symposium, Tulsa, April 4-7
15. Blackwell, R.J., Rayne, J.R., and Terry, W.M., "Factors Influencing the Efficiency of Miscible Displacement", Trans., AIME (1959)
16. Habermann, B., "The Efficiencies of Miscible Displacement as a Function of Mobility Ratio", Trans., AIME (1960)

17. Mahaffey, J.L., Rutherford, W.M., and Matthews, C.W., “Sweep Efficiency by Miscible Displacement in a Five-Spot”, Soc. Pet. Eng. J. (1966) 73-80, Trans., AIME, 237
18. Benham, A.L. and Olson, R.W., “A Model Study of Viscous Fingering”, Soc. Pet. Eng. J. (1963) 138-44, Trans., AIME, 228
19. Greenkorn, R.A., Johnson, C.R., and Haring, R.E.,” Miscible Displacement in a Controlled Natural System”, J. Pet. Tech (1965) 329-35, Trans., AIME, 234
20. Kyle, C.R. and Perrine, R.L., “Experimental Studies of Miscible Displacement Instability”, Soc. Pet. Eng. J. (1965) 189-95, Trans., AIME, 234
21. Slobod, R.L. and Thomas, R.A., “Effect of Transverse Diffusion on Fingering in Miscible Displacement”, Soc. Pet. Eng. J. (1963) 9-15
22. Perkins, T.K., Johnston, O.C., and Hoffman, R.N., “Mechanics of Viscous Fingering in Miscible Systems”, Soc. Pet. Eng. J. (1965) 301-17, Trans., AIME, 234
23. Perrine, R.L., “A Unified Theory for Stable and Unstable Miscible Displacement”, Soc. Pet. Eng. J. (1963) 205-13, Trans, AIME, 228
24. Koval, E.J., “A Method for Predicting the Performance of Unstable Miscible Displacement in Heterogeneous Media”, Soc. Pet. Eng. J. (1963) 145-54, Trans., AIME, 228
25. Pozzi, A.L. and Blackwell, R.J., “Design of Laboratory Models for Study of Miscible Displacement”, Soc. Pet. Eng, J. (1963) 28-40, Trans., AIME, 228
26. van der Poel, C., “Effect of Lateral Diffusivity on Miscible Displacement in Horizontal Reservoirs”, Soc. Pet. Eng. J. (1962) 317-26, Trans., AIME, 225
27. Dougherty, E.L., “Mathematical Model of an Unstable Miscible Displacement”, Soc. Pet. Eng. J. (1963) 155-65
28. Peaceman, D.W. and Rachford, H.H.Jr., “Numerical Calculation of Multidimensional Miscible Displacement”, Soc. Pet. Eng. J. (1962) 327-39, Trans., AIME, 225
29. Perrine, R.L., “Stability Theory and Its Use to Optimize Solvent Recovery of Oil”, Soc. Pet. Eng. J. (1961) 9-16, Trans., AIME, 222
30. Bucley, S.E. and Leverett, M.C., “Mechanisms of Fluid Displacement in Sands”, Trans., AIME (1942) 146, 107-116
31. Brigham, W.E., Reed, P.W., and Dew, J.N., “Experiments on Mixing During Miscible Displacement in Porous Media”, Soc. Pet. Eng. J. (1961) 1-8, Trans., AIME, 222
32. Handy, L.L., “An Evaluation of Diffusion Effects in Miscible Displacement”, Trans., AIME (1959) 216, 61-63

33. Claridge, E.L., “Prediction of Recovery in Unstable Miscible Flooding”, Soc. Pet. Eng. J. (1972) 143-55
34. Peters, E.J., Broman, W.H., and Broman, J.A., “A Stability Theory for Miscible Displacement”, paper SPE 13167 presented at the 1984 SPE Annual Technical Conference and Exhibition, Houston
35. Heller, J.P., “Onset of Instability Patterns Between Miscible Fluids in Porous Media”, J. Appl. Phys. (1966) 37, 1566-79
36. Todd, M.R. and Longstaff, W.J., “The Development, Testing and Application of a Numerical Simulator for Predicting Miscible Flood Performance”, JPT (1972) 874-82, Trans., AIME, 253
37. Warren, J.E. and Skiba, F.F., “Macroscopic Dispersion”, Soc. Pet. Eng. J. (1964) 215-25, Trans., AIME, 231
38. Christie, M.A. and Bond, D.J., “Detailed Simulation of Unstable Processes in Miscible Flooding”, SPERE (1987) 514-22, Trans., AIME, 283
39. Hatziavramidis, D.T., “A New Computational Approach to the Miscible Displacement Problem”, SPERE (1990) 631-38
40. Araktingi, U., Orr, F.M., and Sageev Grader, A., ”Reservoir Characterization for the CO_2 Enhanced Oil Recovery Process”, annual report Contract No. DE-AC21-85MC22042, U.S. DOE, Washington, DC (1987)
41. Giordano, R.M., Salter, S.J., and Mohanty, K.K., “The Effects of Permeability Variations on Flow in Porous Media”, paper SPE 14365 presented at the 1985 SPE Annual Technical Conference and Exhibition, Las Vegas
42. Christie, M.A., “High-Resolution Simulation of Unstable Flows in Porous Media”, SPERE (1989) 297-303, Trans., AIME, 287
43. Slobod, R.L. and Caudle, B.H., “X-Ray Shadowgraph Studies of Areal Sweepout Efficiencies”, Trans., AIME, 195, 265-270 (1972)
44. Dyes, A.B., Caudle, B.H., and Erikson, R.A., “Oil Production after Breakthrough – As Influenced by Mobility Ratio”, Trans., AIME, 201, 81-86 (1954)
45. Craig, F.F.Jr., Geffen, T.M., and Morse, R.A., “Oil Recovery Performance of Pattern Gas or Water Injection Operations from Model Tests”, Trans., AIME, 204, 7-15 (1955)
46. Kimbler, O.K., Caudle, B.H., and Cooper, H.E.Jr., “Areal Sweepout Behavior in a Nine-Spot Injection Pattern”, J. Pet. Tech. 199-202 (1964), Trans., AIME, 231
47. Maloy, K.J., Felder, J., and Jossang, T., “Viscous Fingering Fractals in Porous Media”, Phys. Rev. Lett. 55, 2688-2691 (1985)

48. Stokes, J.P., Weitz, D.A., Gollub, J.P., Dougherty, A., Robbins, M.O., Chaikin, P.M., and Lindsay, H.M., "Interfacial Stability of Immiscible Displacement in a Porous Medium", Phys. Rev. Lett. 57, 1718-1721 (1986)
49. Perkins, T.K. and Johnston, O.C., "A Study of Immiscible Fingering in Linear Models", Soc. Pet. Eng. J. 39-46 (1969)
50. Peters, E.J. and Flock, D.L., "The Onset of Instability During Two-Phase Immiscible Displacement in Porous Media", Paper SPE 8371 presented at the 1979 SPE Annual Technical Conference and Exhibition, Las Vegas
51. Hornof, V. and Morrow, N.R., "Flow Visualization of the Effects of Interfacial Tension on Displacement", SPE Reservoir Engineering, 251-256 (1988)
52. Peters, E.J., Broman, J.A., and Broman, W.H.Jr., "Computer Image Processing: A New Tool for Studying Viscous Fingering in Corfloods", Paper SPE 13668, SPE Reservoir Engineering (1987)
53. Howison, S.D., "Fingering in Hele-Shaw Cells", J. Fluid Mech. (1986) 167 439-53
54. Park, C.W., Gorell, S., and Homsy, G.M., "Two-Phase Displacement in Hele-Shaw Cells: Experimentson Viscously Driven Instabilities", J. Fluid Mech. (1984) 141, 257-87
55. Hele-Shaw, H.S., "Investigation of the Nature of Surface Resistance of Water and of Streamline Motion under Certain Experimental Conditions", Trans. Instn. Nav. Archit., London 40, 21-46 (1898)
56. Saffman, P.G. and Taylor, G., "The Penetration of a Fluid into a Porous Medium or Hele-Shaw Cell Containing a more Viscous Liquid", Proc. Roy. Soc. London A245, 312-329 (1958)
57. Bear, J., "Dynamics of Fluids in Porous Media", American Elsevier Publishing Co., New York, 687-701 (1972)
58. Park, C.W. and Homsy, G.M., "The Instability of Long Fingers in Hele-Shaw Flows", Phys Fluids, 28, 1583-1585 (1985)
59. Claridge, E.L., "A Trapping Hele-Shaw Model for Miscible-Immiscible Flooding Studies", Paper SPE 4105 presented at the 1972 SPE Annual Meeting, San Antonio, October 8-11
60. King, M.J., "Viscous Fingering and Probabilistic Simulation", Standard Oil Research and Development, Cleveland (1988)
61. Fanchi, J.R., Shank, G.D., and Christiansen, R.L., "Chaos: A Source of Miscible Viscous Fingering Instabilities", Petroleum Society of CIM/Soc. Pet. Eng., paper no.CIM/SPE 90-99 (1990)
62. Rachford, H.H.Jr., "Instability in Water Flooding Oil from Water Wet Porous Media Containing Connate Water", Soc. Pet. Eng. J. (1964) 133-148, Trans., AIME, 231

63. Hagoort, J., “Displacement Stability of Water Drives in Water-Wet-Bearing Reservoirs”, Soc. Pet. Eng. J. (1974) 63-74
64. Wooding, R.A., “The Stability of a Viscous Liquid in a Vertical Tube Containing Porous Material”, Proc. R. Soc. London, Ser. A. 252 (1959) 120-130
65. Schowalter, W.R., “Stability Criteria for Miscible Displacement of Fluid from a Porous Medium”, A.I.Ch.E.J. (1965) 99-105
66. Lee, S.T., Gary Li, K.M., and Culham, W.E., “Stability Analysis of Miscible Displacement Processes”, paper SPE 12631 presented at the SPE/DOE Fourth Symposium on Enhanced Oil Recovery in Tulsa (1984)
67. van Damme, H., Obrecht, F., Levitz, P., Gatineau, L., and Laroche, C., “Fractal Viscous Fingering in Clay Slurries”, Nature 320, 731-733 (1986)
68. Mandelbrot, B.B., “How Long is the Coast of Britain? Statistical Self-Similarity and Fractional Dimension”, Science 155, 636-638 (1967)
69. Lake, L.W., “Enhanced Oil Recovery”, Prentice-Hall Inc., New Jersey (1989)
70. Skarestad, M. and Skauge, A., ”PTEK 213 – Reservoarteknikk II”, Universitetet i Bergen, Bergen (2005)
71. Lindley, J., U.S. Department of Energy, Bartesville, Oklahoma
72. http://www.npd.no/NR/exeres/E61B2C94-1AC4-431F-9820-790E43F83458.htm?NRMODE=Unpublished
73. Daccord, G., Nittmann, J., and Stanley, H.E., “Radial Viscous Fingers and Diffusion-Limited Aggregation: Fractal Dimension and Growth Sites”, Phys. Rev. Lett. 56, 336-339 (1986)
74. Gharbi, R.B., Qasem, F., and Peters, E.J., “A relationship Between the Fractal Dimension and Scaling Groups of Unstable Miscible Displacements”, Soc. Pet. Eng., paper first presented at the 2000 SPE Annual Technical Conference and Exhibition, Dallas (2000)
75. Christie, M.A., “Numerical Techniques for High Resolution Simulation of Instabilities”, SPE 16005, presented at 1987 Symposium Reservoir Simulation, San Antonio
76. King, M. and Sher, H., “Probabilistic Stability Analysis of Multiphase Flow in Porous Media”, SPE 14366, presented at the 1985 Annual SPE Mtg., Las Vegas
77. DeGregoria, A.J., “A Predictive Monte-Carlo Simulation of Two-Fluid Flow through Porous Media at Finite Mobility Ratio”, Phys. Fluids 28, 1216-1220
78. King, M. and Scher, H., “A Probabilistic Approach to Multiphase and Multi-component Fluid Flow in Porous Media”, submitted to Phys. Rev. A.

79. Tan, C.T. and Homsy, G.M., “Simulation of Nonlinear Viscous Fingering in Miscible Displacement”, Phys. Fluids 31 (1988) 1330-1338
80. Araktingi, U.G. and Orr, F.M.Jr., “Viscous Fingering in Heterogeneous Porous Media”, SPE Advanced Technology Series, Vol 1, No. 1 (1992)
81. Taylor, G.I., “The Instability of Liquid Surfaces when Accelerated in a Direction Perpendicular to Their Planes”, I, Proc. R. Soc. London, Ser. A, 201, pp.192-196, (1950)
82. Christiansen, R.L. and Fanchi, J.R., “Initiation and Propagation Mechanisms of Miscible Viscous Fingers”, paper presented at the 1990 AIChE Spring National Meeting, Orlando
83. Dumoré, J.M., “Stability Considerations in Downward Miscible Displacement”, Soc. Pet. Eng. J. (1964) 358-362
84. Peters, E.J. and Hardham, W.D., “A Comparison of Unstable Miscible and Immiscible Displacements”, paper SPE 19640 presented at the 64th Annual Technical Conference and Exhibition of the Society of Petroleum Engineers, San Antonio (1989)
85. Peters, E.J. and Flock, D.L., “The Onset of Instability During Two-Phase Immiscible Displacement in Porous Media”, Soc. Pet. Eng., AIME, (1981)
86. van Meurs, P., “The Use of a Transparent Three Dimensional Model for Studying the Mechanism of Flow Processes in Oil Reservoirs”, Trans., AIME (1957) 210, 295-301
87. van Meurs, P. and van der Poel, C., ”A theoretical Description of Water-Drive Processes Involving Viscous Fingering”, Trans., AIME (1957) 213, 103-112
88. Scheidegger, A.E., “On the Stability of Displacement Fronts in Porous Media: A Discussion of the Muskat-Aronofsky Model”, Cdn. J. of Physics (1960) 38, 153-162
89. Flock, D.L., Peters, E.J., Baird, H., Wilborg, R., and Kloepfer, J., “The Influence of Frontal Instabilities During Viscous Oil Displacement”, The Oil Sands of Canada-Venezuela, CIM (1977) 17, 380-385
90. Shupe, R.D., “Chemical Stability of Polyacrylamide Polymers”, Journal of Petroleum Technology, 33 (1981), 1513-1329
91. O’Leary, W.B., Boivin, J.W., Dasinger, B.L., Beck, D., Goldman, I.M., and Wernau, W.C., “Biocide Evaluation Against Xanthan Polymer-Degrading Bacteria”, paper SPE 13588 presented at the 1985 International Symposium on Oilfield and Geothermal Chemistry, Phoenix, April 9-11
92. Flory, P.J., “Principles of Polymer Chemistry”, Ithaca, New York: Cornell University Press, 1953.
93. Meter, D.M. and Bird, R.B., “Tube Flow of Non-Newtonian Polymer Solutions, Parts 1 and 2-Laminar Flow and Rheological Models”, American Institute of Chemical Engineers Journal (1964), 878-881, 1143-1150

94. Jennings, R.R., Rogers, J.H., and West, T.J., “Factors Influencing Mobility Control by Polymer Solutions”, Journal of Petroleum Technology, 23 (1971), 391-401

95. Duda, J.L., Klaus, E.E, and Fan, S.K., “Influence of Polymer Molecule-Wall Interactions on Mobility Control”, Soc. Pet. Eng. J., 2 (1981) 613-622

96. Fanchi, J.R. and Christiansen, R.L., “Applicability of Fractals to the Description of Viscous Fingering”, Soc. Pet. Eng., paper presented at the 64th Annual Technical Conference and Exhibition of the Society of Petroleum Engineers, San Antonio (1989)

97. Brock, D.C. and Orr, F.M., “Flow Visualization of Viscous Fingering in Heterogeneous Porous Media”, Soc. Pet. Eng., paper presented at the 66th Annual Technical Conference and Exhibition of the Society of Petroleum Engineers, Dallas (1991)

98. Majors, P., Li, P., and Peters, E.J., “NMR Imaging of Immiscible Displacements in Porous Media”, Soc. Pet. Eng., paper first presented at the 1995 SPE Annual Technical Conference and Exhibition, Dallas (1997)

99. Delshad, M., Pope, G.A., and Sepehrnoori, K., “A Compositional Simulator for Modeling Surfactant Enhanced Aquifer Remediation”, Journal of Contaminant Hydrology, 23, 303-327

100. Han, P., Delshad, M., Sepehrnoori, K., and Pope, G.A., ”A Fully Implicit, Parallel, Compositional Chemical Flooding Simulator”, Soc. Pet. Eng., paper first presented at the 2005 SPE Annual Technical Conference and Exhibition, Dallas (2007)

101. Technical Documentation of UTCHEM, prepared by Reservoir Engineering Research Program Center for Petroleum and Geosystems Engineering, The University of Texas at Austin, Texas (2000)

102. Lin, E., “A Study of Micellar/Polymer Flooding Using a Compositional Simulator”, Ph.D. dissertation, The University of Texas at Austin, (1981)

103. Sorbie, K.S., “Polymer-Improved Oil Recovery”, CRC Press, Inc., Boca Raton, Florida, (1991)

104. Wreath, D., Pope, G.A., and Sepehrnoori, K.S., “Dependence of Polymer Apparent Viscosity on the Permeable Media and Flow Conditions”, In Situ, 14(3), 263-284, (1990)

105. Hirasaki, G.J. and Pope, G.A., “Analysis of Factors Influencing Mobility and Adsorption in the Flow of Polymer Solution Through Porous Media”, Soc. Pet. Eng. J,. (1974) 337-346

106. Brooks, R.H. and Corey, A.T., “Properties of Porous Media Affecting Fluid Flow”, J. Irrig. Drain. Div., 6, 61, (1966)

107. Leverett, M.C., “Capillary Behavior in Porous Solids”, Trans. AIME, 142, 152, (1941)

108. Delshad, M., Delshad, M., Pope, G.A., and Lake, L.W., ”Two- and Three Phase Relative Permeability of Miellar Fluids”, Paper SPE 13581 presented at the 1985 International Symposium on Oilfield and Geothermal Chemistry, Phoenix, April 9-11

109. Fulcher, R.A., Ertekin, T., and Stahl, C.D., “The Effect of Capillary Number and Its Constituents on Two-Phase Relative Permeability Curves”, Paper SPE 12170 presented at the 1983 SPE Annual Technical Conference and Exhibition, San Francisco, Oct. 5-8

110. Rhamakrishan, T.S, and Wasan, D.T., “The Relative Permeability Function for Two.Phase Flow in Porous Media: Effect of Capillary Number”, paper SPE/DOE 12693 presented at the 1984 SPE/DOE Symposium on EOR Tulsa, April 15-18

111. Harbert, L.W., “Low Interfacial Tension Relative Permeability”, paper SPE 12171 presented at the 1983 SPE Annual Technical Conference and Exhibition, San Francisco, 5-8

12 Appendix

12.1 Appendix 1: Complete picture series for section 5.1 – Effect of numerical dispersion

The complete picture series for the effect of numerical dispersion are presented in Fig. 12.1-6.

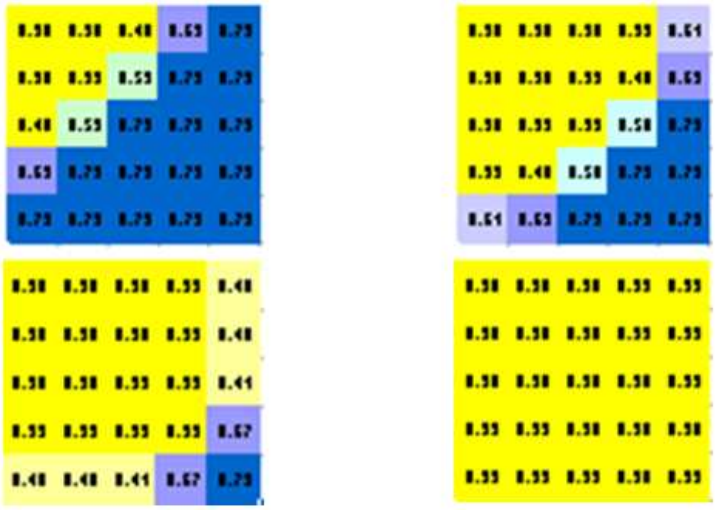

Figure 12.1: The effect of amount and size of grid blocks on the shape of the displacement front for a model of 5x5x1 gridblocks. The yellow and blue colors in the figure represent the water and oil respectively. The figures from left to right are respectively at 1 PV, 2 PV, 3 PV, and 4PV injected.

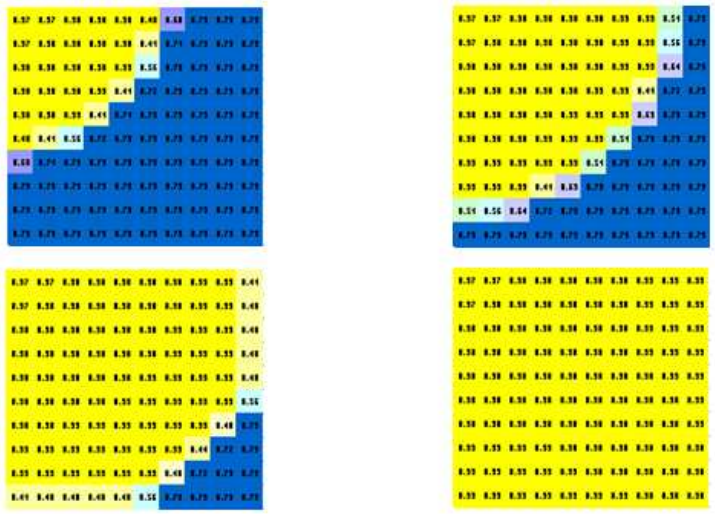

Figure 12.2: The effect of amount and size of grid blocks on the shape of the displacement front for a model of 10x10x1 gridblocks. The yellow and blue colors in the figure represent the water and oil respectively. The figures from left to right are respectively at 1 PV, 2 PV, 3 PV, and 4PV injected.

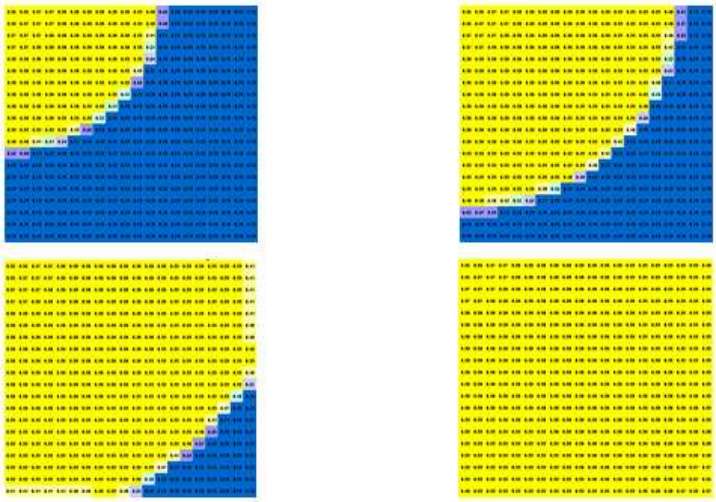

Figure 12.3: The effect of amount and size of grid blocks on the shape of the displacement front for a model of 20x20x1 gridblocks. The yellow and blue colors in the figure represent the water and oil respectively. The figures from left to right are respectively at 1 PV, 2 PV, 3 PV, and 4PV injected.

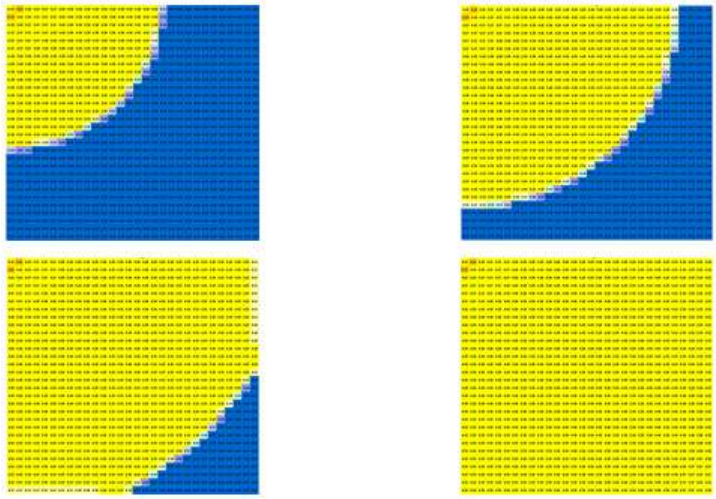

Figure 12.4: The effect of amount and size of grid blocks on the shape of the displacement front for a model of 30x30x1 gridblocks. The yellow and blue colors in the figure represent the water and oil respectively. The figures from left to right are respectively at 1 PV, 2 PV, 3 PV, and 4PV injected.

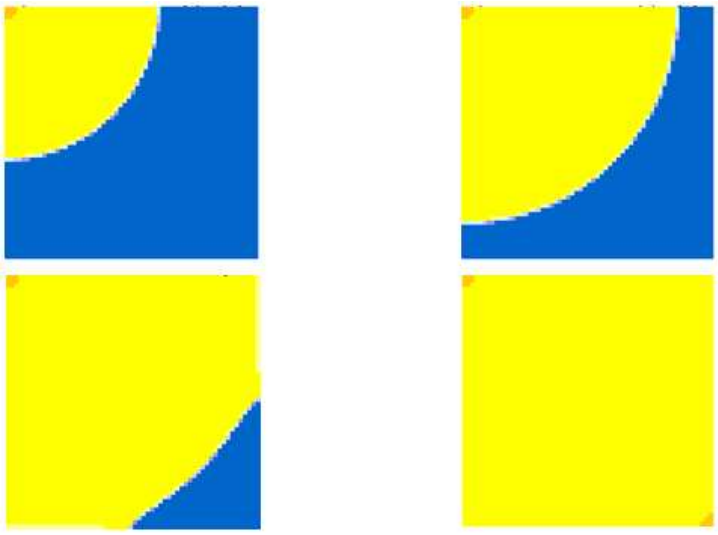

Figure 12.5: The effect of amount and size of grid blocks on the shape of the displacement front for a model of 60x60x1 gridblocks. The yellow and blue colors in the figure represent the water and oil respectively. The figures from left to right are respectively at 1 PV, 2 PV, 3 PV, and 4PV injected.

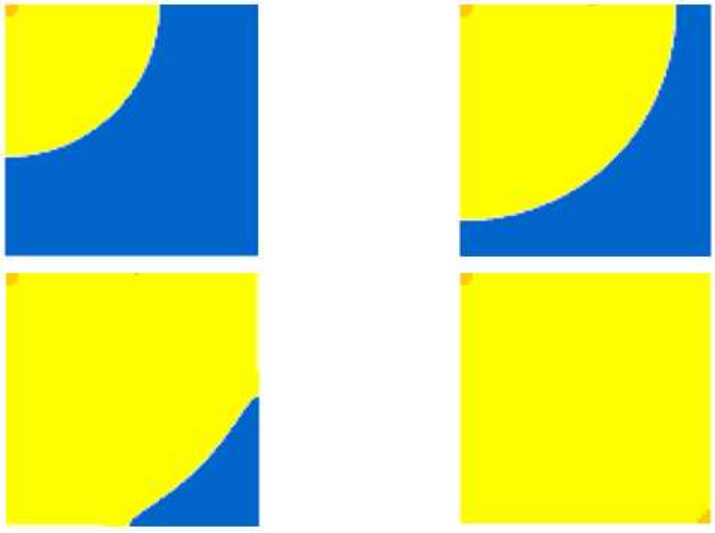

Figure 12.6: The effect of amount and size of grid blocks on the shape of the displacement front for a model of 100x100x1 gridblocks. The yellow and blue colors in the figure represent the water and oil respectively. The figures from left to right are respectively at 1 PV, 2 PV, 3 PV, and 4PV injected.

12.2 Appendix 2: Complete picture series for section 5.2 – Effect of heterogeneities

Complete picture series for section 5.2 in the case where residual saturations and relative permeability curves are independent on capillary number.

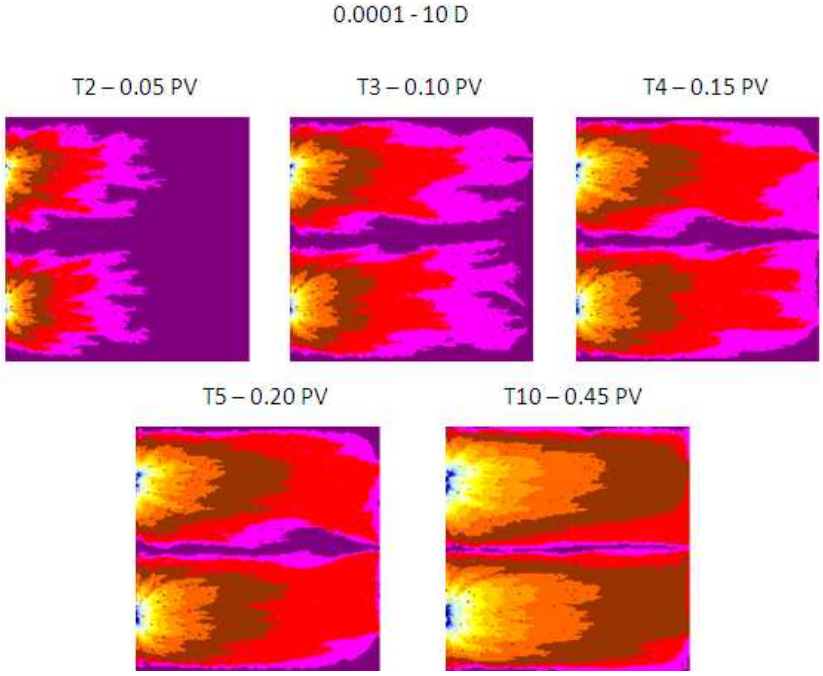

Figure 12.7: Simulated saturation profiles at different PV injected with a heterogeneity variation of 0.0001 – 10D. Residual saturations and relative permeability curves are independent on capillary number.

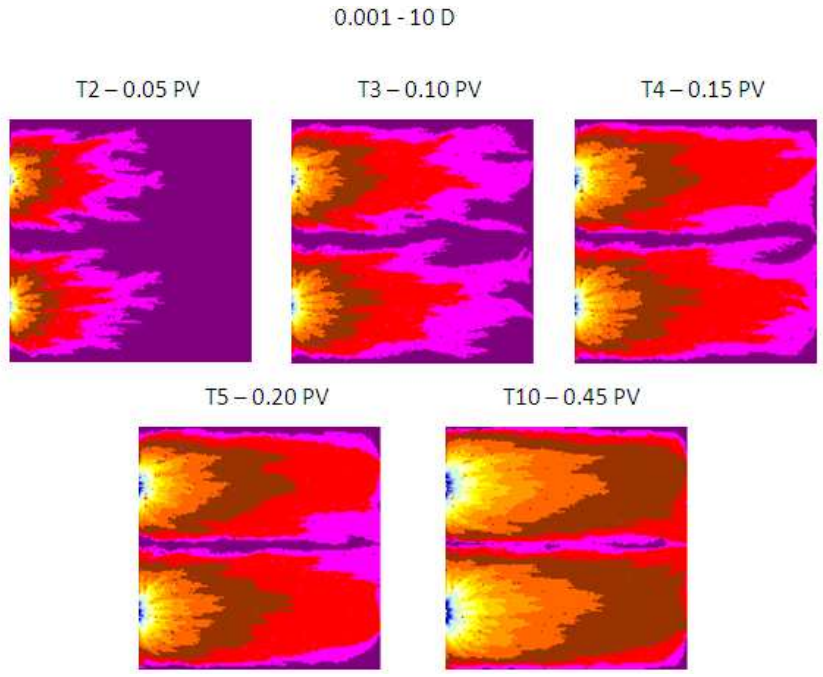

Figure 12.8: Simulated saturation profiles at different PV injected with a heterogeneity variation of 0.001 – 10D. Residual saturations and relative permeability curves are independent on capillary number.

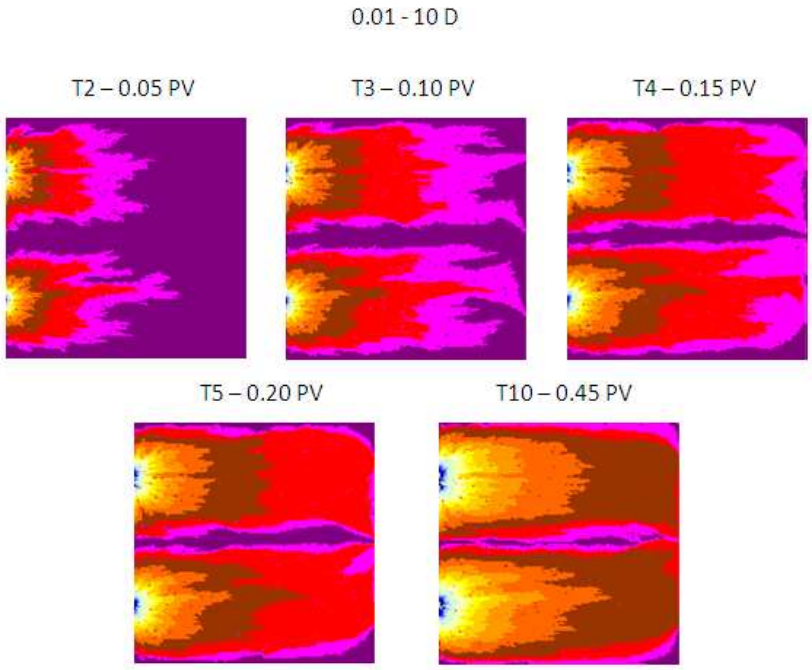

Figure 12.9: Simulated saturation profiles at different PV injected with a heterogeneity variation of 0.01 – 10D. Residual saturations and relative permeability curves are independent on capillary number.

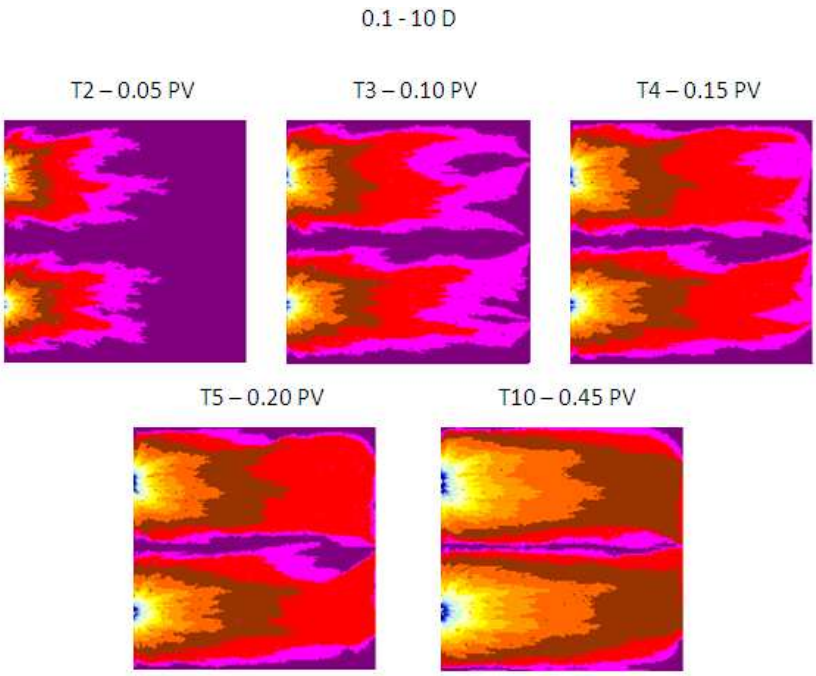

Figure 12.10: Simulated saturation profiles at different PV injected with a heterogeneity variation of 0.1 – 10D. Residual saturations and relative permeability curves are independent on capillary number.

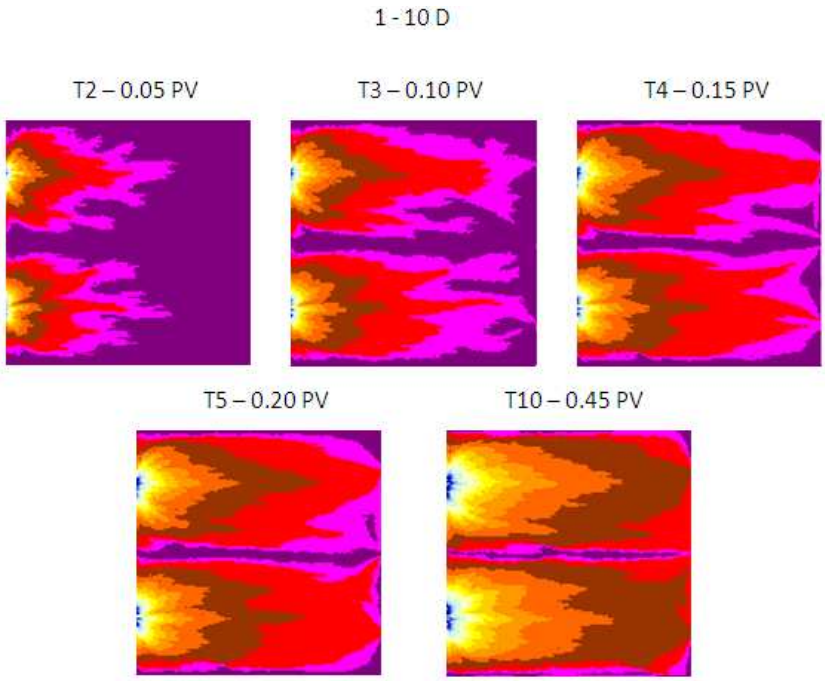

Figure 12.11: Simulated saturation profiles at different PV injected with a heterogeneity variation of 1 – 10D. Residual saturations and relative permeability curves are independent on capillary number.

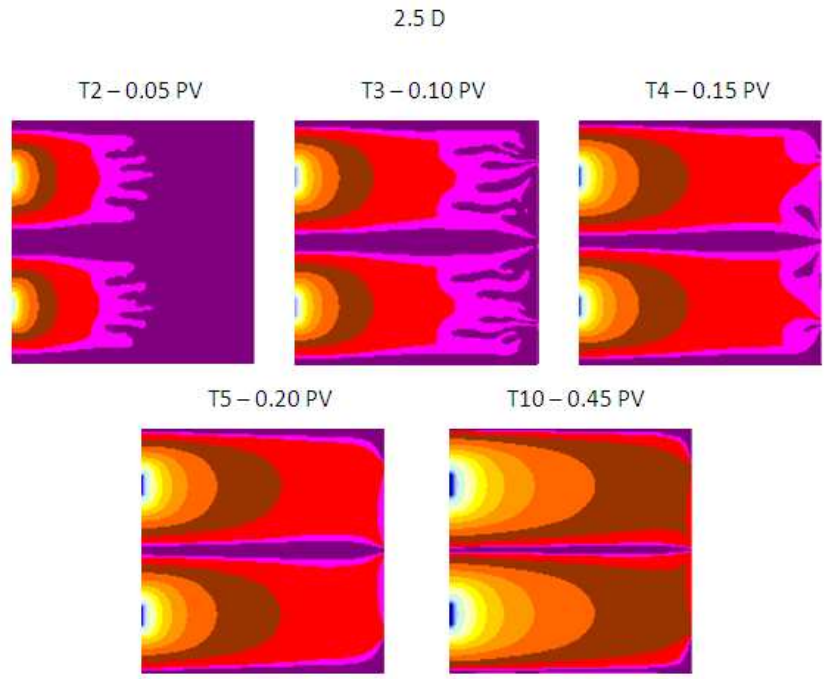

Figure 12.12: Simulated saturation profiles at different PV injected with a heterogeneity variation of 2.5D. Residual saturations and relative permeability curves are independent on capillary number.

Complete picture series for section 5.2 in the case where residual saturations and relative permeability curves are dependent on capillary number.

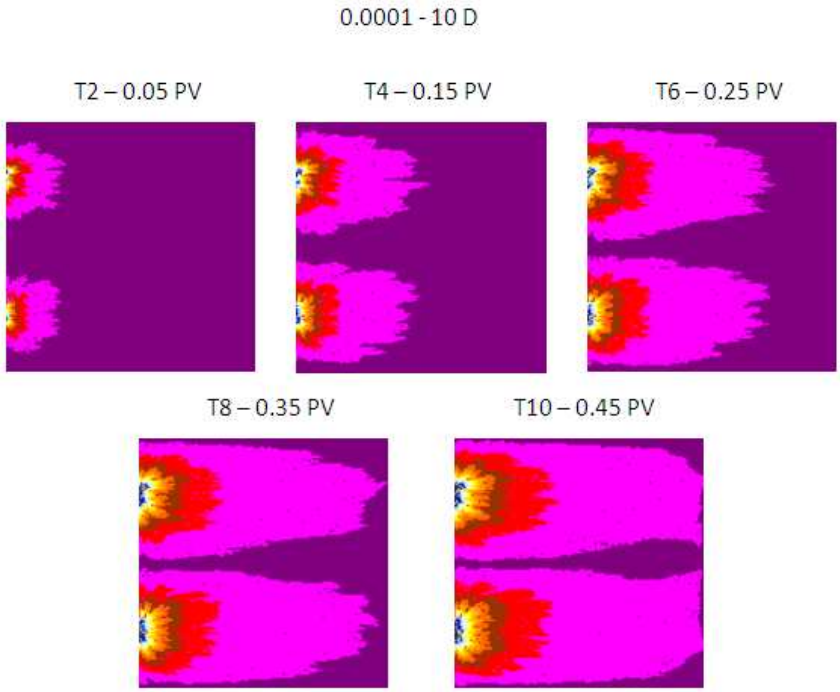

Figure 12.13: Simulated saturation profiles at different PV injected with a heterogeneity variation of 0.0001 – 10D. Residual saturations and relative permeability curves are independent on capillary number.

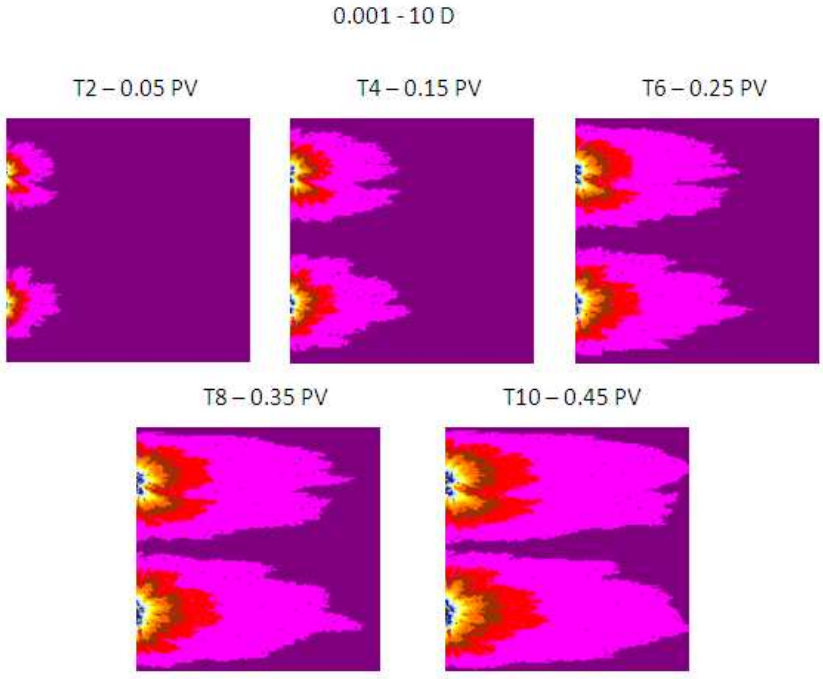

Figure 12.14: Simulated saturation profiles at different PV injected with a heterogeneity variation of 0.001 – 10D. Residual saturations and relative permeability curves are independent on capillary number.

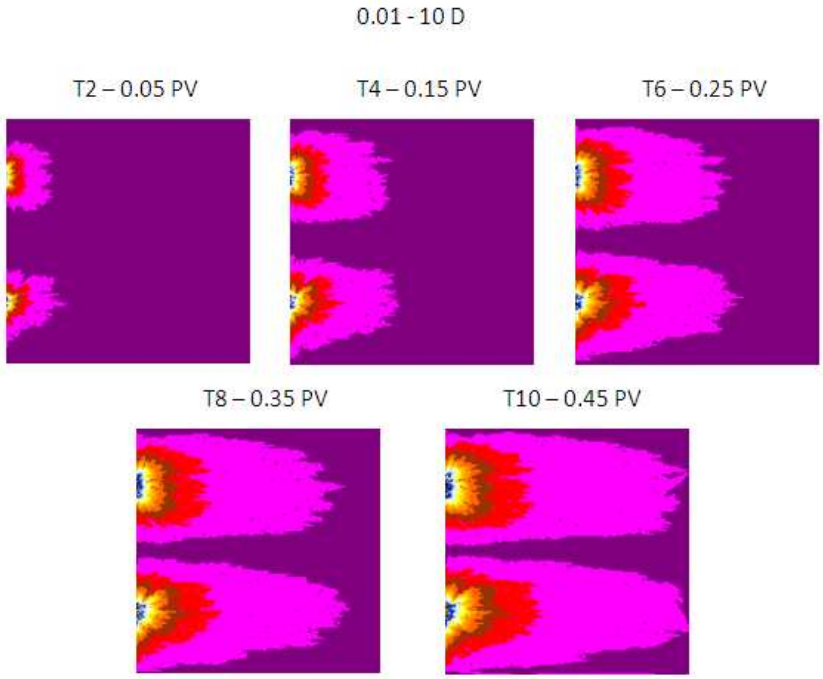

Figure 12.15: Simulated saturation profiles at different PV injected with a heterogeneity variation of 0.01 – 10D. Residual saturations and relative permeability curves are independent on capillary number.

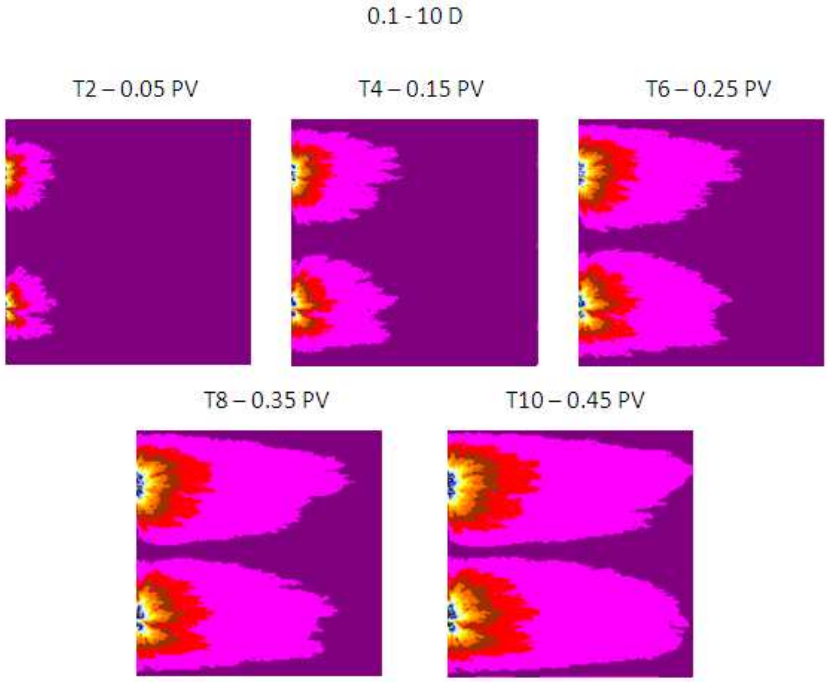

Figure 12.16: Simulated saturation profiles at different PV injected with a heterogeneity variation of 0.1 – 10D. Residual saturations and relative permeability curves are independent on capillary number.

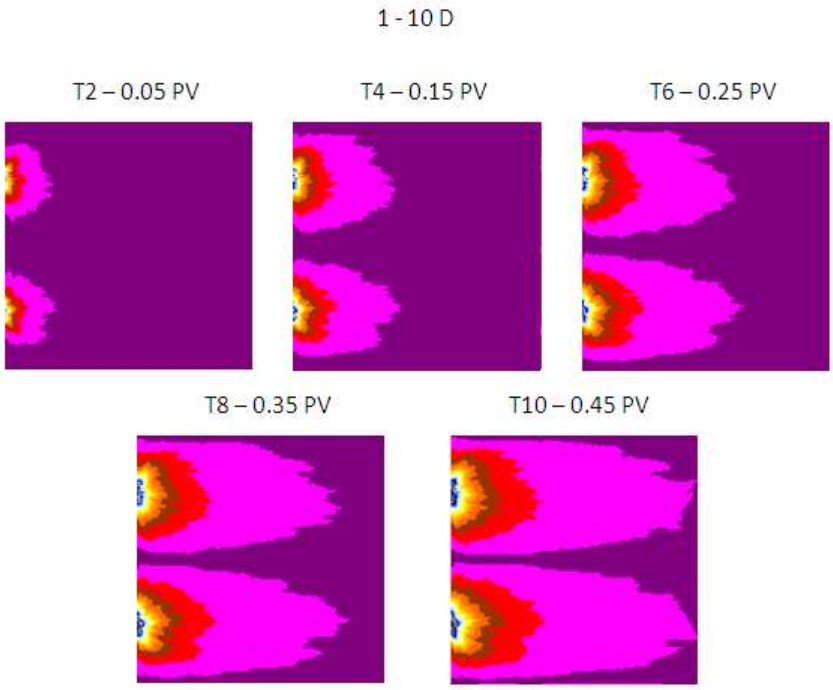

Figure 12.17: Simulated saturation profiles at different PV injected with a heterogeneity variation of 1 – 10D. Residual saturations and relative permeability curves are independent on capillary number.

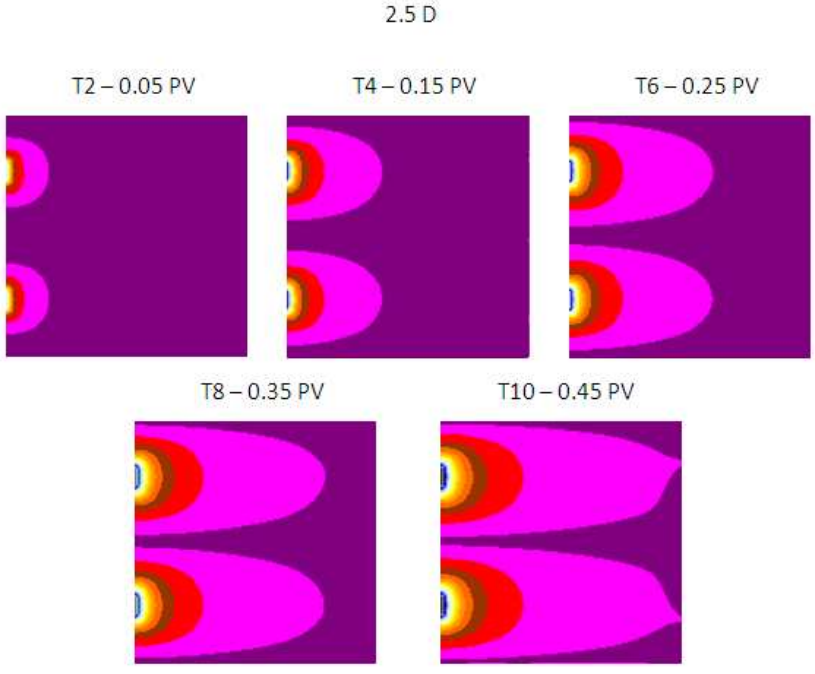

Figure 12.18: Simulated saturation profiles at different PV injected with a heterogeneity variation of 2.5D. Residual saturations and relative permeability curves are independent on capillary number.

12.3 Appendix 3: Theory regarding the dependence of residual saturations on capillary number

Capillary number and the Capillary Desaturation Curve

The capillary number is the dimensionless ratio between viscous and capillary forces, and is usually expressed in Eq. 12.1 [69],

$$N_c = \frac{u\mu}{\sigma} \tag{12.1}$$

where u is the Darcy velocity of the displacing fluid, μ is the displacing fluid viscosity, and σ is the interfacial tension between the displaced and the displacing fluid. UTCHEM operates with this classical definition of capillary number.

The capillary number is closely related to the residual saturations through the Capillary Desaturation Curve, CDC. The CDC defines mobilization of each phase as the capillary number increases, and is often modeled by a log- linear expression similar to Eq. 12.2 [3],

$$S_r = b_0 + b_1 \log N_c \tag{12.2}$$

where S_r is residual saturation, and b_0 and b_1 are linear coefficients. The CDC is largely influenced by wettability and pore-size distribution [3], as illustrated by Fig. 12.19.

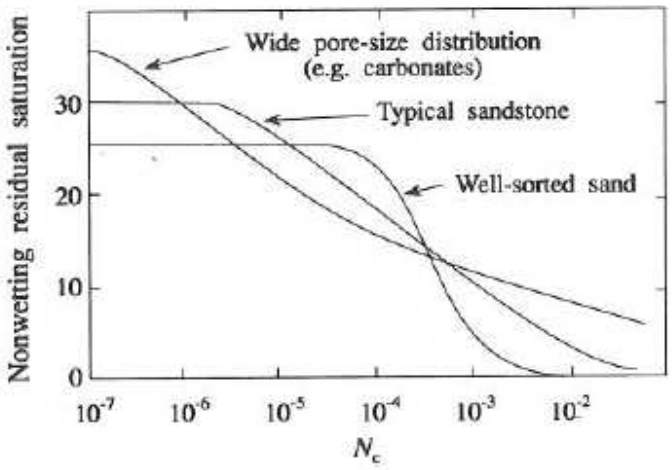

(a) Effect of pore-size distribution on the CDC.

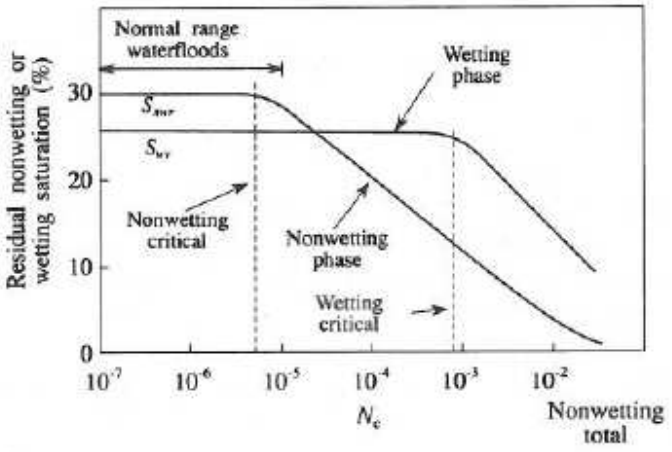

(b) Effect of wettability on the residual saturation of wetting and nonwetting phase.

Figure 12.19: Characteristic Capillary Desaturation Curves [69].

At low capillary numbers, the residual saturations for both wetting and non-wetting phase are fairly constant. A decrease in residual saturations does not occur until a critical capillary number, $N_c^{Critical}$, is reached.

As residual saturations change with increasing capillary number, the endpoints and exponents of the relative permeability curve change [108,109,110,111,112]. Because of this the relative permeability should be measured for several capillary numbers during the decline period. Due to the fact that such measurements are both rather expensive and time consuming, they are usually only performed at one high

and one low capillary number. In the case of a two-phase system the endpoints of the relative permeability is usually modeled as a function of the other phase residual saturation [3].

Bond and Trapping number

The mobilization of residual saturations is also dependent on buoyancy forces represented by the bond number. The bond number is the dimensionless ratio between gravity and capillary forces, Eq. 12.3,

$$N_{B_l} = \frac{kg\left(\rho_l - \rho_{l'}\right)}{\sigma_{ll'}} \tag{12.3}$$

where g is the gravity constant, and k is the permeability.

Resent developments have led to a new dimensionless number, the trapping number, which includes both the viscous and gravitational forces.
The different forces controlling the movement of an oil drop in a porous media are the trapping force due to the capillary pressure, the viscous force due to the hydraulic gradient, and gravity. Depending on the direction of flow, the gravity might act as either a trapping or a driving force. The mobilization criteria for the drop can be expressed as in Eq. 12.4,

$$\text{Hydraulic force + Buoyancy force} \geq \text{Capillary force}$$
$$\Delta L\left|\nabla\Phi_w - g\Delta\rho\right| \geq \Delta P_c \tag{12.4}$$

The left-hand side of this equation defines the trapping number, Eq. 12.5 [101],

$$N_{Tl} = \frac{\left|-\vec{\bar{k}}\cdot\vec{\nabla}\Phi_{l'} - \vec{\bar{k}}\cdot\left[g\left(\rho_{l'} - \rho_l\right)\vec{\nabla}h\right]\right|}{\sigma_{ll'}} \tag{12.5}$$

UTCHEM uses the trapping number to model the residual saturations dependency on interfacial tension. This is necessary in order to model the combined effect of viscous and buoyancy forces. UTCHEM does however offer an option for ignoring the buoyancy forces and only considering the capillary forces.

In UTCHEM the residual saturations are computed as a function of trapping number in the following way, Eq. 12.6 [101],

$$S_{\ell r} = \min\left(S_{\ell}, S_{\ell r}^{high} + \frac{S_{\ell r}^{low} - S_{\ell r}^{high}}{1 + T_{\ell} N_{T_{\ell}}} \right) \tag{12.6}$$

where $S_{\ell r}^{low}$ and $S_{\ell r}^{high}$ are the input residual saturations for phase ℓ at low and high trapping numbers.

In UTCHEM the endpoints and exponents in relative permeability functions are modeled in Eq. 12.7 and 12.8 [101],

$$k_{rl}^{o} = k_{rl}^{o^{low}} + \frac{S_{l'r}^{low} - S_{l'r}}{S_{l'r}^{low} - S_{l'r}^{high}} \left(k_{rl}^{o^{high}} - k_{rl}^{o^{low}} \right) \tag{12.7}$$

$$n_l = n_l^{low} + \frac{S_{l'r}^{low} - S_{l'r}}{S_{l'r}^{low} - S_{l'r}^{high}} \left(n_l^{high} - n_l^{low} \right) \tag{12.8}$$

12.4 Appendix 4: Theory regarding tuning parameters in UTCHEM

The courant number is defined as in Eq. 12.9 [101],

$$C = \frac{Q\Delta t}{\Delta x \Delta y \Delta z \phi} \tag{12.9}$$

where Q is the maximum injection or production for each well block.

This the automatic time-step selection used in thesis is based on a method of relative changes for the first three components (IMES =2). The maximum and minimum time steps in days are computed based on maximum and minimum Courant numbers, Eq. 12.10 and 12.11 [101],

$$\Delta t_{max} = \frac{CNMAX}{\min\limits_{M=1}^{nwell} \left(\max\limits_{i=1}^{nwbc} \frac{Q_i}{\Delta x_i \Delta y_i \Delta z_i \phi_i} \right)} \tag{12.10}$$

and

$$\Delta t_{max} = \frac{CNMIN}{\min\limits_{M=1}^{nwell}\left(\max\limits_{i=1}^{nwbc} \frac{Q_i}{\Delta x_i \Delta y_i \Delta z_i \phi_i} \right)} \tag{12.11}$$

Where C, Courant number, is limited to $CNMIN \le C \le CNMAX$, and CNMIN and CNMAX are input parameters in UTCHEM.

12.5 Appendix 5: Input file for the Basic model

```
CC*****************************************************************
CC                                                *
CC   BRIEF DESCRIPTION OF DATA SET : UTCHEM (VERSION 9)                  *
CC                                                *
CC*****************************************************************
CC                                                *
CC  WATER FLOOD TEST , 150x150x1      UNIT - METRIC                  *
CC  Slab Flood Simulation                                 *
CC  LENGTH (m) : 0.3            PROCESS : miscible  flooding          *
CC  THICKNESS (m) : .01                                               *
CC  WIDTH (m) : .3              COORDINATES : CARTESIAN               *
CC  POROSITY : 0.22               PORE VOLUME SPECIFICATION           *
CC  GRID BLOCKS : 150x150x1           COURANT NUMBER SPECIFICATION      *
CC  UNIFORM GRIDBLOCK SIZES         WELL SKIN = 0                     *
CC                                                *
CC*****************************************************************
CC
CC*****************************************************************
CC                                                *
CC   RESERVOIR DESCRIPTION                                    *
CC                                                *
CC*****************************************************************
CC
CC Run number
*---- RUNNO
CORE-W
CC
CC Title and run description
*---- title(i)
2-D model with three vertical injectors and two vertical producers
Test fingering during a miscible flood

CC
CC SIMULATION FLAGS
*---- IMODE IMES IDISPC ICWM ICAP IREACT IBIO ICOORD ITREAC ITC  IGAS  IENG
     1   2    3     0   0   0     0   1     0     0   0    0
CC
CC no. of gridblocks,flag specifies constant or variable grid size,unit
*---- NX    NY    NZ  IDXYZ  IUNIT
     150   150    1   0     1
CC
CC constant grid block size in x,y,and z
```

```
*---- dx1          dy1          dz1
     0.002        0.002        0.02
CC
CC total no. of components,no. of tracers,no. of gel components
*----n    no    ntw    nta    ngc    ng    noth
    6    0     0      0      0      0     0
CC
CC Name of the components
*----spname(i) for i=1 to n
Water
Oil
Surf.
Polymer
Chloride
Calcium
CC
CC flag indicating if the component is included in calculations or not
*----icf(kc) for kc=1,n
     1  1  0  0  1  1
CC
CC*************************************************************************
CC                                          *
CC    OUTPUT OPTIONS                                    *
CC                                          *
CC*************************************************************************
CC
CC
CC FLAG TO WRITE TO UNIT 3,FLAG FOR PV OR DAYS TO PRINT OR TO STOP THE RUN
*---- ICUMTM  ISTOP  IOUTGMS
     0       0      0
CC
CC FLAG INDICATING IF THE PROFILE OF KCTH COMPONENT SHOULD BE WRITTEN
*---- IPRFLG(KC),KC=1,N
       1  1  0  0  1  1
CC
CC FLAG FOR PRES.,SAT.,TOTAL CONC.,TRACER CONC.,CAP.,GEL, ALKALINE PROFILES
*---- IPPRES IPSAT IPCTOT IPBIO IPCAP IPGEL IPALK IPTEMP IPOBS
       1      1      1      0    0    0    0    0      0
CC
CC FLAG FOR WRITING SEVERAL PROPERTIES TO UNIT 4 (Prof)
*---- ICKL IVIS IPER ICNM ICSE IHYSTP IFOAMP INONEQ
      1    1    1    0    0    0    0    0
CC
CC FLAG  for variables to PROF output file
*---- IADS IVEL IRKF IPHSE
      1    0    1    0
CC
CC*************************************************************************
CC                                          *
CC    RESERVOIR PROPERTIES                                  *
CC                                          *
CC*************************************************************************
CC
CC
CC MAX. SIMULATION TIME ( DAYS)
*---- TMAX
     0.1
CC
CC ROCK COMPRESSIBILITY (1/PSI), STAND. PRESSURE(PSIA)
*---- COMPR              PSTAND
     0                  0
CC
CC FLAGS INDICATING CONSTANT OR VARIABLE POROSITY, X,Y,AND Z PERMEABILITY
*---- IPOR1  IPERMX IPERMY IPERMZ IMOD
     0      0      3      3      0
CC
```

```
CC CONSTANT POROSITY FOR WHOLE RESERVOIR
*---- PORC1
    0.22
CC
CC VARIABLE X PERMEABILITY FOR EACHLAYER
*---- PERMX(I),FOR K=1 TO NZ
    2500
CC
CC Y DIRECTION PERMEABILITY IS DEPENDENT ON X DIRECTION PERMEABILITY
*---- CONSTANT PERMEABILITY MULTIPLIER FOR Y DIRECTION PERMEABILITY
    1
CC
CC Z DIRECTION PERMEABILITY IS DEPENDENT ON X DIRECTION PERMEABILITY
*---- CONSTANT PERMEABILITY MULTIPLIER FOR Z DIRECTION PERMEABILITY
    0.5
CC
CC FLAG FOR CONSTANT OR VARIABLE DEPTH, PRESSURE, WATER SATURATION,INITIAL AQUEOUS PHASE
cOMPOSITIONS
*----IDEPTH  IPRESS  ISWI  ICWI
   0      0     0    -1
CC
CC CONSTANT DEPTH (M)
*---- D111
    0
CC
CC CONSTANT PRESSURE (PSIA)
*---- PRESS1
    101.
CC
CC CONSTANT INITIAL WATER SATURATION
*---- SWI
    0.0001
CC
CC BRINE SALINITY AND DIVALENT CATION CONCENTRATION (MEQ/ML)
*---- C50      C60
    0.293    0

CC*********************************************************************
CC                                        *
CC   PHYSICAL PROPERTY DATA                              *
CC                                        *
CC*********************************************************************
CC
CC
CC OIL CONC. AT PLAIT POINT FOR TYPE II(+)AND TYPE II(-), CMC
*---- c2plc  c2prc   epsme   ihand
    0     1      0.001   0
CC
CC flag indicating type of phase behavior parameters
*---- ifghbn
    0
CC SLOPE AND INTERCEPT OF BINODAL CURVE AT ZERO, OPT., AND 2XOPT SALINITY
CC FOR ALCOHOL 1
*---- hbns70   hbnc70   hbns71   hbnc71   hbns72   hbnc72
    0       0.0600   0       0.0500   0       0.0600              surfactant_input.lxs sheet: Batch 0.0350 0.0268

0.0350
CC SLOPE AND INTERCEPT OF BINODAL CURVE AT ZERO, OPT., AND 2XOPT SALINITY
CC FOR ALCOHOL 2
*---- hbns80  hbnc80  hbns81  hbnc81  hbns82  hbnc82
    0      0      0      0      0      0
CC
CC LOWER AND UPPER EFFECTIVE SALINITY FOR ALCOHOL 1 AND ALCOHOL 2
*---- csel7   cseu7   csel8   cseu8
    0.30    0.40    0       0                                  surfactant_input.lxs sheet: Batch
CC
```

```
CC THE CSE SLOPE PARAMETER FOR CALCIUM AND ALCOHOL 1 AND ALCOHOL 2
*---- beta6    beta7    beta8
     0.8       -2       0
CC
CC FLAG FOR ALCOHOL PART. MODEL AND PARTITION COEFFICIENTS
*---- ialc   opsk7o   opsk7s   opsk8o   opsk8s
     0      0        0        0        0
CC
CC NO. OF ITERATIONS, AND TOLERANCE
*---- nalmax     epsalc
     20         0.0001
CC
CC ALCOHOL 1 PARTITIONING PARAMETERS IF IALC=1
*---- akwc7     akws7    akm7     ak7      pt7
     4.671     1.79     48       35.31    0.222
CC
CC ALCOHOL 2 PARTITIONING PARAMETERS IF IALC=1
*---- akwc8     akws8    akm8    ak8     pt8
     0         0        0       0       0
CC
CC ift model flag
*----  ift
      1
CC
CC INTERFACIAL TENSION PARAMETERS
*---- chuh     ahuh
     0.3       10                                          surfactant_input.lxs sheet: Batch
CC
CC LOG10 OF OIL/WATER INTERFACIAL TENSION
*---- xiftw
     -100
CC
CC ORGANIC MASS TRANSFER FLAG
*---- imass icor
     0     0
CC
CC CAPILLARY DESATURATION PARAMETERS FOR PHASE 1, 2, AND 3
*---- itrap      t11      t22      t33
     0          1865     59074    364.2
CC
CC  FLAG FOR RELATIVE PERMEABILITY AND CAPILLARY PRESSURE MODEL
*---- iperm
     0
CC
CC FLAG FOR CONSTANT OR VARIABLE REL. PERM. PARAMETERS
*---- isrw    iprw    iew
     0       0       0
CC
CC CONSTANT RES. SATURATION OF PHASES 1,2,AND 3 AT LOW CAPILLARY NO.
*---- s1rwc     s2rwc     s3rwc
     0.0001     0.0001      0.0001
CC
CC CONSTANT ENDPOINT REL. PERM. OF PHASES 1,2,AND 3 AT LOW CAPILLARY NO.
*---- p1rwc     p2rwc     p3rwc
     1.0       1.0       1.0
CC
CC CONSTANT REL. PERM. EXPONENT OF PHASES 1,2,AND 3 AT LOW CAPILLARY NO.
*---- e1wc     e2wc     e3wc
     1.4       1.4       1.4
CC
CC WATER AND OIL VISCOSITY , RESERVOIR TEMPERATURE
*---- VIS1    VIS2   TSTAND
     1.0     200   0                          0.678   7.0          surfactant_input.lxs sheet: Vis
CC
CC COMPOSITIONAL PHASE VISCOSITY PARAMETERS
*----   ALPHAV1   ALPHAV2   ALPHAV3   ALPHAV4  ALPHAV5
```

```
      3       3       0       0.9     0.7                 surfactant_input.lxs sheet: Vis
CC
CC PARAMETERS TO CALCULATE POLYMER VISCOSITY AT ZERO SHEAR RATE
*---- AP1     AP2     AP3
    12.54   41      715                                   polymer_input.lxs sheet: Ap
CC
CC PARAMETER TO COMPUTE CSEP,MIN. CSEP, AND SLOPE OF LOG VIS. VS. LOG CSEP
*---- BETAP   CSE1    SSLOPE
    1       0.01    -0.2389                               polymer_input.lxs sheet: Ap
CC
CC PARAMETER FOR SHEAR RATE DEPENDENCE OF POLYMER VISCOSITY
*---- GAMMAC  GAMHF   POWN
    24      450     1.8                                   polymer_input.lxs sheet: shear
CC
CC CC FLAG FOR POLYMER PARTITIONING, PERM. REDUCTION PARAMETERS
*---- IPOLYM  EPHI3   EPHI4   BRK     CRK
    1       1       1       100     0.13                  polymer_input.lxs sheet: perm_red
CC
CC SPECIFIC WEIGHT FOR COMPONENTS 1,2,3,7,8 ,Coeffient of oil and GRAVITY FLAG
*---- DEN1    DEN2    DEN23   DEN3    DEN7    DEN8    IDEN
    1.25    0.73    0.388   0.42    0.346   0       2
CC
CC FLAG FOR CHOICE OF UNITS ( 0:BOTTOMHOLE CONDITION , 1: STOCK TANK)
*----- ISTB
     0
CC
CC COMPRESSIBILITY FOR VOL. OCCUPYING COMPONENTS 1,2,3,7,AND 8
*---- COMPC(1)  COMPC(2)  COMPC(3)  COMPC(7)  COMPC(8)
    0       0       0       0       0
CC
CC CONSTANT OR VARIABLE PC PARAM., WATER-WET OR OIL-WET PC CURVE FLAG
*---- ICPC    IEPC    IOW
    0       0       0
CC
CC CAPILLARY PRESSURE PARAMETER, CPC0
*---- CPC0
    0
CC
CC CAPILLARY PRESSURE PARAMETER, EPC0
*---- EPC0
    2
CC
CC MOLECULAR DIFFUSION COEF. KCTH COMPONENT IN PHASE 1
*---- D(KC,1),KC=1,N
    0       0       0       0       0       0
CC
CC MOLECULAR DIFFUSION COEF. KCTH COMPONENT IN PHASE 2
*---- D(KC,2),KC=1,N
    0       0       0       0       0       0
CC
CC MOLECULAR DIFFUSION COEF. KCTH COMPONENT IN PHASE 3
*---- D(KC,3),KC=1,N
    0       0       0       0       0       0
CC
CC LONGITUDINAL AND TRANSVERSE DISPERSIVITY OF PHASE 1
*---- ALPHAL(1)     ALPHAT(1)
    0.001         0.0001
CC
CC LONGITUDINAL AND TRANSVERSE DISPERSIVITY OF PHASE 2
*---- ALPHAL(2)     ALPHAT(2)
    0.001         0.0001
CC
CC LONGITUDINAL AND TRANSVERSE DISPERSIVITY OF PHASE 3
*---- ALPHAL(3)     ALPHAT(3)
    0.001         0.0001
CC
```

```
CC flag to specify organic adsorption calculation
*---- iadso
    0
CC
CC SURFACTANT AND POLYMER ADSORPTION PARAMETERS
*---- AD31   AD32   B3D   AD41   AD42   B4D   IADK  IADS1   FADS   REFK
    2.85   0.25   1000  4.40   0.0    100  0    0       0      50   surfactant_input.lxs sheet: Ads 2.85 0.25
CC                                                          polymer_input.lxs sheet: Ads
CC PARAMETERS FOR CATION EXCHANGE OF CLAY AND SURFACTANT
*---- QV    XKC   XKS    EQW
    0    0    0     804
CC
CC*********************************************************************
CC                                          *
CC   WELL DATA                                    *
CC                                          *
CC*********************************************************************
CC
CC
CC FLAG FOR SPECIFIED BOUNDARY AND ZONE IS MODELED
*---- IBOUND     IZONE
    0         0
CC
CC TOTAL NUMBER OF WELLS, WELL RADIUS FLAG, FLAG FOR TIME OR COURANT NO.
*---- NWELL   IRO    ITIME    NWREL
    5       2      1        5
CC
CC WELL ID,LOCATIONS,AND FLAG FOR SPECIFYING WELL TYPE, WELL RADIUS, SKIN
*---- IDW    IW    JW    IFLAG    RW     SWELL   IDIR   IFIRST   ILAST   IPRF
    1      150    1    1        0.001  0       1      20       30        0
CC
CC WELL NAME
*----  WELNAM
INJE1
CC
CC ICHEK , MAX. AND MIN. ALLOWABLE BOTTOMHOLE PRESSURE AND RATE
*---- ICHEK     PWFMIN     PWFMAX    QTMIN    QTMAX
    0         0          1251      0        4000
CC
CC WELL ID,LOCATIONS,AND FLAG FOR SPECIFYING WELL TYPE, WELL RADIUS, SKIN
*---- IDW    IW    JW    IFLAG    RW     SWELL   IDIR   IFIRST   ILAST   IPRF
    2      150    1    1        0.001  0       1      70       80      0
CC
CC WELL NAME
*----  WELNAM
INJE2
CC
CC ICHEK , MAX. AND MIN. ALLOWABLE BOTTOMHOLE PRESSURE AND RATE
*---- ICHEK     PWFMIN     PWFMAX    QTMIN    QTMAX
    0         0          1251      0        4000
CC
CC WELL ID,LOCATIONS,AND FLAG FOR SPECIFYING WELL TYPE, WELL RADIUS, SKIN
*---- IDW    IW    JW    IFLAG    RW     SWELL   IDIR   IFIRST   ILAST   IPRF
     3     150    1    1        0.001  0       1      120      130       0
CC
CC WELL NAME
*----  WELNAM
INJE3
CC
CC ICHEK , MAX. AND MIN. ALLOWABLE BOTTOMHOLE PRESSURE AND RATE
*---- ICHEK     PWFMIN     PWFMAX    QTMIN    QTMAX
    0         0          1251      0        4000
CC
CC WELL ID,LOCATIONS,AND FLAG FOR SPECIFYING WELL TYPE, WELL RADIUS, SKIN
*---- IDW    IW    JW    IFLAG    RW     SWELL   IDIR   IFIRST   ILAST   IPRF
    4     1     1     2        0.001  0       1      45       55      0
```

```
CC
CC WELL NAME
*----  WELNAM
PROD1
CC
CC ICHEK , MAX. AND MIN. ALLOWABLE BOTTOMHOLE PRESSURE AND RATE
*---- ICHEK    PWFMIN    PWFMAX   QTMIN   QTMAX
     0        0         1251     0       4000
CC
CC WELL ID,LOCATIONS,AND FLAG FOR SPECIFYING WELL TYPE, WELL RADIUS, SKIN
*---- IDW   IW   JW   IFLAG   RW    SWELL  IDIR  IFIRST  ILAST  IPRF
     5    1    1    2       0.001 0      1     95      105    0
CC
CC WELL NAME
*----  WELNAM
PROD2
CC
CC ICHEK , MAX. AND MIN. ALLOWABLE BOTTOMHOLE PRESSURE AND RATE
*---- ICHEK    PWFMIN    PWFMAX   QTMIN   QTMAX
      0        0       1251     0       4000
CC
CC  ID,INJ. RATE AND INJ. COMP. FOR RATE CONS. WELLS FOR EACH PHASE (L=1,3)
*----  ID    QI(M,L)    C(M,KC,L)
      1     0.001441       1     0  0  0   0.350  0   0   0  0
      1     0              0     0  0  0   0      0   0   0  0
      1     0              0     0  0  0   0      0   0   0  0
CC
CC  ID,INJ. RATE AND INJ. COMP. FOR RATE CONS. WELLS FOR EACH PHASE (L=1,3)
*----  ID    QI(M,L)    C(M,KC,L)
      2     0.001441     1     0  0  0   0.350  0   0   0  0
      2     0            0     0  0  0   0      0   0   0  0
      2     0            0     0  0  0   0      0   0   0  0
CC
CC  ID,INJ. RATE AND INJ. COMP. FOR RATE CONS. WELLS FOR EACH PHASE (L=1,3)
*----  ID    QI(M,L)    C(M,KC,L)
      3     0.001441       1     0  0  0   0.350  0   0   0  0
      3     0              0     0  0  0   0      0   0   0  0
      3     0              0     0  0  0   0      0   0   0  0
CC
CC ID, BOTTOM HOLE PRESSURE FOR PRESSURE CONSTRAINT WELL (IFLAG=2 OR 3)
*----  ID   PWF
      4    101.
CC
CC ID, BOTTOM HOLE PRESSURE FOR PRESSURE CONSTRAINT WELL (IFLAG=2 OR 3)
*----  ID   PWF
      5    101.
CC
CC CUM. INJ. TIME , AND INTERVALS (PV) FOR WRITING TO OUTPUT FILES
*----TINJ   CUMPR1  CUMHI2(SUMARY) WRHPV(HIST) WRPRF(PLOT) RSTC
    0.1166  0.0166   0.0166        0.0166       0.0166        0.0833
CC
CC FOR IMES=2 ,THE INI. TIME STEP,CONC. TOLERANCE,MAX.,MIN. time steps
*----DT     DCLIM   CNMAX   CNMIN
    0.000001     0.002      0.5   0.005
```

12.6 Appendix 6: Input file for the IMMISC1 model

The heterogeneous permeability field in this input file is replaced by a constant value of $2.5\,\mu m^2$

```
CC*****************************************************************
CC                                                               *
CC    BRIEF DESCRIPTION OF DATA SET : UTCHEM (VERSION 9)                    *
CC                                                               *
CC*****************************************************************
CC                                                               *
CC  WATER FLOOD TEST , 50x50x1                                       *
CC  Slab Flood Simulation                                        *
CC  LENGTH (m) : 0.1              PROCESS : water  flooding          *
CC  THICKNESS (m) : .02                                          *
CC  WIDTH (m) : .1                COORDINATES : CARTESIAN            *
CC  POROSITY : 0.22               PORE VOLUME SPECIFICATION          *
CC  GRID BLOCKS : 50x50x1         COURANT NUMBER SPECIFICATION       *
CC  UNIFORM GRIDBLOCK SIZES       WELL SKIN = 0                      *
CC                                                               *
CC*****************************************************************
CC
CC*****************************************************************
CC                                                               *
CC    RESERVOIR DESCRIPTION                                      *
CC                                                               *
CC*****************************************************************
CC
CC Run number
*---- RUNNO
CORE-W
CC
CC Title and run description
*---- title(i)
CORE-W Core Flood assuming a homogeneous permeability field
water flooding

CC
CC SIMULATION FLAGS
*---- IMODE IMES IDISPC ICWM ICAP IREACT IBIO ICOORD ITREAC ITC  IGAS  IENG
     1    2     3     0   0   0     0   1     0     0   0    0
CC
CC no. of gridblocks,flag specifies constant or variable grid size,unit
*---- NX    NY    NZ  IDXYZ  IUNIT
     50    50    1   0      1
CC
CC constant grid block size in x,y,and z
*---- dx1           dy1           dz1
     0.002         0.002         0.02
CC
CC total no. of components,no. of tracers,no. of gel components
*----n    no    ntw    nta    ngc    ng    noth
    6    0     0      0      0      0     0
CC
CC Name of the components
*----spname(i) for i=1 to n
Water
Oil
Surf.
Polymer
Chloride
Calcium
CC
CC flag indicating if the component is included in calculations or not
*----icf(kc) for kc=1,n
     1  1  0  0  1  1
```

```
CC
CC*********************************************************************
CC                                        *
CC    OUTPUT OPTIONS                                  *
CC                                        *
CC*********************************************************************
CC
CC
CC FLAG TO WRITE TO UNIT 3,FLAG FOR PV OR DAYS TO PRINT OR TO STOP THE RUN
*---- ICUMTM  ISTOP  IOUTGMS
    0      0     0
CC
CC FLAG INDICATING IF THE PROFILE OF KCTH COMPONENT SHOULD BE WRITTEN
*---- IPRFLG(KC),KC=1,N
      1  1  0  0  1  1
CC
CC FLAG FOR PRES.,SAT.,TOTAL CONC.,TRACER CONC.,CAP.,GEL, ALKALINE PROFILES
*---- IPPRES IPSAT IPCTOT IPBIO IPCAP IPGEL IPALK IPTEMP IPOBS
      1     1     1     0    0    0    0    0     0
CC
CC FLAG FOR WRITING SEVERAL PROPERTIES TO UNIT 4 (Prof)
*---- ICKL IVIS IPER ICNM ICSE IHYSTP IFOAMP INONEQ
     1    1    1    0    0    0    0    0
CC
CC FLAG  for variables to PROF output file
*---- IADS IVEL IRKF IPHSE
     1    0    1    0
CC
CC*********************************************************************
CC                                        *
CC    RESERVOIR PROPERTIES                                *
CC                                        *
CC*********************************************************************
CC
CC
CC MAX. SIMULATION TIME ( DAYS)
*---- TMAX
    1.0
CC
CC ROCK COMPRESSIBILITY (1/PSI), STAND. PRESSURE(PSIA)
*---- COMPR              PSTAND
    0                0
CC
CC FLAGS INDICATING CONSTANT OR VARIABLE POROSITY, X,Y,AND Z PERMEABILITY
*---- IPOR1  IPERMX IPERMY IPERMZ IMOD
    0     2     3     3     0
CC
CC CONSTANT POROSITY FOR WHOLE RESERVOIR
*---- PORC1
    0.22
CC
CC CONSTANT X-PERMEABILITY FOR WHOLE RESERVOIR
*---- PERMXC
   2500
CC
CC Y DIRECTION PERMEABILITY IS DEPENDENT ON X DIRECTION PERMEABILITY
*---- CONSTANT PERMEABILITY MULTIPLIER FOR Y DIRECTION PERMEABILITY
    1
CC
CC Z DIRECTION PERMEABILITY IS DEPENDENT ON X DIRECTION PERMEABILITY
*---- CONSTANT PERMEABILITY MULTIPLIER FOR Z DIRECTION PERMEABILITY
    0.5
CC
CC FLAG FOR CONSTANT OR VARIABLE DEPTH, PRESSURE, WATER SATURATION,INITIAL AQUEOUS PHASE
cOMPOSITIONS
*----IDEPTH  IPRESS  ISWI  ICWI
```

```
    0      0     0     -1
CC
CC CONSTANT DEPTH (FT)
*---- D111
     0
CC
CC CONSTANT PRESSURE (PSIA)
*---- PRESS1
     101.
CC
CC CONSTANT INITIAL WATER SATURATION
*---- SWI
     .0001
CC
CC BRINE SALINITY AND DIVALENT CATION CONCENTRATION (MEQ/ML)
*---- C50       C60
     0.293     0

CC*********************************************************************
CC                                          *
CC    PHYSICAL PROPERTY DATA                                *
CC                                          *
CC*********************************************************************
CC
CC
CC OIL CONC. AT PLAIT POINT FOR TYPE II(+)AND TYPE II(-), CMC
*---- c2plc  c2prc   epsme   ihand
     0      1       0.001   0
CC
CC flag indicating type of phase behavior parameters
*---- ifghbn
     0
CC SLOPE AND INTERCEPT OF BINODAL CURVE AT ZERO, OPT., AND 2XOPT SALINITY
CC FOR ALCOHOL 1
*---- hbns70   hbnc70   hbns71   hbnc71   hbns72   hbnc72
     0       0.0200   0       0.0150   0       0.0200              surfactant_input.lxs sheet: Batch 0.0350 0.0268 0.0350
CC SLOPE AND INTERCEPT OF BINODAL CURVE AT ZERO, OPT., AND 2XOPT SALINITY
CC FOR ALCOHOL 2
*---- hbns80  hbnc80  hbns81  hbnc81  hbns82  hbnc82
     0       0       0       0       0       0
CC
CC LOWER AND UPPER EFFECTIVE SALINITY FOR ALCOHOL 1 AND ALCOHOL 2
*---- csel7   cseu7   csel8   cseu8
     0.24    0.49    0       0                                   surfactant_input.lxs sheet: Batch
CC
CC THE CSE SLOPE PARAMETER FOR CALCIUM AND ALCOHOL 1 AND ALCOHOL 2
*---- beta6    beta7    beta8
     0.8       -2       0
CC
CC FLAG FOR ALCOHOL PART. MODEL AND PARTITION COEFFICIENTS
*---- ialc   opsk7o   opsk7s   opsk8o   opsk8s
     0      0        0        0        0
CC
CC NO. OF ITERATIONS, AND TOLERANCE
*---- nalmax     epsalc
     20         0.0001
CC
CC ALCOHOL 1 PARTITIONING PARAMETERS IF IALC=1
*---- akwc7     akws7    akm7     ak7      pt7
     4.671     1.79     48       35.31    0.222
CC
CC ALCOHOL 2 PARTITIONING PARAMETERS IF IALC=1
*---- akwc8     akws8    akm8    ak8     pt8
     0         0        0       0       0
CC
CC ift model flag
```

```
*----  ift
       1
CC
CC INTERFACIAL TENSION PARAMETERS
*---- chuh     ahuh
     0.3       10                                        surfactant_input.lxs sheet: Batch
CC
CC LOG10 OF OIL/WATER INTERFACIAL TENSION
*---- xiftw
     1.3
CC
CC ORGANIC MASS TRANSFER FLAG
*---- imass icor
     0     0
CC
CC CAPILLARY DESATURATION PARAMETERS FOR PHASE 1, 2, AND 3
*---- itrap      t11      t22      t33
     0          1865     59074    364.2
CC
CC  FLAG FOR RELATIVE PERMEABILITY AND CAPILLARY PRESSURE MODEL
*---- iperm
     0
CC
CC FLAG FOR CONSTANT OR VARIABLE REL. PERM. PARAMETERS
*---- isrw    iprw    iew
     0       0       0
CC
CC CONSTANT RES. SATURATION OF PHASES 1,2,AND 3 AT LOW CAPILLARY NO.
*---- s1rwc    s2rwc     s3rwc
     0.0001     0.49      0.0001
CC
CC CONSTANT ENDPOINT REL. PERM. OF PHASES 1,2,AND 3 AT LOW CAPILLARY NO.
*---- p1rwc     p2rwc    p3rwc
     0.1       1      1
CC
CC CONSTANT REL. PERM. EXPONENT OF PHASES 1,2,AND 3 AT LOW CAPILLARY NO.
*---- e1wc     e2wc     e3wc
     1.4       4        2
CC
CC WATER AND OIL VISCOSITY , RESERVOIR TEMPERATURE
*---- VIS1    VIS2   TSTAND
     1.0     200.0    0                          0.678   7.0          surfactant_input.lxs sheet: Vis
CC
CC COMPOSITIONAL PHASE VISCOSITY PARAMETERS
*----   ALPHAV1   ALPHAV2   ALPHAV3   ALPHAV4  ALPHAV5
         2         2         0         0.9       0.7                 surfactant_input.lxs sheet: Vis
CC
CC PARAMETERS TO CALCULATE POLYMER VISCOSITY AT ZERO SHEAR RATE
*---- AP1      AP2      AP3
     12.54    41       715                                    polymer_input.lxs sheet: Ap
CC
CC PARAMETER TO COMPUTE CSEP,MIN. CSEP, AND SLOPE OF LOG VIS. VS. LOG CSEP
*---- BETAP    CSE1     SSLOPE
     1        0.01     -0.2389                                polymer_input.lxs sheet: Ap
CC
CC PARAMETER FOR SHEAR RATE DEPENDENCE OF POLYMER VISCOSITY
*---- GAMMAC   GAMHF   POWN
     24       450     1.8                                    polymer_input.lxs sheet: shear
CC
CC CC FLAG FOR POLYMER PARTITIONING, PERM. REDUCTION PARAMETERS
*---- IPOLYM    EPHI3    EPHI4    BRK     CRK
     1         1        1        100     0.13                polymer_input.lxs sheet: perm_red
CC
CC SPECIFIC WEIGHT FOR COMPONENTS 1,2,3,7,8 ,Coeffient of oil and GRAVITY FLAG
*---- DEN1     DEN2    DEN23     DEN3    DEN7    DEN8    IDEN
     1.25    0.862   0.388     0.42    0.346   0       2
```

```
CC
CC FLAG FOR CHOICE OF UNITS ( 0:BOTTOMHOLE CONDITION , 1: STOCK TANK)
*----- ISTB
      0
CC
CC COMPRESSIBILITY FOR VOL. OCCUPYING COMPONENTS 1,2,3,7,AND 8
*---- COMPC(1)  COMPC(2)  COMPC(3)  COMPC(7)  COMPC(8)
    0        0        0        0        0
CC
CC CONSTANT OR VARIABLE PC PARAM., WATER-WET OR OIL-WET PC CURVE FLAG
*---- ICPC    IEPC   IOW
    2       0     0
CC
CC CAPILLARY PRESSURE PARAMETER, CPC0
*---- CPC0
     700
CC
CC CAPILLARY PRESSURE PARAMETER, EPC0
*---- EPC0
    2
CC
CC MOLECULAR DIFFUSION COEF. KCTH COMPONENT IN PHASE 1
*---- D(KC,1),KC=1,N
    0       0       0       0       0       0
CC
CC MOLECULAR DIFFUSION COEF. KCTH COMPONENT IN PHASE 2
*---- D(KC,2),KC=1,N
    0       0       0       0       0       0
CC
CC MOLECULAR DIFFUSION COEF. KCTH COMPONENT IN PHASE 3
*---- D(KC,3),KC=1,N
    0       0       0       0       0       0
CC
CC LONGITUDINAL AND TRANSVERSE DISPERSIVITY OF PHASE 1
*---- ALPHAL(1)     ALPHAT(1)
    0.0         0.000
CC
CC LONGITUDINAL AND TRANSVERSE DISPERSIVITY OF PHASE 2
*---- ALPHAL(2)     ALPHAT(2)
    0.0         0.000
CC
CC LONGITUDINAL AND TRANSVERSE DISPERSIVITY OF PHASE 3
*---- ALPHAL(3)     ALPHAT(3)
    0.0         0.000
CC
CC flag to specify organic adsorption calculation
*---- iadso
    0
CC
CC SURFACTANT AND POLYMER ADSORPTION PARAMETERS
*---- AD31    AD32   B3D    AD41   AD42   B4D   IADK  IADS1   FADS   REFK
    2.85    0.25   1000   4.40   0.0    100   0     0       0      50   surfactant_input.lxs sheet: Ads 2.85 0.25
CC                                                                      polymer_input.lxs sheet: Ads
CC PARAMETERS FOR CATION EXCHANGE OF CLAY AND SURFACTANT
*---- QV    XKC   XKS    EQW
    0     0     0      804
CC
CC*****************************************************************
CC                                          *
CC    WELL DATA                                   *
CC                                          *
CC*****************************************************************
CC
CC
CC FLAG FOR SPECIFIED BOUNDARY AND ZONE IS MODELED
*---- IBOUND     IZONE
```

```
    0         0
CC
CC TOTAL NUMBER OF WELLS, WELL RADIUS FLAG, FLAG FOR TIME OR COURANT NO.
*---- NWELL   IRO    ITIME    NWREL
    2       2      1        2
CC
CC WELL ID,LOCATIONS,AND FLAG FOR SPECIFYING WELL TYPE, WELL RADIUS, SKIN
*---- IDW    IW    JW    IFLAG    RW     SWELL   IDIR   IFIRST   ILAST   IPRF
    1      50    1    1        0.0001   0       1      20        30       0
CC
CC WELL NAME
*----  WELNAM
INJECTOR
CC
CC ICHEK , MAX. AND MIN. ALLOWABLE BOTTOMHOLE PRESSURE AND RATE
*---- ICHEK     PWFMIN     PWFMAX    QTMIN    QTMAX
    0         0          1251      0        4000
CC
CC WELL ID,LOCATIONS,AND FLAG FOR SPECIFYING WELL TYPE, WELL RADIUS, SKIN
*---- IDW    IW    JW    IFLAG    RW     SWELL   IDIR   IFIRST   ILAST   IPRF
    2      1    1    2        0.0001   0       1      20        30       0
CC
CC WELL NAME
*----  WELNAM
PRODUCER
CC
CC ICHEK , MAX. AND MIN. ALLOWABLE BOTTOMHOLE PRESSURE AND RATE
*---- ICHEK     PWFMIN     PWFMAX    QTMIN    QTMAX
    0         0          1251      0        4000
CC
CC ID,INJ. RATE AND INJ. COMP. FOR RATE CONS. WELLS FOR EACH PHASE (L=1,3)
*----  ID     QI(M,L)       C(M,KC,L)
     1      0.004323  1      0      0      0      0.200  0
     1      0             0      0      0      0      0      0
     1      0             0      0      0      0      0      0
CC
CC ID, BOTTOM HOLE PRESSURE FOR PRESSURE CONSTRAINT WELL (IFLAG=2 OR 3)
*----  ID    PWF
     2     101
CC
CC CUM. INJ. TIME , AND INTERVALS (PV OR DAY) FOR WRITING TO OUTPUT FILES
*---- TINJ     CUMPR1     CUMHI1     WRHPV     WRPRF     RSTC
    0.00116      0.0000116      0.0000116        0.0000116     0.0000116       0.05
CC
CC FOR IMES=2 ,THE INI. TIME STEP,CONC. TOLERANCE,MAX.,MIN. courant numbers
*----  DT         DCLIM     CNMAX      CNMIN
     0.00000001   0.005      0.001        0.000000005
```

12.7 Appendix 7: X-ray images from the first immiscible process in the laboratory experiment

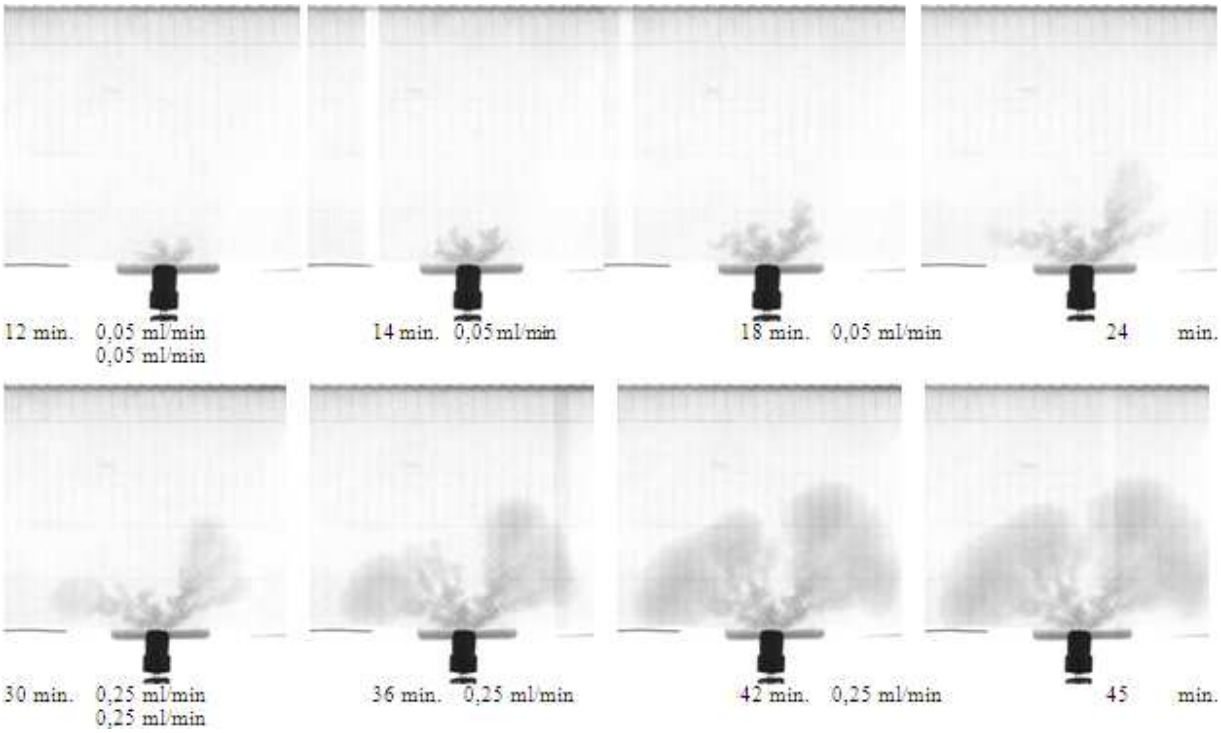

Figure 12.20: X-ray images displaying 11 x 11 cm of the Bentheimer slab. Start of water injection at S_o=1, from port 2 [6].

12.8 Appendix 8: X-ray images from the second immiscible process in the laboratory experiment

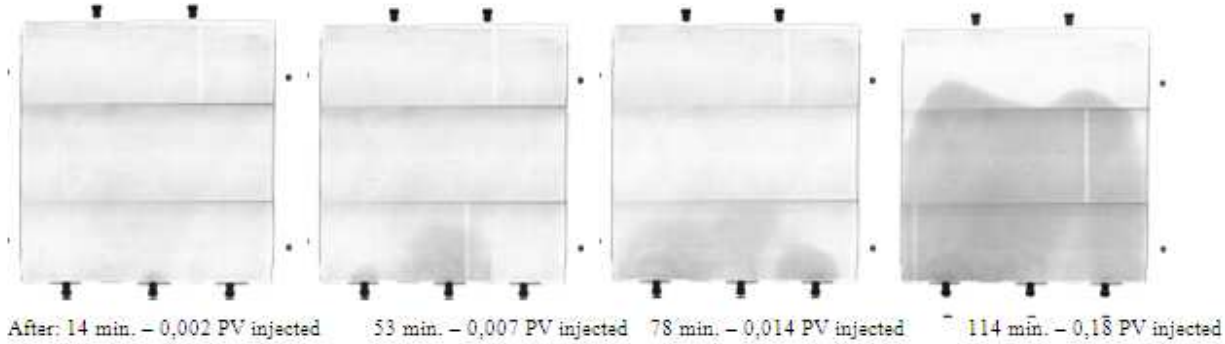

Figure 12.21: X-ray images displaying the 30 x 30 cm Bentheimer slab. Start of water injection at S_w=0.12, from port 2 [6].

12.9 Appendix 9: Input file for the POLY2 model

```
CC*****************************************************************
CC                                                               *
CC    BRIEF DESCRIPTION OF DATA SET : UTCHEM (VERSION 9)                    *
CC                                                               *
CC*****************************************************************
CC                                                               *
CC  WATER FLOOD TEST , 150x150x1      UNIT - METRIC                       *
CC  Slab Flood Simulation                                        *
CC  LENGTH (m) : 0.3            PROCESS : polymer  flooding          *
CC  THICKNESS (m) : 0.02                                         *
CC  WIDTH (m) : .0.3              COORDINATES : CARTESIAN                *
CC  POROSITY : 0.22               PORE VOLUME SPECIFICATION              *
CC  GRID BLOCKS : 150x150x1           COURANT NUMBER SPECIFICATION       *
CC  UNIFORM GRIDBLOCK SIZES         WELL SKIN = 0                        *
CC                                                               *
CC*****************************************************************
CC
CC*****************************************************************
CC                                                               *
CC    RESERVOIR DESCRIPTION                                          *
CC                                                               *
CC*****************************************************************
CC
CC Run number
*---- RUNNO
CORE-W
CC
CC Title and run description
*---- title(i)
2-D model with three vertical injectors and two vertical producers
Test fingering during a miscible flood

CC
CC SIMULATION FLAGS
*---- IMODE IMES IDISPC ICWM ICAP IREACT IBIO ICOORD ITREAC ITC  IGAS  IENG
     1    2     3      0    0    0      0    1      0      0    0     0
CC
CC no. of gridblocks,flag specifies constant or variable grid size,unit
*---- NX    NY    NZ  IDXYZ  IUNIT
     150    150    1   0      1
CC
CC constant grid block size in x,y,and z
*---- dx1          dy1          dz1
     0.002        0.002        0.02
CC
CC total no. of components,no. of tracers,no. of gel components
*----n    no    ntw    nta    ngc    ng    noth
    6    0     0      0      0     0      0
CC
CC Name of the components
*----spname(i) for i=1 to n
Water
Oil
Surf.
Polymer
Chloride
Calcium
CC
CC flag indicating if the component is included in calculations or not
*----icf(kc) for kc=1,n
     1  1  0  1  1  1
CC
CC*****************************************************************
CC                                                               *
```

```
CC    OUTPUT OPTIONS                                    *
CC                                                *
CC*****************************************************************
CC
CC
CC FLAG TO WRITE TO UNIT 3,FLAG FOR PV OR DAYS TO PRINT OR TO STOP THE RUN
*---- ICUMTM  ISTOP  IOUTGMS
     1      1     0
CC
CC FLAG INDICATING IF THE PROFILE OF KCTH COMPONENT SHOULD BE WRITTEN
*---- IPRFLG(KC),KC=1,N
      1 1 0 1 1 1
CC
CC FLAG FOR PRES.,SAT.,TOTAL CONC.,TRACER CONC.,CAP.,GEL, ALKALINE PROFILES
*---- IPPRES IPSAT IPCTOT IPBIO IPCAP IPGEL IPALK IPTEMP IPOBS
      1     1     1     0    0    0    0    0     0
CC
CC FLAG FOR WRITING SEVERAL PROPERTIES TO UNIT 4 (Prof)
*---- ICKL IVIS IPER ICNM ICSE IHYSTP IFOAMP INONEQ
     1   1   1   0   0   0   0   0
CC
CC FLAG  for variables to PROF output file
*---- IADS IVEL IRKF IPHSE
     1   0   1   0
CC
CC*****************************************************************
CC                                                *
CC    RESERVOIR PROPERTIES                                *
CC                                                *
CC*****************************************************************
CC
CC
CC MAX. SIMULATION TIME ( DAYS)
*---- TMAX
     25
CC
CC ROCK COMPRESSIBILITY (1/PSI), STAND. PRESSURE(PSIA)
*---- COMPR               PSTAND
     0                   0
CC
CC FLAGS INDICATING CONSTANT OR VARIABLE POROSITY, X,Y,AND Z PERMEABILITY
*---- IPOR1  IPERMX IPERMY IPERMZ IMOD
     0     0     3     3     0
CC
CC CONSTANT POROSITY FOR WHOLE RESERVOIR
*---- PORC1
     0.22
CC
CC VARIABLE X PERMEABILITY FOR EACHLAYER
*---- PERMX(I),FOR K=1 TO NZ
     2500
CC
CC Y DIRECTION PERMEABILITY IS DEPENDENT ON X DIRECTION PERMEABILITY
*---- CONSTANT PERMEABILITY MULTIPLIER FOR Y DIRECTION PERMEABILITY
     1
CC
CC Z DIRECTION PERMEABILITY IS DEPENDENT ON X DIRECTION PERMEABILITY
*---- CONSTANT PERMEABILITY MULTIPLIER FOR Z DIRECTION PERMEABILITY
     0.5
CC
CC FLAG FOR CONSTANT OR VARIABLE DEPTH, PRESSURE, WATER SATURATION,INITIAL AQUEOUS PHASE
cOMPOSITIONS
*----IDEPTH  IPRESS  ISWI  ICWI
    0      0     0    -1
CC
CC CONSTANT DEPTH (M)
```

```
*---- D111
    0
CC
CC CONSTANT PRESSURE (PSIA)
*---- PRESS1
    101.
CC
CC CONSTANT INITIAL WATER SATURATION
*---- SWI
    0.53
CC
CC BRINE SALINITY AND DIVALENT CATION CONCENTRATION (MEQ/ML)
*---- C50      C60
    0.293    0

CC*********************************************************************
CC                                        *
CC   PHYSICAL PROPERTY DATA                              *
CC                                        *
CC*********************************************************************
CC
CC
CC OIL CONC. AT PLAIT POINT FOR TYPE II(+)AND TYPE II(-), CMC
*---- c2plc  c2prc   epsme   ihand
    0     1      0.001   0
CC
CC flag indicating type of phase behavior parameters
*---- ifghbn
    0
CC SLOPE AND INTERCEPT OF BINODAL CURVE AT ZERO, OPT., AND 2XOPT SALINITY
CC FOR ALCOHOL 1
*---- hbns70   hbnc70   hbns71   hbnc71   hbns72   hbnc72
    0       0.0600   0       0.0500   0       0.0600              surfactant_input.lxs sheet: Batch 0.0350 0.0268 0.0350
CC SLOPE AND INTERCEPT OF BINODAL CURVE AT ZERO, OPT., AND 2XOPT SALINITY
CC FOR ALCOHOL 2
*---- hbns80  hbnc80  hbns81  hbnc81  hbns82  hbnc82
    0      0      0      0      0      0
CC
CC LOWER AND UPPER EFFECTIVE SALINITY FOR ALCOHOL 1 AND ALCOHOL 2
*---- csel7   cseu7   csel8   cseu8
    0.30   0.40   0      0                                   surfactant_input.lxs sheet: Batch
CC
CC THE CSE SLOPE PARAMETER FOR CALCIUM AND ALCOHOL 1 AND ALCOHOL 2
*---- beta6    beta7    beta8
    0.8      -2      0
CC
CC FLAG FOR ALCOHOL PART. MODEL AND PARTITION COEFFICIENTS
*---- ialc   opsk7o   opsk7s   opsk8o   opsk8s
    0     0       0       0       0
CC
CC NO. OF ITERATIONS, AND TOLERANCE
*---- nalmax     epsalc
    20         0.0001
CC
CC ALCOHOL 1 PARTITIONING PARAMETERS IF IALC=1
*---- akwc7     akws7    akm7     ak7      pt7
    4.671     1.79     48       35.31    0.222
CC
CC ALCOHOL 2 PARTITIONING PARAMETERS IF IALC=1
*---- akwc8     akws8    akm8    ak8     pt8
    0         0       0      0      0
CC
CC ift model flag
*----  ift
     1
CC
```

```
CC INTERFACIAL TENSION PARAMETERS
*---- chuh     ahuh
     0.3       10                                          surfactant_input.lxs sheet: Batch
CC
CC LOG10 OF OIL/WATER INTERFACIAL TENSION
*---- xiftw
     1.4
CC
CC ORGANIC MASS TRANSFER FLAG
*---- imass icor
     0     0
CC
CC CAPILLARY DESATURATION PARAMETERS FOR PHASE 1, 2, AND 3
*---- itrap      t11      t22      t33
     0          1865     59074    364.2
CC
CC  FLAG FOR RELATIVE PERMEABILITY AND CAPILLARY PRESSURE MODEL
*---- iperm
     0
CC
CC FLAG FOR CONSTANT OR VARIABLE REL. PERM. PARAMETERS
*---- isrw    iprw    iew
     0       0       0
CC
CC CONSTANT RES. SATURATION OF PHASES 1,2,AND 3 AT LOW CAPILLARY NO.
*---- s1rwc    s2rwc     s3rwc
     0.14     0.31      0.0001
CC
CC CONSTANT ENDPOINT REL. PERM. OF PHASES 1,2,AND 3 AT LOW CAPILLARY NO.
*---- p1rwc     p2rwc    p3rwc
     0.1       1.0      1.0
CC
CC CONSTANT REL. PERM. EXPONENT OF PHASES 1,2,AND 3 AT LOW CAPILLARY NO.
*---- e1wc     e2wc     e3wc
     1.4       4        2
CC
CC WATER AND OIL VISCOSITY , RESERVOIR TEMPERATURE
*---- VIS1    VIS2   TSTAND
     1.0     200.0  0                       0.678   7.0          surfactant_input.lxs sheet: Vis
CC
CC COMPOSITIONAL PHASE VISCOSITY PARAMETERS
*----   ALPHAV1   ALPHAV2   ALPHAV3   ALPHAV4  ALPHAV5
       3         3         0         0.9       0.7                  surfactant_input.lxs sheet: Vis
CC
CC PARAMETERS TO CALCULATE POLYMER VISCOSITY AT ZERO SHEAR RATE
*---- AP1      AP2      AP3
     200     2000      1000                                    polymer_input.lxs sheet: Ap
CC
CC PARAMETER TO COMPUTE CSEP,MIN. CSEP, AND SLOPE OF LOG VIS. VS. LOG CSEP
*---- BETAP    CSE1     SSLOPE
     1        0.01     0                                  polymer_input.lxs sheet: Ap
CC
CC PARAMETER FOR SHEAR RATE DEPENDENCE OF POLYMER VISCOSITY
*---- GAMMAC   GAMHF   POWN
     24       180     1.8                                   polymer_input.lxs sheet: shear
CC
CC CC FLAG FOR POLYMER PARTITIONING, PERM. REDUCTION PARAMETERS
*---- IPOLYM    EPHI3    EPHI4    BRK     CRK
     1         1        1        100     0                      polymer_input.lxs sheet: perm_red
CC
CC SPECIFIC WEIGHT FOR COMPONENTS 1,2,3,7,8 ,Coeffient of oil and GRAVITY FLAG
*---- DEN1     DEN2    DEN23     DEN3    DEN7    DEN8    IDEN
     1.25    0.862   0.388     0.42    0.346   0       2
CC
CC FLAG FOR CHOICE OF UNITS ( 0:BOTTOMHOLE CONDITION , 1: STOCK TANK)
*----- ISTB
```

```
     0
CC
CC COMPRESSIBILITY FOR VOL. OCCUPYING COMPONENTS 1,2,3,7,AND 8
*---- COMPC(1)  COMPC(2)  COMPC(3)  COMPC(7)  COMPC(8)
    0        0        0        0        0
CC
CC CONSTANT OR VARIABLE PC PARAM., WATER-WET OR OIL-WET PC CURVE FLAG
*---- ICPC    IEPC   IOW
    0      0     0
CC
CC CAPILLARY PRESSURE PARAMETER, CPC0
*---- CPC0
    0.
CC
CC CAPILLARY PRESSURE PARAMETER, EPC0
*---- EPC0
    2
CC
CC MOLECULAR DIFFUSION COEF. KCTH COMPONENT IN PHASE 1
*---- D(KC,1),KC=1,N
    0       0       0       0       0       0
CC
CC MOLECULAR DIFFUSION COEF. KCTH COMPONENT IN PHASE 2
*---- D(KC,2),KC=1,N
    0       0       0       0       0       0
CC
CC MOLECULAR DIFFUSION COEF. KCTH COMPONENT IN PHASE 3
*---- D(KC,3),KC=1,N
    0       0       0       0       0       0
CC
CC LONGITUDINAL AND TRANSVERSE DISPERSIVITY OF PHASE 1
*---- ALPHAL(1)     ALPHAT(1)
    0.001         0.0001
CC
CC LONGITUDINAL AND TRANSVERSE DISPERSIVITY OF PHASE 2
*---- ALPHAL(2)     ALPHAT(2)
    0.001         0.0001
CC
CC LONGITUDINAL AND TRANSVERSE DISPERSIVITY OF PHASE 3
*---- ALPHAL(3)     ALPHAT(3)
    0.001         0.0001
CC
CC flag to specify organic adsorption calculation
*---- iadso
    0
CC
CC SURFACTANT AND POLYMER ADSORPTION PARAMETERS
*---- AD31    AD32   B3D    AD41   AD42   B4D   IADK  IADS1   FADS   REFK
    2.85    0.25   1000   4.8   0.0    100  0     0       0      50   surfactant_input.lxs sheet: Ads 2.85 0.25
CC                                                          polymer_input.lxs sheet: Ads
CC PARAMETERS FOR CATION EXCHANGE OF CLAY AND SURFACTANT
*---- QV    XKC   XKS    EQW
    0     0     0      804
CC
CC*************************************************************************
CC                                          *
CC    WELL DATA                                     *
CC                                          *
CC*************************************************************************
CC
CC
CC FLAG FOR SPECIFIED BOUNDARY AND ZONE IS MODELED
*---- IBOUND     IZONE
    0         0
CC
CC TOTAL NUMBER OF WELLS, WELL RADIUS FLAG, FLAG FOR TIME OR COURANT NO.
```

```
*---- NWELL   IRO    ITIME    NWREL
    5       2      1        5
CC
CC WELL ID,LOCATIONS,AND FLAG FOR SPECIFYING WELL TYPE, WELL RADIUS, SKIN
*---- IDW    IW    JW    IFLAG    RW     SWELL   IDIR   IFIRST   ILAST   IPRF
    1      150    1    1        0.001  0       1      20       30       0
CC
CC WELL NAME
*----  WELNAM
INJE1
CC
CC ICHEK , MAX. AND MIN. ALLOWABLE BOTTOMHOLE PRESSURE AND RATE
*---- ICHEK     PWFMIN     PWFMAX    QTMIN    QTMAX
    0         0          1251      0        4000
CC
CC WELL ID,LOCATIONS,AND FLAG FOR SPECIFYING WELL TYPE, WELL RADIUS, SKIN
*---- IDW    IW    JW    IFLAG    RW     SWELL   IDIR   IFIRST   ILAST   IPRF
    2      150    1    1        0.001  0       1      70       80      0
CC
CC WELL NAME
*----  WELNAM
INJE2
CC
CC ICHEK , MAX. AND MIN. ALLOWABLE BOTTOMHOLE PRESSURE AND RATE
*---- ICHEK     PWFMIN     PWFMAX    QTMIN    QTMAX
    0         0          1251      0        4000
CC
CC WELL ID,LOCATIONS,AND FLAG FOR SPECIFYING WELL TYPE, WELL RADIUS, SKIN
*---- IDW    IW    JW    IFLAG    RW     SWELL   IDIR   IFIRST   ILAST   IPRF
     3     150    1    1        0.001  0       1      120      130      0
CC
CC WELL NAME
*----  WELNAM
INJE3
CC
CC ICHEK , MAX. AND MIN. ALLOWABLE BOTTOMHOLE PRESSURE AND RATE
*---- ICHEK     PWFMIN     PWFMAX    QTMIN    QTMAX
    0         0          1251      0        4000
CC
CC WELL ID,LOCATIONS,AND FLAG FOR SPECIFYING WELL TYPE, WELL RADIUS, SKIN
*---- IDW    IW    JW    IFLAG    RW     SWELL   IDIR   IFIRST   ILAST   IPRF
    4     1     1    2        0.001  0       1      45       55      0
CC
CC WELL NAME
*----  WELNAM
PROD1
CC
CC ICHEK , MAX. AND MIN. ALLOWABLE BOTTOMHOLE PRESSURE AND RATE
*---- ICHEK     PWFMIN     PWFMAX    QTMIN    QTMAX
    0         0          1251      0        4000
CC
CC WELL ID,LOCATIONS,AND FLAG FOR SPECIFYING WELL TYPE, WELL RADIUS, SKIN
*---- IDW    IW    JW    IFLAG    RW     SWELL   IDIR   IFIRST   ILAST   IPRF
    5     1     1    2        0.001  0       1      95       105      0
CC
CC WELL NAME
*----  WELNAM
PROD2
CC
CC ICHEK , MAX. AND MIN. ALLOWABLE BOTTOMHOLE PRESSURE AND RATE
*---- ICHEK     PWFMIN     PWFMAX    QTMIN    QTMAX
     0         0          1251      0        4000
CC
CC  ID,INJ. RATE AND INJ. COMP. FOR RATE CONS. WELLS FOR EACH PHASE (L=1,3)
*----  ID     QI(M,L)     C(M,KC,L)
     1      0.002882        1      0  0  0.    0.350   0    0    0   0
```

```
     1     0          0     0  0  0   0      0   0   0  0
     1     0          0     0  0  0   0      0   0   0  0
CC
CC  ID,INJ. RATE AND INJ. COMP. FOR RATE CONS. WELLS FOR EACH PHASE (L=1,3)
*----  ID     QI(M,L)     C(M,KC,L)
     2     0.002882      1      0   0   0.    0.350   0    0    0   0
     2     0          0     0  0  0   0      0   0   0  0
     2     0          0     0  0  0   0      0   0   0  0
CC
CC  ID,INJ. RATE AND INJ. COMP. FOR RATE CONS. WELLS FOR EACH PHASE (L=1,3)
*----  ID     QI(M,L)     C(M,KC,L)
     3     0.002882       1      0   0   0.    0.350   0    0    0   0
     3     0          0     0  0  0   0      0   0   0  0
     3     0          0     0  0  0   0      0   0   0  0
CC
CC ID, BOTTOM HOLE PRESSURE FOR PRESSURE CONSTRAINT WELL (IFLAG=2 OR 3)
*----  ID    PWF
     4     101.
CC
CC ID, BOTTOM HOLE PRESSURE FOR PRESSURE CONSTRAINT WELL (IFLAG=2 OR 3)
*----  ID    PWF
     5     101.
CC
CC CUM. INJ. TIME , AND INTERVALS (PV OR DAY) FOR WRITING TO OUTPUT FILES
*---- TINJ     CUMPR1     CUMHI1     WRHPV     WRPRF      RSTC
     9  9       9        9      9    4.0
CC
CC FOR IMES=2 ,THE INI. TIME STEP,CONC. TOLERANCE,MAX.,MIN. time steps
*----DT            DCLIM     CNMAX   CNMIN
    0.000001     0.002      0.2     0.02
CC
CC
*---- IBMOD
     0
CC
CC IRO, ITIME, NEW FLAGS FOR ALL THE WELLS (POLYMER DRIVE)
*---- IRO ITIME IFLAG
     2  1     1  1  1  2  2
CC
CC NUMBER OF WELLS changes IN LOCATION OR SKIN OR PWF
*----NWEL1
     0
CC
CC NUMBER OF WELLS WITH RATE changes, id
*----NWEL1   Id
    3      1  2  3
CC
CC  ID,INJ. RATE AND INJ. COMP. FOR RATE CONS. WELLS FOR EACH PHASE (L=1,3)
*----  ID     QI(M,L)     C(M,KC,L)
     1     0.002882       1      0   0   0.5    0.350   0    0    0   0
     1     0          0     0  0  0   0      0   0   0  0
     1     0          0     0  0  0   0      0   0   0  0
CC
CC  ID,INJ. RATE AND INJ. COMP. FOR RATE CONS. WELLS FOR EACH PHASE (L=1,3)
*----  ID     QI(M,L)     C(M,KC,L)
     2     0.000      1     0   0   0.5    0.350   0    0    0   0
     2     0          0     0  0  0   0      0   0   0  0
     2     0          0     0  0  0   0      0   0   0  0
CC
CC  ID,INJ. RATE AND INJ. COMP. FOR RATE CONS. WELLS FOR EACH PHASE (L=1,3)
*----  ID     QI(M,L)     C(M,KC,L)
     3     0.001441       1      0   0   0.5    0.350   0    0    0   0
     3     0          0     0  0  0   0      0   0   0  0
     3     0          0     0  0  0   0      0   0   0  0
CC
CC CUM. INJ. TIME , AND INTERVALS (PV OR DAY) FOR WRITING TO OUTPUT FILES
```

```
*---- TINJ     CUMPR1     CUMHI1     WRHPV     WRPRF      RSTC
      9.07   0.01        0.01        0.01      0.01    4.0
CC
CC FOR IMES=2 ,THE INI. TIME STEP,CONC. TOLERANCE,MAX.,MIN. time steps
*----DT            DCLIM     CNMAX   CNMIN
    0.000001     0.002      0.2     0.02
CC
CC
*---- IBMOD
     0
CC
CC IRO, ITIME, NEW FLAGS FOR ALL THE WELLS (POLYMER DRIVE)
*---- IRO ITIME IFLAG
      2   1     1  1  1  2  2
CC
CC NUMBER OF WELLS changes IN LOCATION OR SKIN OR PWF
*----NWEL1
     0
CC
CC NUMBER OF WELLS WITH RATE changes, id
*----NWEL1   Id
    2       1   3
CC
CC id,INJ. RATE AND INJ. COMP. FOR RATE CONS. WELLS FOR EACH PHASE (L=1,3)
*----id  QI(M,L)  C(M,KC,L)
     1     0.00014411     1     0   0   0.5    0.350   0    0    0
     1     0           0     0  0  0   0       0    0    0
     1     0           0     0  0  0   0       0    0    0
CC
CC id,INJ. RATE AND INJ. COMP. FOR RATE CONS. WELLS FOR EACH PHASE (L=1,3)
*----id  QI(M,L)  C(M,KC,L)
     3     0.00014411     1     0   0   0.5  0.350   0    0    0
     3     0           0     0  0  0   0       0    0    0
     3     0           0     0  0  0   0       0    0    0
CC
CC CUM. INJ. TIME , AND INTERVALS (PV) FOR WRITING TO OUTPUT FILES
*----TINJ   CUMPR1  CUMHI2(SUMARY) WRHPV(HIST) WRPRF(PLOT) RSTC
    9.4   0.33    0.33        0.33       0.33         4.0
CC
CC FOR IMES=2 ,THE INI. TIME STEP,CONC. TOLERANCE,MAX.,MIN. time steps
*----DT     DCLIM   CNMAX   CNMIN
    0.000001     0.002      0.2   0.02
CC
CC
*---- IBMOD
     0
CC
CC IRO, ITIME, NEW FLAGS FOR ALL THE WELLS (POLYMER DRIVE)
*---- IRO ITIME IFLAG
      2   1     1  1  1  2  2
CC
CC NUMBER OF WELLS changes IN LOCATION OR SKIN OR PWF
*----NWEL1
     0
CC
CC NUMBER OF WELLS WITH RATE changes, id
*----NWEL1   Id
    2       1   3
CC
CC id,INJ. RATE AND INJ. COMP. FOR RATE CONS. WELLS FOR EACH PHASE (L=1,3)
*----id  QI(M,L)  C(M,KC,L)
     1     0.0001441     1     0   0   0.5    0.350   0    0    0
     1     0           0     0  0  0   0       0    0    0
     1     0           0     0  0  0   0       0    0    0
CC
CC id,INJ. RATE AND INJ. COMP. FOR RATE CONS. WELLS FOR EACH PHASE (L=1,3)
```

```
*----id  QI(M,L)  C(M,KC,L)
     3     0.0001441     1     0   0   0.5    0.350   0    0    0
     3     0           0     0   0   0    0       0    0    0
     3     0           0     0   0   0    0       0    0    0
CC
CC CUM. INJ. TIME , AND INTERVALS (PV) FOR WRITING TO OUTPUT FILES
*----TINJ   CUMPR1  CUMHI2(SUMARY) WRHPV(HIST) WRPRF(PLOT) RSTC
    9.67   0.01    0.01        0.01       0.01         2.0
CC
CC FOR IMES=2 ,THE INI. TIME STEP,CONC. TOLERANCE,MAX.,MIN. time steps
*----DT     DCLIM   CNMAX   CNMIN
    0.000001     0.002      0.2   0.02
CC
CC
*---- IBMOD
     0
CC
CC IRO, ITIME, NEW FLAGS FOR ALL THE WELLS (POLYMER DRIVE)
*---- IRO ITIME IFLAG
      2   1     1  1  1  2  2
CC
CC NUMBER OF WELLS changes IN LOCATION OR SKIN OR PWF
*----NWEL1
     0
CC
CC NUMBER OF WELLS WITH RATE changes, id
*----NWEL1   Id
    2       1   3
CC
CC id,INJ. RATE AND INJ. COMP. FOR RATE CONS. WELLS FOR EACH PHASE (L=1,3)
*----id  QI(M,L)  C(M,KC,L)
     1     0.0001441     1     0   0   0.5    0.350   0    0    0
     1     0           0     0   0   0    0       0    0    0
     1     0           0     0   0   0    0       0    0    0
CC
CC id,INJ. RATE AND INJ. COMP. FOR RATE CONS. WELLS FOR EACH PHASE (L=1,3)
*----id  QI(M,L)  C(M,KC,L)
     3     0.0001441     1     0   0   0.5    0.350   0    0    0
     3     0           0     0   0   0    0       0    0    0
     3     0           0     0   0   0    0       0    0    0
CC
CC CUM. INJ. TIME , AND INTERVALS (PV) FOR WRITING TO OUTPUT FILES
*----TINJ   CUMPR1  CUMHI2(SUMARY) WRHPV(HIST) WRPRF(PLOT) RSTC
    11.0   1.33    1.33        1.33       1.33         2.0
CC
CC FOR IMES=2 ,THE INI. TIME STEP,CONC. TOLERANCE,MAX.,MIN. time steps
*----DT     DCLIM   CNMAX   CNMIN
    0.000001     0.002      0.2   0.02
CC
CC
*---- IBMOD
     0
CC
CC IRO, ITIME, NEW FLAGS FOR ALL THE WELLS (POLYMER DRIVE)
*---- IRO ITIME IFLAG
      2   1     1  1  1  2  2
CC
CC NUMBER OF WELLS changes IN LOCATION OR SKIN OR PWF
*----NWEL1
     0
CC
CC NUMBER OF WELLS WITH RATE changes, id
*----NWEL1   Id
    2       1   3
CC
CC id,INJ. RATE AND INJ. COMP. FOR RATE CONS. WELLS FOR EACH PHASE (L=1,3)
```

```
*----id  QI(M,L)  C(M,KC,L)
     1     0.0001441     1      0   0   0.5    0.350   0    0    0
     1     0             0      0   0   0    0       0    0    0
     1     0             0      0   0   0    0       0    0    0
CC
CC id,INJ. RATE AND INJ. COMP. FOR RATE CONS. WELLS FOR EACH PHASE (L=1,3)
*----id  QI(M,L)  C(M,KC,L)
     3     0.0001441     1      0   0   0.5    0.350   0    0    0
     3     0             0      0   0   0    0       0    0    0
     3     0             0      0   0   0    0       0    0    0
CC
CC CUM. INJ. TIME , AND INTERVALS (PV) FOR WRITING TO OUTPUT FILES
*----TINJ   CUMPR1  CUMHI2(SUMARY) WRHPV(HIST) WRPRF(PLOT) RSTC
    13.0   1.0    1.0        1.0        1.0         2.0
CC
CC FOR IMES=2 ,THE INI. TIME STEP,CONC. TOLERANCE,MAX.,MIN. time steps
*----DT     DCLIM   CNMAX   CNMIN
    0.000001     0.002      0.2   0.02
```